Transilvania University of Braşov

HABILITATION THESIS

Title: MULTIFUNCTIONAL THIN SOLID FILMS

Domain: Materials Engineering

Author: Lect. Dr. Eng. Daniel CRISTEA

University: Transilvania University of Braşov

BRAŞOV, 2021

CONTENT

Acknowledgements 4

List of abbreviations 5

(A1) Abstract 7

(A2) Rezumat 9

(B) Scientific and professional achievements and the evolution and development plans for career development

(B1) Professional achievements 11

(B2) Scientific achievements 20

Chapter 1. Multifunctional thin solid films: means of development 20

1.1 Background and overview of reactive magnetron sputtering 20

1.1.1 Sputtering 21

1.1.2 The influence of the applied magnetic field on the sputtering process 23

1.2 Reactive magnetron sputtering process control 24

Motivation of the thesis subject 27

Chapter 2 Transition metal oxynitride thin films 28

2.1 Motivation 28

2.1.1 Pure tantalum 28

2.1.2 Tantalum oxide coatings 29

2.1.3 Tantalum nitride coatings 30

2.1.4 Tantalum oxynitride coatings 30

2.2 Sample preparation 31

2.3 Results and discussions 33

2.3.1. Chemical composition, chemical states, structural development 33

2.3.2 Electrical, photocatalytic and antibacterial properties 48

2.3.3 Thermal treatment structural effects 68

Chapter 3 Ceramic composite thin films 73

3.1. Motivation and theoretical aspects 73

3.1.1 Compound characteristics 76

3.2 Sample preparation 78

3.3 Results and discussions 79

3.3.1. Composition and morphology 79

3.3.2 Mechanical characterization 82

Chapter 4 Magnesium-based ternary nitride thin films 87

4.1 Motivation and theoretical aspects 87

4.2. Experimental details and results 89

Conclusions 104

(B3) The evolution and development plans for career development 106

B3.1 Teaching activities 106

B3.2 Research topics 106

B3.2.1 Complex oxynitride coatings 107

B3.2.2 Refractory metal and magnesium-based coatings 110

B3.2.3 Refractory metal ternary nitrides (Me1Me2N) 111

(B4) Bibliography 115

Acknowledgements

The research results presented in this habilitation thesis have been financially supported by several national and international grants:

- Sectoral Operational Programme Human Resources Development (SOP HRD), financed from the European Social Fund and by the Romanian Government under the project number POSDRU/159/1.5/S/134378 is gratefully acknowledged for providing an 18-month postdoctoral fellowship ("Tantalum oxynitride multifunctional thin films applications").
- PRO-DD (POS-CCE, O.2.2.1., ID 123, SMIS 2637, ctr. No 11/2009) is gratefully acknowledged for providing some of the infrastructure used for sample analysis.
- Transilvania University of Brasov, Romania is acknowledged for financing the Young Researchers Grant Unitbv 8022/2017 – "Wear resistant thin solid films".
- DAAD German Academic Exchange Service - Research Stays for University Academics and Scientists is acknowledged for the financial support of the project "RM-Mg-N multiple component nitride-type thin films, obtained by simultaneous sputtering of two metallic targets". Host Institution (2020): FEM (forschunginstitut edelmetalle + metallchemie), Schwäbisch Gmünd, Germany.
- Multilayer inorganic/organic tribological coatings for space applications - financed in the Research-Development-Innovation for Aerospace Technologies and Advanced Research Program (STAR) - ctr. no. 68/2013. 2013 – 2016, financed by the Romanian Space Agency.
- European Union's Horizon 2020 research and innovation programme under grant agreement No 823802 is gratefully acknowledged for the access to infrastructure. Sfera III Access Grant: "Concentrated solar radiation fast sintering of novel metastable Al-Si-Ni alloys, as potential raw materials for additive manufacturing", Middle Eastern Technical University, Ankara, Turkey, 2019; SFERA III Access Grant: "Novel Ti-based biocompatible alloy coatings from powders sintered onto Ti6Al4V substrates using concentrated solar radiation", PROMES-CNRS, Odeillo, France, 2020.

My scientific development would not have been possible without the work done with my collaborators from the following institutions: Transilvania University of Brasov, Romania; National Institute for Laser, Plasma and Radiation Physics, Romania; The National Institute for Research and Development for Optoelectronics, Romania; Alexandru Ioan Cuza University of Iaşi, Romania; National Institute of Materials Physics, Romania; University of Minho, Physics Department, Portugal; Research Institute for Precious Metals and Metal Chemistry, Germany; Horia Hulubei National Institute for Physics and Nuclear Engineering, Romania; The Institute for Nuclear Research Pitesti, Romania; The National Institute for Research and Development in Electrical Engineering ICPE-CA Romania; The National Institute of Research and Development for Technical Physics, Romania.

List of abbreviations

AFM – atomic force microscopy

ALD – atomic layer deposition

BFTEM – bright field transmission electron microscopy

CFU – colony-forming unit

CSP – concentrated solar power

CTE – coefficient of thermal expansion

DC – direct current

E_{CB} – conduction band edge potential

ECR – Electron Cyclotron Resonance

EDS - Energy-dispersive X-ray spectroscopy

E_g – optical band gap energy

E_U – Urbach energy

E_{VB} – valence band edge potential

fcc – face centered cube

GND – grounded

HiPIMS – high-power impulse magnetron sputtering

HRTEM – high resolution transmission electron microscopy

HSS – high speed steel

HTXRD – high temperature x-ray diffraction

ICDD – International Centre for Diffraction Data

JCPDS - Joint Committee on Powder Diffraction Standards

MB – methylene blue

MIM – metal insulator metal

MIS – metal insulator semiconductor

MO – methyl orange

MOS – metal oxide semiconductor

MOSFET – metal oxide semiconductor field effect transitor

NHE – normal hydrogen electrode

NSS – neutral salt spray

OCP – open circuit potential

OCV – open circuit voltage

PBS – phosphate buffered solution

PLD – pulsed laser deposition

PVD – physical vapour deposition

RBS – Rutherford backscattering spectrometry

RF – radio frequency

RM – refractory metal

RMS – root mean square roughness

SBF – simulated body fluid

sccm – standard cubic centimeters per minute

SEM – scanning electron microscopy

SHE – standard hydrogen electrode

SOFC – solid oxide fuel cell

TEM – transmission electron microscopy

UV – ultra violet radiation

VEC – valence electron concentration

VIS – visible radiation

XPS – x-ray photoelectron spectroscopy

XRD – x-ray diffraction

XRR – x-ray reflectivity

Abstract

My PhD thesis, successfully defended in 2013, titled: "**Research on the synthesis and characterization of MeO_xN_y system thin films deposited by reactive magnetron sputtering**" presents the development of oxynitride-type thin films (MeO_xN_y, where Me = Ta), deposited by reactive magnetron sputtering. One of the most frequently used methods to alter the surface properties of a material is to deposit a thin film or coating on top of the base material, which will significantly improve the functionality of the final part, in terms of its mechanical, electrical, optical, chemical properties, and so on.

After the completion of the PhD program, my research had the main objective of improving the research on tantalum oxynitride thin films, by extending the studies towards the most promising application directions.

Moreover, I was involved in the research and development of several types of multicomponent thin films, evidenced in the majority of the ISI-WOS published articles: **45 ISI-WOS papers** (45 indexed, 40 in journals and 5 proceedings papers) and **14 BDI papers**. The thin film research and development, mainly by Physical Vapor Deposition (DC sputtering, pulsed laser deposition, High-power impulse magnetron sputtering (HiPIMS), etc.), was complemented by surface characterization (nanoindentation, wear and tribology, adherence of thin films to substrates, corrosion resistance, biocompatibility, photocatalysis, electrical, and optical analysis).

The habilitation thesis titled **Multifunctional thin solid films** represents the accumulation of knowledge in the field of surface engineering, based on my work with reactive magnetron sputtering deposition and several analysis techniques. The scope of this habilitation thesis is to show that reactive magnetron sputtering is a powerful technique which is able to obtain complex thin solid films, with multifunctional properties, which can be tailored to suit the desired application.

The first part of the habilitation thesis presents my professional track after the completion of my PhD program, with emphasis on the accomplishments and results. The scientific results are presented in the following section, which is structured in four chapters. A short description of the content of each chapter is presented hereinafter.

Chapter one contains relevant information regarding the theoretical aspects of sputtering, some information on the role of the applied magnetic field, and key information regarding the reactive sputtering process, with emphasis on some factors that govern the stability and reproducibility of the reactive magnetron sputtering deposition.

Chapter two presents results obtained after the completion of my PhD program, on optimized tantalum oxynitride TaO_xN_y thin solid films, regarding certain possible applications: i) photocatalytic

behavior, observed through the photodegradation of some solutions of methylene blue, respectively methyl-orange, with or without hydrogen peroxide, under the action of the ultraviolet spectrum, respectively of the visible spectrum, in the presence of the tantalum oxynitride thin solid films; ii) as a material with tunable electrical properties, where the electrical resistivity increases with increasing reactive gas partial pressure, starting from characteristic values of metallic compounds to characteristic values of oxides, and the high resistivity samples exhibit permittivity values up to 41, significantly higher than those for other tantalum-based films found in the literature; iii) as a potential biomaterial due to its adequate antibacterial/antibiofilm capacity against certain pathogens.

Chapter three presents results concerning the composition, morphological and mechanical characteristics for ceramic composite magnetron sputtered (Ti + TiB_2 + WC) coatings. The films were obtained by simultaneous standard/reactive magnetron sputtering from three targets (Ti, TiB_2 and WC). The films are hard (instrumented indentation hardness values between 20 and 22 GPa), but if they are deposited on softer materials, they exhibit poor adhesion to the substrate, which can be certainly improved by adjusting the deposition parameters. These films show promising results concerning their wear resistance, especially if the films would be paired with an appropriate substrate material.

Chapter four presents preliminary results concerning the development of single stage deposition ternary hard coatings with improved corrosion properties. The purpose of the research presented herein was to study refractory metal multiple component nitride-type thin films, obtained by simultaneous sputtering of two metallic targets, with the addition in various proportions of reactive gas. The refractory metal candidate was chosen after preliminary tests in respect to the corrosion behavior of the coatings. The second stage of the research was to deposit multiple component coatings, and to analyze them in terms of corrosion protection capacity, but coupled with as high as possible mechanical properties.

The last section of this habilitation thesis presents the career development plan, related to teaching activities, as well as to future research directions. The future research subjects are reliant on the gained knowledge since the completion of my PhD program. The proposed subjects are: **i)** developing complex oxynitride coatings, such as $Me_1Me_2O_xN_y$-type materials, which can be tailored to answer certain industrial requirements; **ii)** due to multiple unanswered questions regarding the coatings presented in chapter 4 of this thesis, the research activities will be devoted towards understanding the physical phenomena displayed by this system. Secondly, further research is planed using the same hypothesis, namely pairing two elemental targets, to obtain single stage corrosion resistant complex coatings; **iii)** the development of multiple component nitride-type compounds due to their potential original properties compared to their nitride parents.

Rezumat

Teza mea de doctorat, susținută cu succes în 2013, intitulată: „**Cercetări privind sinteza și caracterizarea straturilor subțiri din sistemul MeO_xN_y obținute prin pulverizare reactivă în sistem magnetron**” prezintă dezvoltarea filmelor subțiri de tip oxinitrură (MeO_xN_y, unde Me = Ta), depuse prin pulverizare reactivă în regim magnetron. Una dintre metodele cele mai frecvent utilizate pentru a modifica proprietățile de suprafață ale unui material este depunerea unei pelicule subțiri sau a unei acoperiri deasupra materialului de bază, care va îmbunătăți semnificativ funcționalitatea piesei, în ceea ce privește proprietățile mecanice, electrice, optice, și așa mai departe.

După finalizarea programului de doctorat, cercetarea mea a avut ca principal obiectiv îmbunătățirea proprietăților filmelor subțiri de tip oxinitrură de tantal, prin extinderea studiilor către cele mai promițătoare direcții de utilizare.

Mai mult decât atât, am fost implicat în cercetarea și dezvoltarea mai multor tipuri de filme subțiri multicomponent, prezentate în majoritatea articolelor publicate: **45 de lucrări ISI-WOS** (45 indexate, 40 în reviste și 5 lucrări de tip proceeding) și **14 articole de tip BDI**. Cercetarea și dezvoltarea filmelor subțiri, în principal prin depunerea fizică din stare de vapori (pulverizare în current continuu, depunere laser pulsată, etc.), a fost completată de caracterizarea materialelor prin diverse tehnici de analiză (nanoindentare, uzură și tribologie, aderență a filmelor subțiri la substraturi, rezistență la coroziune, biocompatibilitate, fotocataliză, analiză electrică și optică).

Teza de abilitare intitulată **Multifunctional thin solid films** reprezintă acumularea de cunoștințe în domeniul ingineriei suprafețelor, pe baza cercetărilor mele legate de depunerea reactivă prin pulverizare în regim magnetron. Scopul acestei teze de abilitare este de a demonstra că pulverizarea în regim magnetron este o tehnică importantă care este capabilă să obțină filme complexe subțiri, cu proprietăți multifuncționale, care pot fi adaptate pentru a răspunde aplicației dorite.

Prima parte a tezei de abilitare prezintă traseul meu profesional după finalizarea programului de doctorat, cu accent pe realizări și rezultate. Rezultatele științifice sunt prezentate în secțiunea următoare, care este structurată în patru capitole. O scurtă descriere a conținutului fiecărui capitol este prezentată în continuare.

Capitolul 1 conține informații relevante cu privire la aspectele teoretice legate de fenomenul de pulverizare, unele informații cu privire la rolul câmpului magnetic aplicat și informații cheie privind procesul de pulverizare reactivă, cu accent pe anumiți factori care influențează stabilitatea și reproductibilitatea depunerii reactive prin pulverizare în regim magnetron.

Capitolul 2 prezintă rezultatele obținute după finalizarea programului de doctorat, pe filme solide subțiri optimizate de oxinitrură de tantal TaO_xN_y, cu privire la anumite aplicații posibile: i) comportament fotocatalitic, observat prin fotodegradarea unor soluții de albastru de metilen, respectiv metil-oranj, cu

sau fără peroxid de hidrogen, sub acțiunea spectrului ultraviolet, respectiv a spectrului vizibil, în prezența filmelor solide subțiri de oxinitrură de tantal; ii) ca material cu proprietăți electrice variabile, unde rezistivitatea electrică crește odată cu creșterea presiunii parțiale, începând de la valorile caracteristice ale compușilor metalici la valorile caracteristice ale oxizilor, iar probele de rezistivitate ridicată prezintă valori ale permitivității de până la 41, semnificativ mai mari decât cele pentru alte filme bazate pe tantal găsite în literatură; iii) ca posibil biomaterial datorită capacității sale antibacteriene adecvate împotriva anumitor agenți patogeni.

Capitolul 3 prezintă rezultate privind compoziția, caracteristicile morfologice și mecanice pentru acoperirile ceramice compozite obținute prin pulverizare, bazate pe Ti + TiB_2 + WC. Filmele au fost obținute prin pulverizarea simultană în regim magnetron, standard sau reactiv, a trei ținte (Ti, TiB_2 și WC). Filmele sunt dure (valori de duritate între 20 și 22 GPa), dar dacă sunt depuse pe materiale mai moi, prezintă o aderență slabă la substrat, care poate fi cu siguranță îmbunătățită prin ajustarea parametrilor de depunere. Aceste filme prezintă rezultate promițătoare în ceea ce privește rezistența la uzură, mai ales dacă filmele ar fi depuse pe un material adecvat.

Capitolul 4 prezintă rezultate preliminare privind dezvoltarea de acoperiri ternare obținute prin depunere într-o singură etapă, cu rezistență la coroziune îmbunătățită. Scopul cercetării prezentate în acest capitol a fost studierea filmelor subțiri de tip nitruri multicomponent, bazate pe metale tranziționale, obținute prin pulverizarea simultană a două ținte metalice, cu adăugarea în diferite proporții de gaz reactiv. Materialele metalice au fost alese după testele preliminare în ceea ce privește comportamentul la coroziune al acoperirilor de tip nitruri binare. A doua etapă a cercetării a fost depunerea acoperirilor multicomponent și analizarea acestora în ceea ce privește capacitatea de protecție împotriva coroziunii, dar cuplată cu proprietăți mecanice cât mai bune.

Ultima secțiune a acestei teze de abilitare prezintă planul de dezvoltare a carierei, în ceea ce privește activitățile didactice, precum și direcțiile viitoare de cercetare. Viitoarele subiecte de cercetare se bazează pe cunoștințele acumulate de la finalizarea programului meu de doctorat. Subiectele propuse sunt: **i)** dezvoltarea de acoperiri complexe de tip oxinitrură, cum ar fi materiale de tip $Me_1Me_2O_xN_y$, care pot fi adaptate pentru a răspunde anumitor cerințe industriale; **ii)** din cauza mai multor neclarități cu privire la acoperirile prezentate în capitolul 4 al acestei teze, activitățile de cercetare vor fi dedicate înțelegerii fenomenelor fizice asociate acestui sistem. În al doilea rând, cercetări ulterioare sunt planificate bazându-se pe aceeași ipoteză, și anume combinarea a două ținte, pentru a obține acoperiri complexe într-o etapă, rezistente la coroziune; **iii)** dezvoltarea compușilor de tip nitrură multicomponent datorită proprietăților lor originale în comparație cu nitrurile binare.

(B) Scientific and professional achievements and the evolution and development plans for career development

(B1) Professional achievements

The habilitation thesis consists in some of the research results obtained after defending my PhD thesis, in September 2013. My professional background and my career evolution can be summarized as follows:

I obtained the Bachelor's degree in Materials Science from the Materials Science and Engineering Faculty from Transilvania University of Brasov, in 2009. In 2011, I graduated from the Master's programme titled "Engineering and Management of Advanced Metallic, Ceramic and Composite Materials", from the Materials Science and Engineering Faculty from Transilvania University of Brasov. From 2009 to 2011 I was hired as a mechanical engineer at a fasteners manufacturing company (Brasov Fasteners Inc.).

I started my doctoral studies in 2010, in the Materials Engineering domain at the Materials Science Department, Transilvania University of Brasov, successfully defending in 2013 the PhD thesis titled: **"Research on the synthesis and characterization of MeO_xN_y system thin films deposited by reactive magnetron sputtering"**. The PhD thesis is the result of a collaboration program between Transilvania University of Brasov and Minho University, Physics Department, Portugal. The research subject was the development of oxynitride-type thin films (MeO_xN_y, where Me = transitional metal: Zr, Ti, Ta, Mo), deposited by sputtering. Considering the complexity of these classes of thin films (possible structures and properties, depending on the processing parameters, mainly due to their tunability (i.e., changing the ratio between the component elements), and furthermore the relative scarcity of scientific reports, up to that date, concerning the TaO_xN_y system, the research was focused on this particular system. The sample preparation and part of the characterization was carried out in the Physics Department of Minho University, Braga, Portugal, where I first dealt with the intricacies of reactive magnetron sputtering and sample analysis, and data processing and interpretation.

After the successful completion of the PhD program, the postdoctoral fellowship of 18 months, awarded by the European Social Fund and by the Romanian Government, had the main objective of improving the research on tantalum oxynitride thin films, by extending the studies towards the most promising application directions: photocatalysis and dielectric films. Consequently, my research was devoted to the deposition and in-depth analysis of TaO_xN_y films using conditions that previously indicated good results concerning the aforementioned applications.

During the PhD program, since 2012, I started my teaching activities at the Materials Department, Transilvania University of Brasov. From March 2015 I joined the department staff as a full-time member, namely as a Lecturer. My teaching activities involve courses, seminars and practical laboratories covering materials science, surface engineering, materials for renewable energy technologies, nanomaterials, biomaterials, scientific writing and ethics, at the bachelor's and master's degree levels, as well as tutoring of undergraduate and master students for their final projects.

I was involved in the research and development of several types of multicomponent thin films, evidenced in the majority of the ISI-WOS published articles: **45 ISI-WOS papers** (45 indexed, 40 in journals and 5 proceedings papers) and **14 BDI papers**. The thin film research and development, mainly by Physical Vapor Deposition (DC sputtering, pulsed laser deposition, High-power impulse magnetron sputtering (HiPIMS), etc.), was complemented by surface characterization (nanoindentation, wear and tribology, adherence of thin films to substrates, corrosion resistance, biocompatibility, photocatalysis, electrical, and optical analysis. I worked with several types of thin films: titanium carbides (TiC), zirconium carbides (ZrC), tantalum oxynitrides (TaO_xN_y), silicon carbides (SiC), titanium oxides embedded with gold or silver nanoparticles (TiO_2-Au, TiO_2-Ag), titanium/copper and titanium/aluminium nanocomposite thin films (TiCu, TiAl), diamond-like carbon films (a-C:H), combinatorial silicon carbide/zirconium nitride films (SiC/ZrN), lanthanum hexaborides (LaB_6), molybdenum disulphides (MoS_2), tungsten carbides (WC), titanium diborides (TiB_2), and many more.

In order to further develop my research capabilities, I attended several traineeship or research exchange programs, as follows:

- Instrumented indentation at Queen Mary University of London, United Kingdom, 2017;
- Dual magnetron sputtering and corrosion analysis at the Research Institute for Precious Metals and Metal Chemistry, Germany, 2020;
- Concentrated solar energy experiments at PROMES-CNRS, Odeillo, France, 2020;
- Simulated concentrated solar energy experiments at Middle Eastern Technical University, Ankara, Turkey, 2019;
- Sputtering deposition chamber maintenance and repair at Minho University, Physics Department, Portugal, 2019;
- Additive manufacturing summer school at University of Modena and Reggio Emilia, Italy, 2019.

Furthermore, I am a reviewer for the following ISI-WOS journals:

- Applied Surface Science (Elsevier),
- Surface & Coatings Technology (Elsevier),
- ACS Applied Materials & Interfaces (American Chemical Society),

- Colloids and Surfaces A (Elsevier),
- Materials Research Express (IOP Science),
- Materials (MDPI),
- Coatings (MDPI),
- Physics Open (Elsevier),
- PloS One,
- Arabian Journal for Science and Engineering (Springer),
- Metals (MDPI),
- ACS Combinatorial Science (American Chemical Society),
- Applied Sciences (MDPI),
- Materials Research Express (IOP),
- Surface and Interface Analysis (Wiley),
- Materials Letters (Elsevier),
- Results in Physics (Elsevier),
- Journal of Environmental Chemical Engineering (Elsevier),
- Journal of Materials Science (Springer),
- Polymers (MDPI),
- Materials Today Communications (Elsevier).

Several research grants were successfully completed or are under development, at the international and national level, as follows:

a). Director/Partner responsible:

1. Postdoctoral fellowship awarded by the Sectoral Operational Programme Human Resources Development (SOP HRD), financed from the European Social Fund and by the Romanian Government under the project number POSDRU/159/1.5/S/134378 ("Tantalum oxynitride multifunctional thin films applications").
2. Young Researchers Grant (Transilvania University of Brasov) 8022/2017 – "Wear resistant thin solid films".
3. "RM-Mg-N multiple component nitride-type thin films, obtained by simultaneous sputtering of two metallic targets". DAAD German Academic Exchange Service - Research Stays for University Academics and Scientists Host Institution (2020): FEM (forschunginstitut edelmetalle + metallchemie), Schwäbisch Gmünd, Germany.
4. Sfera III Access Grant: "Concentrated solar radiation fast sintering of novel metastable Al-Si-Ni alloys, as potential raw materials for additive manufacturing", Middle Eastern Technical University, Ankara, Turkey, 2019;

5. SFERA III Access Grant: "Novel Ti-based biocompatible alloy coatings from powders sintered onto Ti6Al4V substrates using concentrated solar radiation", PROMES-CNRS, Odeillo, France, 2020.
6. PN-III-P1-1.1-TE-2019-1209: "Magnetron sputtered Me-Me binary oxynitride multifunctional thin solid films", financed by: UEFISCDI nr.ctr: TE 59 - 31/08/2020, 2020-2022
7. "Performing mechanical and tribological tests for samples with tribological coatings (Hardness Test, Scratch Test, Pin/Ball on Disk Tribometer Test)" financed by: IFIN-HH Horia Hulubei National Institute for Physics and Nuclear Engineering, Magurele, Romania, nr.ctr: 13440 - 16/11/2020 (value 72000 RON), 2020-2021.

b). Project member:

1. RIA - Horizon 2020, (2016 - 2019) - FOF-13-2016: Photonics Laser-based production: DREAM (Driving up reliability and efficiency of additive manufacturing). Project member. Main responsibilities: sample preparation, results dissemination through reports and publications.
2. PN-III-P2-2.1-BG-2016-0241 - Optimizing the inductive quenching eco-technology for large bearing rings. Bridge Grant 2016-2018. Project member. Main responsibilities: sample preparation, mechanical characterization (microindentation, tribology), results dissemination through reports and publications.
3. Multilayer inorganic/organic tribological coatings for space applications - financed in the Research-Development-Innovation for Aerospace Technologies and Advanced Research Program (STAR) - ctr. no. 68/2013. 2013 – 2016. Project member. Main responsibilities: thin film mechanical characterization and interpretation (nanoindentation, scratch testing, tribology), results dissemination through publications.
4. Grant FP7-INFRA-312643- SFERA II (2016): "Researches regarding the influence of the heat treatments with solar energy over the wear resistant steels properties". Project member. Main responsibilities: sample preparation (at the HÉLIODYSSÉE - Grand Four Solaire d'Odeillo (Odeillo Solar Furnace) facility, located in Font-Romeu-Odeillo-Via, France); mechanical characterization (microindentation, tribology, corrosion resistance), results dissemination through publications.
5. Survey Services: Surface Features of Dental Implants: Mechanical Characteristics. Period: 2017-2018 Funding: DENTIX contract no: 144 / 09.01.2017. Project member. Main responsibilities: surface mechanical characterization and interpretation (nanoindentation, roughness testing, tribology), results dissemination through publications.
6. New Diagnosis and Treatment Methodologies: Active Challenges and Technological Solutions Based on Nanomaterials and Biomaterials - Acronym: SANOMAT, period 2018-2020, financed

by UEFISCDI. Project member. Main responsibilities: thin film mechanical characterization and interpretation (sample preparation, heat treatments, nanoindentation, scratch testing, tribology), results dissemination through publications.

7. "Solar-assisted treatment of some new stainless steels for biomedical applications", Acronym: SOLARBIOMAT CIEMAT-PSA contract no: FP7-INFRA-312643 code P1701100227/2017, period: 2017. Project member. Main responsibilities: sample preparation (at the PSA-CIEMAT facilities, Almeria, Spain); mechanical characterization (microindentation, tribology, corrosion resistance), results dissemination through publications.
8. Premiere H2020 – DREAM, 2017-2019 financed by UEFISCDI nr.ctr: 15/2017 PN-III-P3-3.6-H2020-2016-0077. Project member. Main responsibilities: sample preparation and analysis, results dissemination through reports and publications.

I am an author of the following books:

1. I. Ghiuta, **D. Cristea**. *Silver nanoparticles for delivery purposes* (Chapter) - Nanoengineered Biomaterials for Advanced Drug Delivery 1st Edition, Elsevier, isbn: 9780081029855, 2020;
2. **Daniel Cristea**, Luis Cunha, Aurel Crișan, Daniel Munteanu. *Oxinitride thin solid films*, Transilvania University Publishing, isbn: 978-606-19-0450-1, 2014, 201 Pages;
3. Ioana Ghiuță, **Daniel Cristea**, Daniel Munteanu. *Metallic nanoparticles synthesis,* Transilvania University Publishing, isbn: 978-606-19-1011-3, 2018, 183 Pages;
4. Camelia Gabor, **Daniel Cristea**, Mariana Axente. *Isostatic compaction of thin layers obtained by thermal spraying*, Printech, isbn: 978-606-23-0988-6, 2019, 319 Pages;
5. **Daniel Cristea**. *Advanced materials for renewable energies*, Printech, isbn: 978-606-23-1156-8, 2020, 204 Pages;
6. **Daniel Cristea**. *Nanomaterials*, Printech, isbn: 978-606-23-1144-5, 2020, 254 Pages.

The scientific content of this habilitation thesis is based on information presented in the following articles published in scientific journals after the PhD thesis was defended:

1. **D Cristea,** A Crisan, D Munteanu, M Apreutesei, MF Costa, L Cunha. *Tantalum oxynitride thin films: Mechanical properties and wear behavior dependence on growth conditions*, journal: **Surface and Coatings Technology** 2014 **WOS:000346895000071** IF = 2,90
2. **D Cristea,** A Crisan, N Cretu, J Borges, C Lopes, L Cunha, V Ion, M Dinescu, NP Barradas, E Alves, M Apreutesei, D Munteanu. *Structure dependent resistivity and dielectric characteristics of tantalum oxynitride thin films produced by magnetron sputtering*, journal: **Applied Surface Science** 2015 **WOS:000363673500009** IF = 4,43
3. **D Cristea,** M Pătru, A Crisan, D Munteanu, D Crăciun, NP Barradas, E Alves, M Apreutesei, C Moura, L Cunha. *Composition and structure variation for magnetron sputtered tantalum*

oxynitride thin films, as function of deposition parameters, journal: **Applied Surface Science** 2015 **WOS:000366220500002** IF = 4,43

4. L Cunha, M Apreutesei, C Moura, E Alves, NP Barradas, **D Cristea***. *In-situ XRD vs ex-situ vacuum annealing of tantalum oxynitride thin films: Assessments on the structural evolution,* journal: **Applied Surface Science** 2018 **WOS:000425731200003** IF = 4,43
5. **Daniel Cristea,** Luis Cunha, Camelia Gabor, Ioana Ghiuta, Catalin Croitoru, Alexandru Marin, Laura Velicu, Alexandra Besleaga, Vasile Bogdan. *Tantalum Oxynitride Thin Films: Assessment of the Photocatalytic Efficiency and Antimicrobial Capacity*, journal: **Nanomaterials** 2019 **WOS:000464450100003** IF = 3,50
6. V Jinga, AO Mateescu, G Mateescu, LS Craciun, C Ionescu, C Samoila, D Ursutiu, D Munteanu, **D Cristea**. *Mechanical and tribological behaviour of the multilayer dry lubricant coatings with ternary composition from compound materials (Ti_xN_y; $TiB_2/Ti_xB_yN_z$; $WC/W_xC_yN_z$)* journal: **Journal of Optoelectronics and Advanced Materials** 2015 **WOS:000357766600040** IF = 0.39
7. AO Mateescu, G Mateescu, V Jinga, **D Cristea**, C Samoilă, D Ursutiu, D Munteanu. *Physical and technological interpretation of mechanical properties for single and multi-layer films with properties of dry lubricants*, journal: **Journal of Optoelectronics and Advanced Materials** 2015 **WOS:000359967600039** IF = 0.39
8. V Jinga, AO Mateescu, **D Cristea**, G Mateescu, I Burducea, C Ionescu, LS Crăciun, I Ghiută, C Samoilă, D Ursutiu, D Munteanu. *Compositional, morphological and mechanical investigations of monolayer type coatings obtained by standard and reactive magnetron sputtering from Ti, TiB_2 and WC* journal: **Applied Surface Science** 2015 **WOS:000366220500011** IF = 4.43
9. C Lopes, C Gabor, **D Cristea**, R Costa, RP Domingues, MS Rodrigues, J Borges, E Alves, NP Barradas, D Munteanu, F Vaz. *Evolution of the mechanical properties of Ti-based intermetallic thin films doped with different metals to be used as biomedical devices*, journal: **Applied Surface Science** 2020 **WOS:000510846500142** IF = 5.15
10. D Feldiorean, **D Cristea**, M Tierean, C Croitoru, C Gabor, L Jakab-Farkas, L Cunha, NP Barradas, E Alves, V Craciun, A Marin, C Moura, J Leme, M Socol, D Craciun, M Cosnita, D Munteanu. *Deposition temperature influence on the wear behaviour of carbon-based coatings deposited on hardened steel*, journal: **Applied Surface Science** 2019 **WOS:000458482100090** IF = 4.43

A comparison between the minimum criteria specified by the Romanian National Council for Titles, Diplomas and Certificates, and by the Materials Engineering Commission, according to OMENCS Nr. 6129/20.12.2016, Annex 7, and the scores achieved up to the date of the submission of this thesis is presented in the following table.

Nr. crt	Field of activities	Type of activities	Categories and restrictions	Subcategories	Minimum criteria	Achieved	Achieved score
1	Didactic and professional activity	1.1 Books and chapters in specialty books in recognized publishers	1.1.1 Books / chapters as an author	1.1.1.1 International	-	1	**6.25**
				1.1.1.2 National; of which: minimum 2 for Professor, of which 1 first author	2 Books, of which 1 first author	3, 1 as first author	**43.51**
			1.1.2 Books / chapters as an editor	1.1.2.1 International	-	-	-
				1.1.2.2 National	-	-	-
		1.2 Teaching support	1.2.1 Teaching manuals, monographs, including electronic: For Professor at least 2, of which 1 as first author		Minimum 2, of which 1 as first author	2, single author	**45.8**
			1.2.2 Laboratory guides / applications		-	-	-
				Score (A1)	60		95.56
2	Research activity	2.1 Articles in ISI Thomson Reuters-Web of science Core Collection and ISI Proceedings indexed volumes	2.1.1 Minimum 15 articles for Professor, of which minimum 10 in ISI Th.R. (of which min. 5 with impact factor of min. 1, and minimum 5 as main author with F.I. min. 0.5		15 articles for Professor, of which at least 10 in ISI-listed journals, at least 5 as main author with F.I. min 0.5	40 ISI (8 as main author, F.I. >1) 5 ISI Proc.	**782.31**
		2.2 Journal articles and volumes of BDI indexed scientific events			-	14 BDI	**13.37**
		2.3 Patents			-	-	-
			2.4.1 Director / Partner Manager	2.4.1.1 International	Minimum 2	3	**60**

		2.4 Grants / projects won through competition	(Minimum 2 for Professor)	2.4.1.2 National		2	15
			2.4.2 Team member	2.4.2.1 International	-	3	20
				2.4.2.2 National	-	5	22
				Score (A2)	320		912.68
3	Recognition and impact of the activity	3.1 Citations in ISI-listed journals - Web of Science Core Collection and other BDIs	Minimum 30 citations for Professor, in ISI Thomson - Web of Science and SCOPUS	3.1.1 ISI	30 citations	197	522.56
				3.1.2 BDI		3	0.82
		3.2 Invited presentations in the plenary of national and international scientific events			-	-	-
					-	-	-
					-	-	-
		3.3 Member of the editorial boards or scientific committees of scientific journals and events / Reviewer of scientific journals and events		3.3.1 ISI	-	Reviewer for 20 journals	103
				3.3.2 BDI	-	Reviewer for 3 journals	9
				3.3.3 National and international non-indexed	-	-	-
		3.4 Expert evaluation of research projects		3.4.1 International	-	-	-
				3.4.2 National	-	-	-
				Score (A3)	120		635.38
Optional criteria		3.5 Awards		3.5.1 Romanian Academy	-	-	-
				3.5.2 ASAS, AOSR, branch academies and CNCSIS	-	-	-
				3.5.3 International awards	-	-	-

				3.5.4 National awards	-	-	-
		3.6 Member of academies, organizations, prestigious professional associations, national and international, membership in organizations in the field of education and research	3.6.1 Romanian Academy		-	-	-
			3.6.2 ASAS, AOSR, branch academies		-		
			3.6.3 Leading professional associations		-	-	-
					-	-	-
			3.6.4 Professional associations	3.6.4.1 International	-	-	-
				3.6.4.2 National	-	ATTR Member	2
			3.6.5 Education and research organizations	3.6.5.1 Management	-	Vicedean	10
				3.6.5.2 Member	-	Member of the Faculty Council	2
				Optional criteria score	**-**		**14**
				TOTAL SCORE	Minimum required **500**		**Achieved 1657.62**

(B2) Scientific achievements

Chapter 1 - Multifunctional thin solid films: means of development

1.1 Background and overview of reactive magnetron sputtering

One of the most frequently used methods to alter the surface properties of a material is to deposit a thin film or coating on top of the base material, which will significantly improve the functionality of the final part, in terms of its mechanical, electrical, optical, chemical properties, and so on. Hence, it is not surprising that an overwhelming amount of scientific and technical papers is published each year on this topic. Out of the significant number of deposition techniques, which include but are not limited to physical vapour deposition (PVD) techniques, sputter deposition stands out as a reliable, cost-effective, and flexible means of surface properties enhancement. In most cases, sputter deposition uses a magnetically enhanced glow discharge or magnetron discharge to produce the ions which bombard and sputter the cathode material. Apart from the atoms released from the sputtering target, the glow discharge causes the emission of secondary electrons. This electron emission during ion bombardment is essential to sustain the discharge. Indeed, the emitted electrons are accelerated from the target and can ionize gas atoms. The formed ions bombard again the target, thus making the process self-sustainable.

When a reactive gas is added to the discharge, or when the sputtering process is applied to at least two targets from the same chamber simultaneously, it becomes possible to deposit compound materials. This process is called reactive sputter deposition. One of the major problems of the reactive sputter process is its complexity and several fundamental aspects of the process have not been elucidated yet.

Although, at the technical level, sputter deposition is relatively easy to use and to implement at laboratory or industrial scales, it conceals enough challenges to remain scientific interesting. This explains its popularity in the academic world. Reactive magnetron sputtering remains an interesting and often used technique, due to its flexibility and scalability. In the last decades, there has been a vast increase in the range of material types which can be deposited, the complexity of thin films which can be successfully deposited, the ability to deposit precisely controlled heterostructures and the reproducibility of film deposition (Feldiorean, 2019). The key aspect of this success is the understanding in more detail of all relevant processes during the thin film deposition, in order to maximize the level of control. A good understanding of the reactive sputtering process is essential when tailoring the thin film properties.

This chapter contains relevant information regarding the theoretical aspects of sputtering, some information on the role of the applied magnetic field, and key information regarding the reactive

sputtering process, with emphasis on some factors that govern the stability and reproducibility of the reactive magnetron sputtering deposition, namely: the reactivity of the materials, the sputtering yield, the influence of the pumping speed, the effect of the target size, the effects related to using compound or elemental targets, and process control when dealing with more than one reactive gas.

1.1.1 Sputtering

Sputtering is one of the most common processes of deposition of thin layers, with applicability in the automotive industry, electronics industry, aerospace industry, and many more. Materials that would be difficult to deposit by other methods, due to their high melting temperature, can be easily deposited by sputtering. Coatings characterized by high hardness, wear resistance, corrosion resistance, etc. can be obtained by sputtering.

Figure 1.1 shows the simplified diagram of the direct current (DC) sputtering system. The target is represented by a plate made of the material to be deposited and from which a thin layer will be synthesized. Because it is connected to the negative terminal of a DC (or radiofrequency RF) power source, the target is also known as the cathode. The substrate, which is positioned in front of the cathode (target), can be connected to ground, to a positive or negative potential, cooled, additionally heated, or a combination of the above. After vacuuming (pumping down) the deposition chamber, an inert gas, usually argon or a mixture of argon and helium (Rawal, 2010-1), is introduced into the chamber. After a sustained glow discharge occurs, it can be seen later that a thin layer condenses on the substrate.

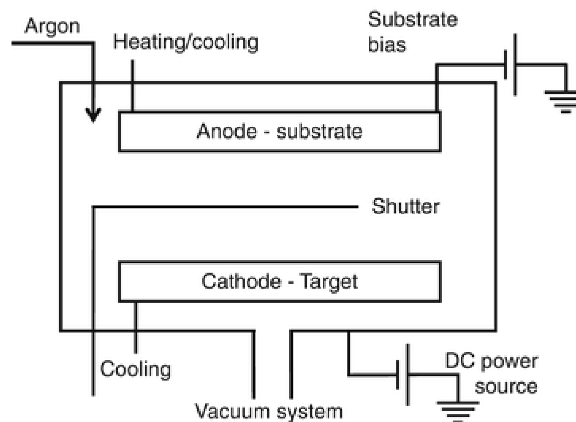

Fig. 1.1 Direct current sputtering system schematic.

Thusly, sputtering represents the detachment of material at the atomic level from a target due to the impact of ions from a glow discharge plasma. In order to be able to understand and control high efficiency sputtering processes, it is necessary to firstly understand the phenomena related to the collision of ions with surfaces. Some of these interactions appear schematically in figure 1.2.

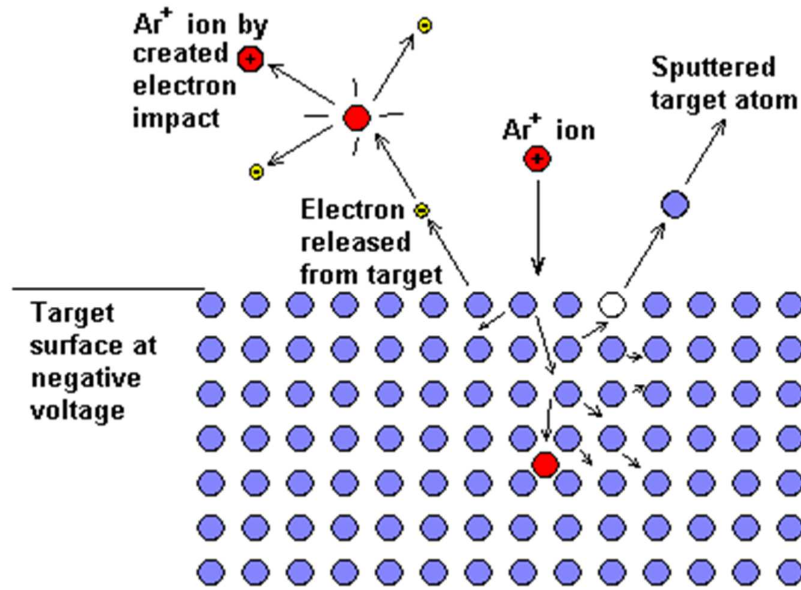

Fig 1.2. Interactions in the case of ion collisions with the surface of a material.

The ion energy must be high enough to cause multiple collisions in the target surface area. The transfer of energy and momentum leads to structural changes in the surface area of the target and to a partial emission of atoms or groups of atoms. The species of interest in the case of sputtering are represented by the sputtered atoms, which will condense on the surface of the substrate thus forming the thin layer, and the emitted electrons, also called secondary electrons. The latter are of particular importance in maintaining a self-sustaining plasma as well as increasing its ionization.

The number of sputtered atoms as function of the number of incident ions is known as the sputtering yield. This parameter depends on the masses and energies of the incident ions, but also on the target atoms and the surface bond energy of the target atoms and/or possible compounds which can be formed at the target surface, a phenomenon generally reffered to as *target poisoning*.

Argon is the gas generally used to obtain a stable, easily ionizable, blue-violet plasma. Argon atoms contain free electrons in the upper atomic layers due to a weak natural ionization. During the discharge process, the Ar atoms are susceptible to the ionization process, a process that changes their initially insulating state to an electrically conductive state. Positive argon ions are attracted to the target surface, and the atoms necessary to obtain the thin layer are released due to the impact of these argon ions. This neutral gas will not react with atomic species in its mechanical movement inside the vacuum chamber, therefore it will not produce unwanted chemical compounds. The occurrence of the sputtering phenomenon depends on the following condition: the energy of the argon ions is higher than the bonding energy between the target atoms.

1.1.2 The influence of the applied magnetic field on the sputtering process

The introduction of a magnetic field in the proximity of the target has the role of intensifying ionization by confining secondary electrons near the target material. These secondary electrons are a by-product resulting from the impact of argon ions. In a planar magnetron the magnetic field is oriented perpendicularly to the direction of the electric field. For this reason, the secondary electrons are forced to describe a helical trajectory near the target. Consequently, the current density increases significantly (the density of ionized argon atoms hitting the target) and the development of the process can be further continued by applying lower voltages.

Fig. 1.3 The erosion track on a rectangular titanium target with gold spots.

By producing a more intense ionization in the proximity of the target, higher deposition rates are thus generated, in the conditions of lower working pressures and maintaining the discharge in this working regime. A lower pressure in the deposition chamber can lead to impurity-free layers. However, these advantages are minimized by a major disadvantage, namely: due to the confinement of secondary electrons in the area of influence of the magnetic field lines, the erosion area of the target follows this positioning of the permanent magnets, as seen in figure 1.3 (Cristea, 2011-1). This means that the use of the target material is limited to a percentage between 25-30 % of the total surface, on the so-called *erosion track*. However, magnetron sputtering deposition chambers have been designed to overcome this disadvantage, by rotating either the target or the permanent magnets, to increase the area of sputtering. Consequently, an erosion zone with a larger area of the total target can be used.

1.2 Reactive magnetron sputtering process control

When adding a reactive gas to the deposition chamber during the sputtering process, the sputtered metal atoms and the reactive gas molecules may chemically react, leading to the formation of compounds. Consequently, one can obtain oxides, nitrides, borides, carbides, oxynitrides, oxycarbides, etc. To distinguish inert argon sputtering from the process where reactive gases are added, the latter process is commonly referred to as a *reactive sputtering process*. At first glance, one may believe that reactive sputtering processes may be as easy to carry out as the simple and straightforward inert sputtering processes, where only argon is employed. Unfortunately, this is not the case. The addition of the reactive gas significantly changes the behaviour of the sputtering process. Both deposition rate as well as the composition of the film will be heavily influenced by the flow of the reactive gas (Berg, 2005).

Figure 1.4 represents a schematic of a typical variation of the sputter erosion rate as function of the flow of the reactive gas. One can observe that the curve takes different pathways when the reactive gas flow is increased, versus when the reactive gas flow is decreased (this is indicated by the arrows in the figure). As can be seen, this curve shows a hysteresis behaviour. Increasing the reactive gas flow slightly beyond the processing point A in the figure will result in a sudden decrease in the sputter erosion rate, down to point B in the graph. Decreasing the reactive gas flow from high values down to just below point C will result in a sudden increase in the sputter erosion rate, from C up to D in the figure. It is these avalanche-like transitions that primarily make process control rather complicated for reactive sputtering processes.

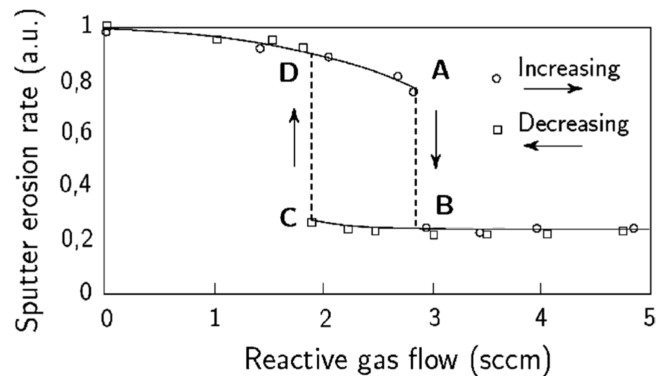

Fig. 1.4. Typical experimental curve for a reactive sputtering process (Depla, 2008)

It is generally agreed upon that the sputtering yield of elemental targets is significantly higher than the sputtering yield of their respective compounds. This is one of the reasons for the complex behaviour of the processing curves. Originally (with zero flow of reactive gas) the sputter erosion rate from the target is determined by the sputtering yield of the pure metal. A slight increase of the flow of reactive gas will not significantly change the composition of the target surface, consequently the deposition

rate will not significantly change. Sputtered atoms, however, will be deposited at a far larger substrate surface than the eroded target surface area. This results in a higher fraction of compound at the deposited substrate areas. This means that almost all of the reactive gas is used up to form the compound at the substrate. Consequently, the target is said to operate in metallic mode. The fact that almost all of the reactive gas is used to form the compound layer on the substrate leads to the phenomenon consisting in almost no partial pressure being generated in the processing chamber.

The compound is also formed on the target, but due to the relatively high sputter erosion rate, less compound will be formed at the target than at the substrate. This explains the slow decrease of the erosion rate up to position A from figure 1.4. At this position, conditions are generated that force the partial pressure to increase dramatically to position B. This new reactive gas partial pressure is high enough to completely form the compound also on the whole target surface. From this position, the target is said to work in the poisoned mode. It has been “poisoned” by the reactive gas and a layer of compound has been formed on the target surface. As a consequence, the deposition rate will be determined by the low sputtering yield value of the compound, instead of the much larger sputtering yield value for the metallic target. This explains the drastic drop in deposition rate at position A. The reactive gas that is not used up to form the compound will contribute to building up of the partial pressure. This will be valid until the nitrogen partial pressure will not be large enough to completely form the compound on the target. From this position (C), the target converts to being substantially metallic again.

There are several factors that significantly affect the reactive sputtering deposition process. Brief theoretical information will be presented for some of these factors, as follows:

- **Target reactivity**. The reactivity between the gas and the target metal is clearly important. The hysteresis should be less pronounced for low reactivity processes. Some reactive gas/target material combinations could be absolutely free of the hysteresis effect. The reactivity between the target and the reactive gas was obviously considered when depositing the samples presented in the following chapters, especially when depositing with two reactive gases.
- **Sputtering yield**. The sputtering yield value for the metallic target is typically significantly higher than the sputtering yield value for the corresponding compound. The hysteresis is very sensitive to the ratio between these two values. It must be understood that reactivity and the ratio between the sputtering yields are fundamental material properties. It is therefore not possible to freely choose these values in a specific processing condition.
- **Pumping speed**. The pumping speed of the vacuum system may be controlled externally and set to a desired value. The higher the value of the pumping speed, the hysteresis will be less pronounced. For a pumping speed value high enough, the hysteresis disappears (Kadlec, 1987). This is often

used in smaller lab systems where sufficient pumping speed may be achieved. In large-sized industrial systems, however, the required pumping speed value for hysteresis-free operation is often unattainably high.

- **Target size.** In a specific system it may be possible to select the size of the target. The hysteresis will be less pronounced for small target areas. This behaviour is generally valid and is not caused by the fact that a smaller target will be exposed to a higher argon sputtering flux for identical total target current. Altering the target current for the small target does not change the shape of the processing curve.
- **Mixed targets**. It has been found that some target mixtures may affect the reactive sputtering process in such a way that no hysteresis will appear (Hoshi, 2004). It has been suggested to fabricate a mixture of a metal and its corresponding metal compound. The metal compound is the one expected to be formed by the metal and the reactive gas in the process. Having different concentrations of compound in such a target may strongly affect the processing curves. The deposition rate depends on the actual composition of the target, but it is always higher than from the corresponding pure metal target operated in compound mode.
- **Two reactive gases**. Oxygen and nitrogen may be added to the deposition chamber, to form an oxynitride of some target material. It is likely that one of the gases may be more reactive than the other. Normally oxides are formed more easily than nitrides. Due to this difference in reactivity, an additional reaction must be considered. With a certain probability, the most reactive gas may break up the metal compound formed by the less reactive gas and replace this by a metal compound based on the more reactive gas atoms.
- **Reactive co-sputtering.** In certain applications, it may be favourable to use two separate targets as sputtering sources. This is convenient when studying properties of films with different compositions of two materials (Lopes, 2020). Carrying out reactive sputtering from two metal targets, however, increases significantly the complexity of the process (Martin, 1999). The main reason for this is that both target surfaces will be exposed to identical partial pressure of the reactive gas. This implies that two metals having quite different reactivity to the reactive gas will not form the stoichiometric compound at the same partial pressure value.
- **Ion implantation.** In a self-sustained sputtering plasma, argon ions are generated by electron impact ionization. Upon arrival at the target, a 500 eV argon ion may be implanted some 30–50 Å. The effect of this implantation, however, is assumed not to influence the target material at the penetration depth. In reactive sputtering, however, also the reactive gas may be ionized. These ions may also be accelerated by the electric field and implanted into the target. These implanted reactive gas ions will easily react with the target metal atoms and form compound molecules. Due to this effect, there will always be some compound formation in the whole surface region reaching into

the ion penetration depth. This effect will increase the response time for a reactive sputtering process when shifting from one processing point to another.

Motivation of the thesis subject.

The last two decades have seen the gradual rise at a steady but consistent pace of scientific publications relates to reactive sputtering, as shown in the following images. It could be concluded that, even if the subject of surface science and engineering could be considered a niche topic, especially when one talks about the ubiquity of the materials science domain, it also has an important role in the advancement of materials science.

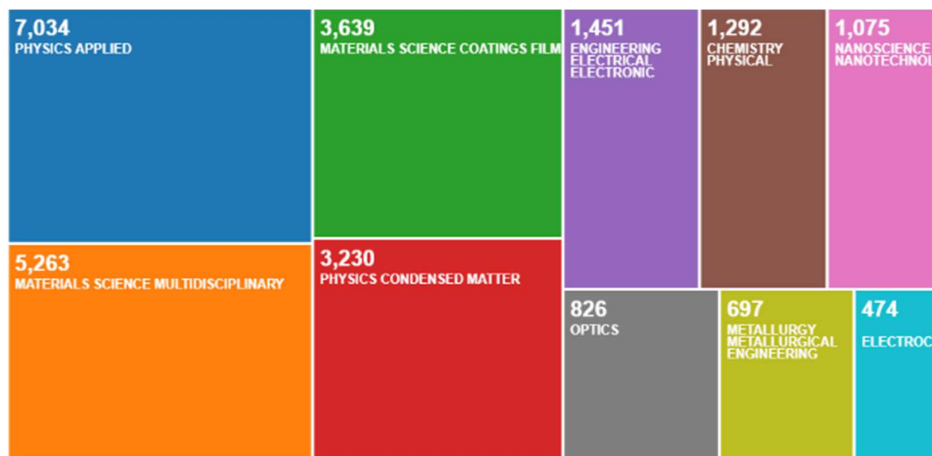

Fig. 1.5. Number of publications on the topic of reactive sputtering, separated by field (accessed Dec 2020).

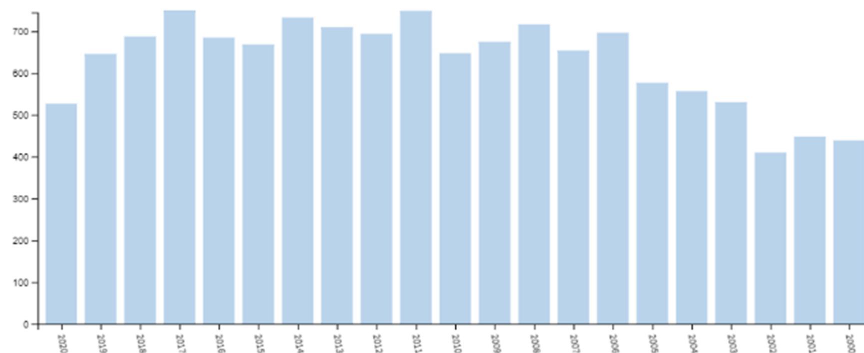

Fig. 1.6. Number of publications on the topic of reactive sputtering, per year, for the last two decades.

The results presented in this thesis are meant to highlight the importance of the fundamental research in the field of reactive sputtering, considering that the obtained coatings can be applied in several industrial sectors, from automotive to optics, from microelectronics to aerospace, from biomaterials to renewable energies, and many more. Secondly, the motivation behind this habilitation thesis rises from the requirements related to academic career advancement.

Chapter 2 - Transition metal oxynitride thin films

2.1 Motivation.

Transition metal oxynitride-like coatings are a group of ceramic materials which are characterized by the possibility of changing the ratio between nitrogen and oxygen, which leads to a variety of properties: optical properties, especially colors in a wide range, which can be used as decorative coatings; electrical properties, which can extend from the conductive area, characteristic of metals to the insulating area, characteristic of oxides; mechanical properties, variable hardness, all due to changes in the N_2 / O_2 ratio (Cristea, 2011-2; Cristea, 2014).

Oxynitride coatings based on transition metals (MeO_xN_y) can potentially benefit from the properties of the respective oxides or nitrides of the particular metal, or can be characterized by entirely new properties, distinct from those of the oxides or nitrides.

My research was aimed towards studying tantalum oxynitride coatings, therefor continuing the ideas from the Ph.D. program, with emphasis on the applications which showed greater potential. The properties of this type of oxynitride are dependent on the possible structures encountered, namely structures of pure tantalum, oxides, nitrides and tantalum oxynitrides (Cristea, 2013-1). Consequently, some information on some physico-chemical characteristics, methods of deposition and applications of pure tantalum layers, tantalum oxides, tantalum nitrides, and tantalum oxynitrides will be briefly presented.

2.1.1 Pure tantalum.

The element Tantalum is discovered in Sweden by A.G. Ekeberg in 1802. The concentration of tantalum in the earth's crust is 1.7 ppm, comparable to that of As (1.8 ppm) and that of Ge (1.5 ppm). Usually Ta is found accompanied by Nb (Niobium) in the mineral of the form $(Fe,Mn)M_2O_6$ where M represents Ta and/or Nb, a mineral called columbite or tantalite, depending on the preponderance of the main component metal. The corrosion resistance of Ta at normal temperatures (due to the presence of an extremely tenacious oxide layer) makes this element suited for coating various surfaces in chemical plants. Due to its inactivity with the fluids of the human body, this metal is ideal to be used for prostheses, bone repair elements, etc. Furthermore, it is used extensively in the electronics industry in the manufacture of capacitors, where the oxide layer is an effective insulator, and as a filament for incandescent lamps. Tantalum was used to replace carbon filaments until the introduction of tungsten (Greenwood, 1997). The applicability of tantalum-based compounds in microelectronics has expanded, for example in resistive elements due to their long-term stability. In addition, Ta layers are used as diffusion barriers between metallic Cu layers and Si-based substrates, as an adhesion promoter in the case of thin platinum layers, with applicability at high temperatures, and as surface coatings which

require a high resistance to wear and corrosion (Grosser, 2009). Due to its high melting temperature (2980 °C (Greenwood, 1997)), sputtering is used as the main technique for the deposition of thin layers of tantalum, but there are reports in the literature related to deposition by electron beam evaporation (Jankowski, 2007) or by electrochemical synthesis from molten salt baths (Lee, 1999).

The crystallographic structures of tantalum depend mainly on the temperature of the synthesis process as well as on the nature of the substrate on which the deposition is made. Thus, there are two structures, namely, the stable phase α-Ta in the base centered cubic form, respectively the tetragonal metastable phase β-Ta. Usually, the metastable phase is encountered when there are no external influences that can lead to the formation of the stable phase α-Ta, such as high substrate temperature or the presence of intermediate layers that promote germination, for example substrates of aluminum, titanium or titanium nitride. The stable α-Ta phase can also occur after annealing treatments on the β-Ta structure, at temperatures above 700 °C (Feinstein, 1974; Liu, 2001).

2.1.2 Tantalum oxide coatings.

Results concerning a wide variety of tantalum oxides can be currently found in the literature. One of the most common variants is Ta_2O_5 tantalum pentoxide. It is extensively studied due to its high dielectric constant, high refractive index and good thermal and chemical stability, properties that make it a strong candidate for microelectronics applications. Other applications of tantalum pentoxide include: anti-reflection coatings on the surface of solar cells, optical transmission paths (optical fibers), insulating material in devices requiring high permittivity (Jagadeesh, 2008), as well as in the construction of metal-oxide-semiconductor field effect transistors (MOSFET) (Wei, 2011). Tantalum pentoxide can also be used as protective coatings, as components of storage capacitors in HDRAM (High-density random-access memory) units. Related to the example presented above, there are a number of disadvantages that should be overcome, the most important being related to the fact that at temperatures above 600 °C, tantalum pentoxide crystallizes, with negative effects on its performance (Jagadeesh, 2008). Tantalum pentoxide is also a potentially biocompatible material due to its high chemical stability (Yang, 2007). Tantalum pentoxide could be used as a catalytic material for wastewater treatment and for the decomposition of water into components, to obtain hydrogen as a future fuel (Jagadeesh, 2011).

Several methods of preparation of tantalum oxide layers can be employed: anodizing or thermal oxidation (Atanassova, 1998), ion beam deposition (Lee, 2005; Yoon, 2005), chemical vapor deposition (Ionescu, 2009), electron beam evaporation (Todorova, 2006), pulsed laser deposition PLD (Atanassova, 2006), reactive DC magnetron sputtering (Hermann, 1981), reactive RF sputtering (Jagadeesh, 2010; Ono, 2006).

Even though several compositions of tantalum oxide can be found in the literature, the only stable phase seems to be tantalum pentoxide. It has been observed that if the preparation of this material takes place at temperatures below 600-650 °C, its structure is amorphous. At temperatures above these values, tantalum pentoxide crystallizes in two main phases: orthorhombic and hexagonal. The orthorhombic structure can be divided into two forms, due to a reversible phase transformation which occurs at 1360 °C. These structural changes, which occur mainly due to the processing temperature, influence the properties of the thin films, regardless of the deposition method.

2.1.3 Tantalum nitride coatings.

Transition metal nitrides are known for their remarkable properties which include high hardness, high temperature stability, chemical stability, etc. These nitrides can be used as wear-resistant coatings, protective coatings, structural elements in integrated circuits, and others. Tantalum nitride can be used as thin-layer resistors (Sun, 1993), diffusion barriers (Kim, 2005), wear-resistant hard layers (Aryasomayajula, 2006; Westergard, 1997), and in the manufacture of high-speed printheads (Shibata, 1976).

The properties of tantalum nitride thin films depend on the microstructure and morphology of the materials. A search in the literature regarding the reported tantalum nitride phases resulted in the following list: $TaN_{0.05}$, Ta_2N, $TaN_{0.8-0.9}$, and TaN (Swisher, 1972), ε-TaN, θ-TaN and δ-TaN (Liu, 2010), Ta_2N, Ta_5N_6, and Ta_3N_5 (Stampfl, 2005), among others. The electronic properties range from good conductor (Ta_2N), to more resistive phases (Ta_5N_6) to insulating phases (Ta_3N_5) (Stampfl, 2005).

2.1.4 Tantalum oxynitride coatings

Due to the demands from the industry for thin layers with dielectric character and thickness in the nano range, attempts are currently made to replace silicon dioxide with other materials with improved properties. TaO_xN_y type coatings are promising alternatives for this particular application. The behavior of these layers in metal-insulator-metal (MIM - Al / TaON / Ru / Si) and metal-insulator-semiconductor (MIS - Al / TaON / Si) cells was studied (Kato, 2009). In this particular report, the deposition was performed using the ECR Plasma Deposition technique (Electron Cyclotron Resonance), by controlling the oxygen flow while the nitrogen flow was maintained at a fixed value. TaO_xN_y layers with a dielectric constant of more than 30 were obtained. However, as the dielectric constant increases, the loss currents also increase. Furthermore, the reliability of integrated circuits with capacitors based on TaO_xN_y, was reported to be implemented, among others, in mobile telephony devices (Verchiani, 2008). The main cause of failure of these MIM (metal-insulator-metal) type circuits is represented by electrostatic discharges.

Another potential application of tantalum oxynitrides is as a photocatalytic material. TaO_xN_y nanoparticles can be obtained following this protocol (Gao, 2011): an amount of $TaCl_5$ is added to a solution of methanol, then in the same solution calcium carbonate is dissolved, resulting in the release of CO_2. A variable amount of urea is then added, and the solution is left at room temperature to turn into a gel. The gel is transferred to an oven and kept under N_2 atmosphere, followed by calcination at 775 °C. The powder is then treated with HCl to remove traces of Ca. The TaO_xN_y particles thus obtained have potential applications, as photocatalytic material, as pigments, or for the manufacture of optoelectronic devices.

A theoretical study on $TaO_{1-x}N_{1+x}$ type materials (Al-Aqtash, 2013) concludes that the band gap energy decreases from 2.3 eV to 1.7 eV as the N/O ratio increases from 3/5 to 5/3, which translates into increased absorption in the visible spectrum, the material thus becoming suitable for photocatalysis in the visible field. In addition to these observations, for good performance in the field of (electro) catalysis, the stoichiometry and homogeneity of this material must be strictly controlled (Abbondanza, 2012). Furthermore, TaO_xN_y coatings obtained by sputtering elemental Ta, followed by oxidation and nitriding of the Ta layer, exhibit increased potential for photocatalysis in the visible spectrum, which was demonstrated through the photodegradation of methylene blue (Hsieh, 2011).

Analyzing the information presented in the previous paragraphs, it can be concluded that tantalum oxynitride type (TaO_xN_y) coatings can benefit from the properties of the extreme structures, namely the oxides and the nitrides of the component metal, due to the possibility of adjusting the oxygen/nitrogen ratio, thus conffering to these materials a multifunctional character, as function of their properties.

2.2 Sample preparation.

Thin layers based on tantalum, either oxide, nitride or oxynitride-type, are characterized by remarkable properties, useful in various fields, from microelectronics, to protective coatings, to optical coatings, to biocompatible coatings, etc.

The main objective of the experimental work conducted after the completion of the Ph.D. program was to isolate and improve certain key configurations of samples from the TaO_xN_y class, to characterize these layers in terms of structural development, morphology, and key promising properties, to identify correlations between the deposition parameters and these properties, focused on 3 main potential applications:

1. Material with special electrical properties;
2. Photocatalytic material;
3. Biocompatible material.

The TaO_xN_y type coatings were deposited by reactive magnetron sputtering, using a mixture of reactive gases whose composition remained constant ($O_2 + N_2$ = 15% + 85%), while varying the total flow of reactive gas mixture introduced into the deposition chamber. A high purity tantalum target was used for all sets of depositions.

The experimental program involved the deposition and analysis of 3 sets of samples, as follows:

1. Series A, of 5 depositions, with varying reactive gas mixture flow rates, and a negative potential of -50V on the substrate holder.
2. Series B, of 9 depositions, with varying reactive gas mixture flow rates, and the substrate holder not connected to the potential (non-biased = GND).
3. Series C, of 8 depositions. The conditions used for this series of samples were chosen in order to complete the first two series, thus using reactive gas flow values as well as negative potential values not used in the case of Series A and Series B.

To determine the different characteristics of the coatings, the following types of substrates were prepared:

a. Glass slides, for determining the electrical resistivity, respectively the photocatalytic behavior.
b. Silicon wafers (100), for the determination of structure by X-ray diffraction, chemical composition by RBS (Rutherford backscattering spectrometry), X-Ray Reflectivity (XRR), transmission electron microscopy (TEM), scanning electron microscopy (SEM).
c. High-speed steel (AISI M2) for determining the dielectric characteristics by making a flat capacitor, where the deposited layer represents the dielectric (metal-insulator-metal = HSS / TaON / gold pads, sputter deposited).

The substrates were cut to the appropriate size (glass and silicon), and the steel ones were subjected to a sanding / polishing treatment, in order to obtain a surface with minimal roughness. An emulsion containing diamond particles with an average grain size of 3μm was used to finish the surfaces. Prior to introduction into the deposition system, the samples were cleaned with ethanol. Before introducing the reactive gas mixture, a plasma cleaning process (ion etching) was applied for a period of 500s.

A laboratory PVD deposition system was used for the deposition of tantalum oxynitride type thin layers, composed of: deposition chamber, antechamber, a vacuum system, a gas flow control system, an electrical system and a control unit. The chamber is cylindrical, with an inside diameter of approximately 0.4 m and a volume of approximately 0.14 m^3. A single type II unbalanced magnetron was used for the depositions. The target is positioned in front of a water-cooled magnetron and has the dimensions of 200 × 100 × 6 mm. The sample holder is positioned in the center of the deposition chamber and can operate both statically and in rotation mode, and can also be biased (connected to a

negative potential). The vacuum system consists of two rotary pumps (Trivac D8B and Balzers DUO 012A), necessary to obtain the preliminary vacuum of approximately 0.5Pa, the final vacuum being obtained due to two turbomolecular pumps (Balzers TPU200 and Alcatel PTM5400) connected in parallel. The pressure in the deposition chamber was monitored by two manometers, one for the preliminary vacuum and one for the final vacuum. The power sources consist of two Hüttinger direct current (DC) generators of 2.5 and 7.5 kW, respectively.

2.3 Results and discussions.

2.3.1. Chemical composition, chemical states, structural development.

Chemical composition. The chemical composition, in atomic percentages, for the three series of samples is shown in Table 2.1. The samples are ordered primarily according to the flow rate of the reactive gas mixture used during the deposition and secondly according to the bias voltage applied to the substrate holder. Table 1 contains also the thickness of the coatings, obtained by ball cratering, and certain ratios between the constituent elements.

Rutherford Backscattering Spectrometry (RBS) measurements were performed using $^{1}H^{+}$ with an energy of 2.25 MeV and an incidence angle of 0°, in the presence of 3 detectors, one standard at an angular position of 140 °, and two pin-diode detectors positioned symmetrically to each other, both at an angular position of 165° (detector 3 on the same side as standard detector 2).

The evolution of non-metallic components in relation to the metal content of the film is shown in Figure 2.1, depending on the flow rate of reactive gases. As expected, increasing the flow of reactive gases has the effect of increasing the non-metal fraction in the films. Looking at the graph in figure 2.1 we can also see that the ratio (N + O)/Ta reaches or even exceeds the value of 2.5, characteristic of certain compounds, such as α-Ta_2O_5 or β-Ta_2O_5, once the flow of 30 sccm is exceeded. In the case of samples obtained with a flow rate of 30 sccm, those obtained with the substrate connected to the negative potential have the ratio (N + O)/Ta = 2.84 (bias potential = -50V), respectively 2.57 (bias potential = -100V), while samples obtained with a flow rate of 35 sccm the non-metal/metal ratio is equal to 2.84, for the sample obtained with the grounded substrate, respectively 2.70 for the sample with -50V bias potential. One can also observe the effect of the substrate bias in terms of the content of non-metallic elements in the film. As a trend, with the exception of the samples obtained with the highest flow of reactive gases (35 sccm), the non-metal content of the layer is always higher, for samples obtained with similar flow of reactive gas, in the case of coatings obtained with the polarized substrate. This observation can be explained by taking into account the effect of polarizing the substrate: argon ions in the plasma are also attracted towards the surface of the samples, not only to the target. This ion bombardment seems to promote the appearance of bonds between non-metallic elements and tantalum.

Table 2.1 Deposition conditions, thickness and chemical composition of TaO_xN_y type layers:

- U_{subst} - bias voltage;
- F (N_2 + O_2) - flow rate of the reactive gas mixture;
- t_f - the thickness of the layers.

Sample	$F(N_2+O_2)$ (sccm)	$U_{subst.}$ (V)	t_f (μm)	Ta [at%]	N [at%]	O [at%]	(N+O)/Ta	N/Ta	O/Ta
B1	2.5	GND	1.15 ± 0.10	90	7	3	0.11	0.07	0.03
C1		-50V	0.91±0.10	76	24	0	0.31	0.31	0
A1	4.5	-50	1.21 ± 0.06	62	28	10	0.61	0.45	0.16
B2	5	GND	1.26 ± 0.07	68	18	14	0.47	0.26	0.20
C2	7.5	GND	0.70±0.11	54	37	9	0.85	0.68	0.16
C3		-50V	0.89±0.06	50	41	9	1.00	0.82	0.18
B3	10	GND	1.30 ± 0.08	50	28	22	1.00	0.56	0.44
A2		-50V	0.98 ± 0.05	43	33	24	1.32	0.76	0.55
B4	15	GND	1.34 ± 0.09	49	27	24	1.04	0.55	0.48
A3		-50V	1.04 ± 0.05	39	35	26	1.56	0.89	0.66
B5	20	GND	1.37 ± 0.08	47	22	31	1.12	0.46	0.65
B6	22.5	GND	1.31 ± 0.10	43	18	39	1.32	0.41	0.90
B7	25	GND	1.21 ± 0.04	43	17	40	1.32	0.39	0.93
A4		-50V	1.04 ± 0.05	35	35	30	1.85	1.00	0.85
C4	30	GND	1.01±0.09	33	21	46	2.03	0.63	1.39
C5		-50V	0.73±0.05	26	14	60	2.84	0.53	2.30
C6		-100V	1.26±0.08	28	14	58	2.57	0.50	2.07
C7	35	GND	0.14±0.02	26	8	66	2.84	0.30	2.53
C8		-50V	0.11±0.02	27	9	64	2.70	0.33	2.37

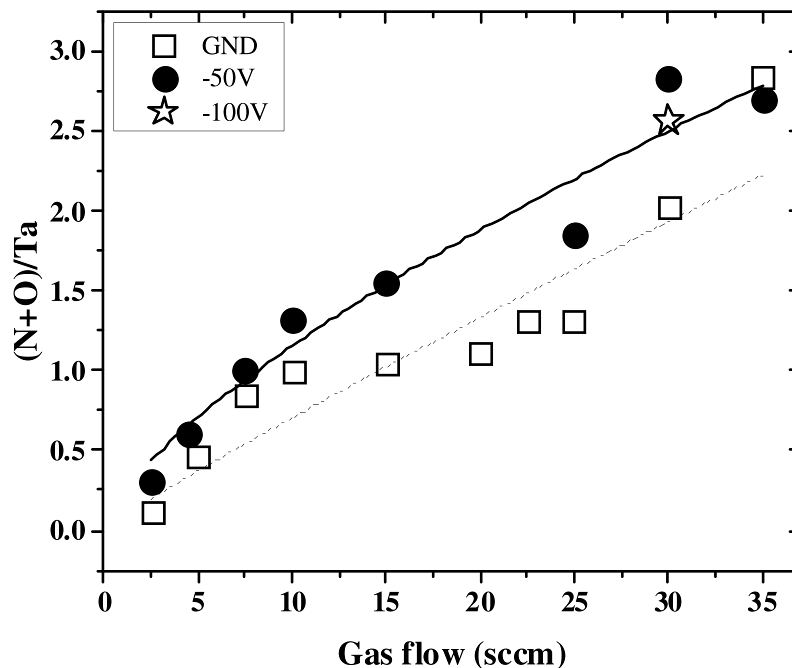

Fig. 2.1 Variation of the non-metallic content in the layers, depending on the flow of reactive gases.

<u>Chemical states.</u> X-ray Photoelectron Spectroscopy (XPS) measurements were performed on selected silicon substrate samples (the coatings deposited with the grounded substrate holder), with an Escalab 250 system (Thermo Scientific) equipped with a monochromated Al K_{α} (1486.6 eV) X-ray source and a 10^{-8} Pa base pressure in the analysis chamber. The acquired spectra were calibrated with respect to the C1s line of surface adventitious carbon at 284.8 eV. An electron flood gun was used to compensate for the charging effect in insulating samples. A gentle removal of the contaminants confined on the outermost surface layers of the thin films was performed prior to the XPS surface chemical analysis. An Ar^{+} ion gun operated with a low energy ion beam of 1.0 keV was rastered over a (3 × 3) mm^2 area and a 0.5 min sputter time was used for surface etching.

No impurities or contaminants were detected in the samples analyzed by XPS. The relative atomic concentration of the films, as a function of the partial pressure of the reactive gases ($P(N_2 + O_2)$), is depicted in figure 2.2. The equivalency between the reactive gas mixture flow and the partial pressure for the samples analyzed by XPS can be observed in Table 2.2.

Table 2.2. Equivalency between the reactive gas mixture flow and the partial pressure:

Reactive gas flow (sccm)	Partial pressure N_2+O_2 (Pa)
2.5	0.02
5	0.04
10	0.08
15	0.13
20	0.17
22.5	0.20
25	0.22
30	0.24

XPS was used to access the bonding state of atoms across the surface layers and, after quantitative analysis, to find the elements' relative concentration and corresponding chemical states. The spectra revealed the characteristic XPS transitions of tantalum, oxygen, and nitrogen, thus proving the chemical interaction between metal atoms and the reactive gas mixture from the deposition chamber.

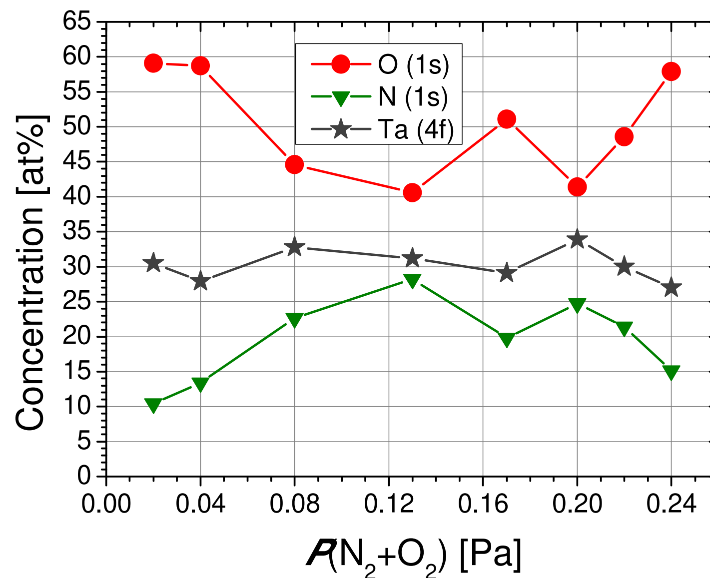

Fig. 2.2. Atomic concentration of the films, as function of the reactive mixture partial pressure, obtained from O (1s), N (1s) and Ta (4f) of XPS spectra.

To probe the surface chemistry of the films, O1s, N1s and Ta4f XPS high resolution spectra were acquired. The surface chemical response of tantalum, as a function of nitrogen/oxygen flow ratio, is portrayed in figure 2.3. The tantalum chemical states were assessed after curve-fitting of the complex Ta4f envelops. Figure 2.2 summarizes the relative chemical concentrations. It is very important to mention that the data in the literature and databases are spread over a rather wide binding energy range.

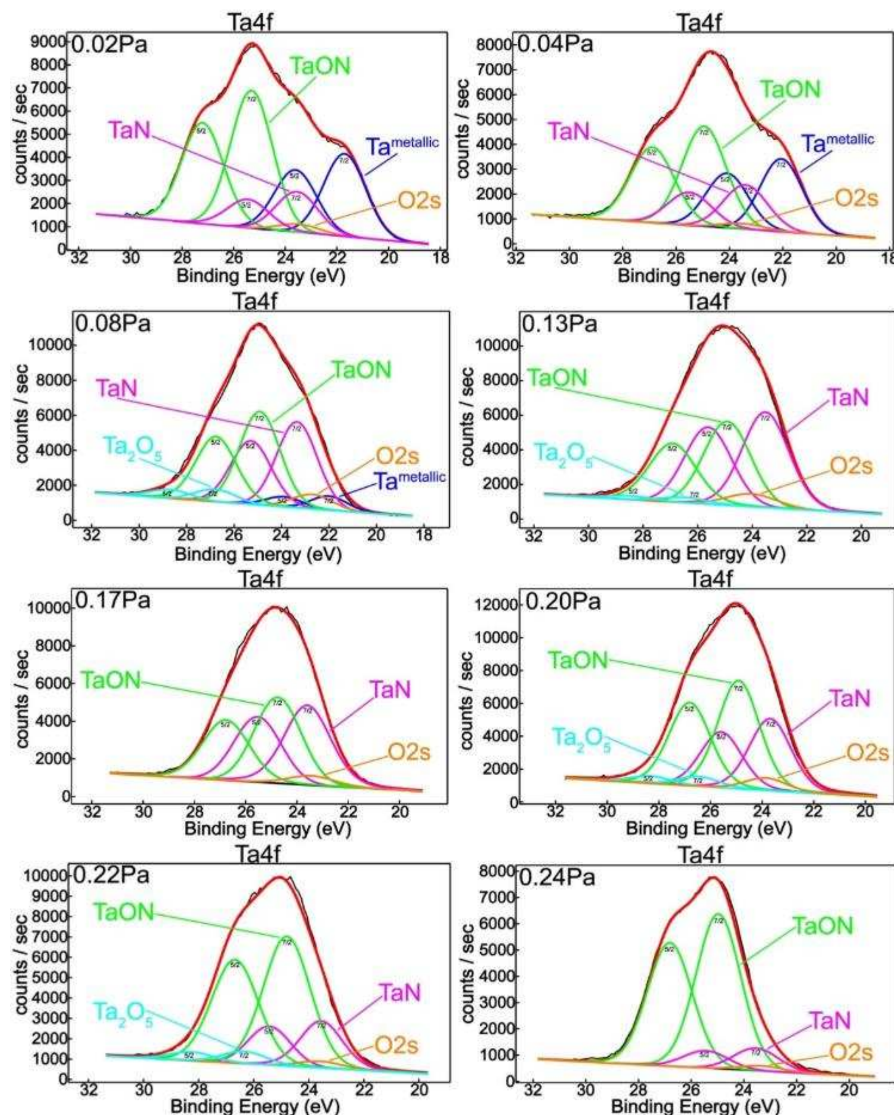

Fig. 2.3. XPS deconvoluted Ta4f spectrum for samples obtained with different reactive gas partial pressures.

The feature located at 22.0 eV can be ascribed to metallic Ta (Ishihara, 2008; Yamajo, 2019; Rumble, 1992; Arranz, 2000; Chun, 2003), while the peak at 23.5 eV corresponds to tantalum nitride (Ishihara, 2008; Rumble, 1992; Arranz, 2000; Zhang, 1997; Shi, 2005; Lamour, 2008). The photoelectron binding energy peaks located at 25.0 eV and 26.5 eV can be attributed to tantalum oxynitride (Lamour, 2008;

Maeda, 2008) and to Ta^{5+} oxidation state correspondent to the tantalum pentoxide Ta_2O_5, respectively (Yamajo, 2019; Rumble, 1992; Chun, 2003; Zhang, 1997; Hara, 2003). Chun and Ishihara reported 25.8 eV for the binding energy corresponding to tantalum oxynitride bonding, closely in agreement with previous findings in the literature (Ishihara, 2008; Chun, 2003).

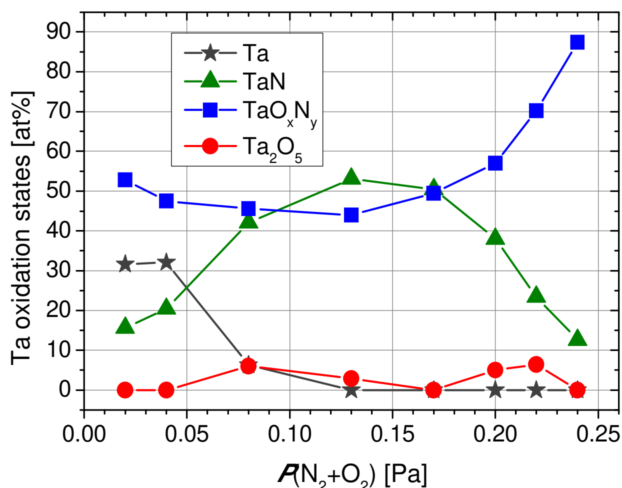

Fig. 2.4. Tantalum chemical states relative concentrations based on the fitting process of Ta 4f XPS peak.

From figure 2.4 one can notice a dramatic decrease of metallic Ta with the increase of the reactive gas mixture partial pressure, from ~32% to ~6% when $P(N_2+O_2)$ increases from 0.02 and 0.08 Pa, and completely vanishes for higher values of $P(N_2+O_2)$. This is a consequence of increasing nitrogen relative concentration (Figure 2.2) in association with the corresponding increase of tantalum nitride content (Figure 2.3). Although the oxygen decreasing trend was accompanied by decreasing oxynitride contribution, tantalum presents a fully oxidized state for 0.13 Pa and higher reactive gas partial pressures.

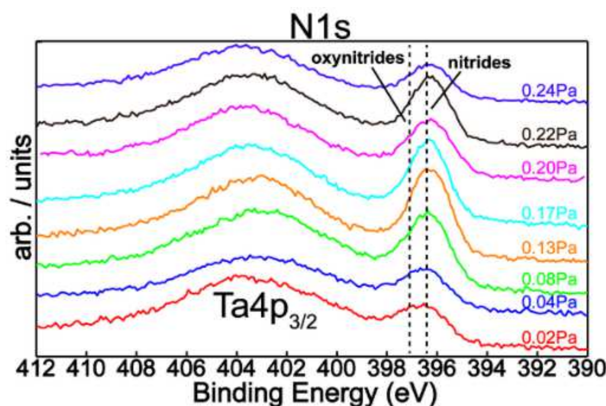

Fig. 2.5. N1s XPS superimposed spectra for different reactive gas partial pressures.

A completely opposite chemical behavior was observed in the case of films prepared with high partial pressure conditions. Thus, a decreasing tendency of nitride contribution followed by an increase of oxynitride feature was established by increasing $P(N_2+O_2)$ from 0.17 to 0.24 Pa, in good agreement with element relative concentrations (Figure 2.2). A peculiar chemical behavior of Ta_2O_5 can be explained by the occurrence of a threshold pressure value at 0.13 Pa in which diffusion/segregation processes take place that have an influence on the surface chemistry of deposited layers.

Figure 2.5 shows the N1s superimposed core level spectra for all mixed reactive gas atmospheres indicating a similar chemical behavior with small quantitative differences regarding the nitrogen content. In addition, spectral deconvolution of N1s (Figure. 2.6) of the samples produced with $P(N_2+O_2)$ = 0.02 Pa and $P(N_2+O_2)$ = 0.24 Pa reinforce the assessment of metallic nitride and oxynitride films formation, in good agreement with tantalum chemistry (Figure 2.3). Therefore, the observed features in the nitrogen spectra are located at 396.5 eV and 397.2 eV, respectively, the former being ascribed to metal nitrides (Ishihara, 2008, Rumble, 1992; Arranz, 2000; Chun, 2003; Zhang, 1997) and the latter to metal oxynitrides (Chun, 2003).

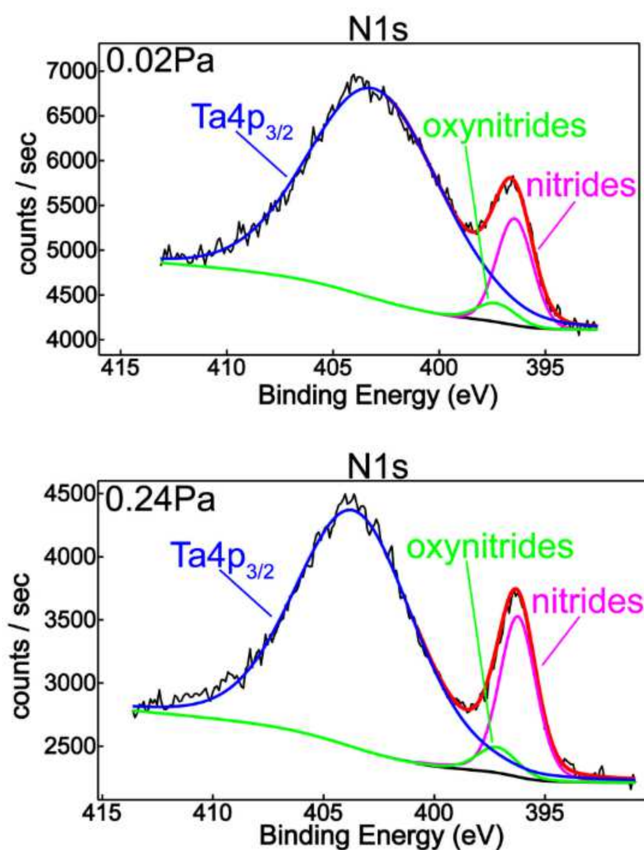

Fig. 2.6. XPS deconvoluted N1s spectrum for samples obtained with different reactive gas mixture partial pressures: a) 0.02Pa; b) 0.24Pa.

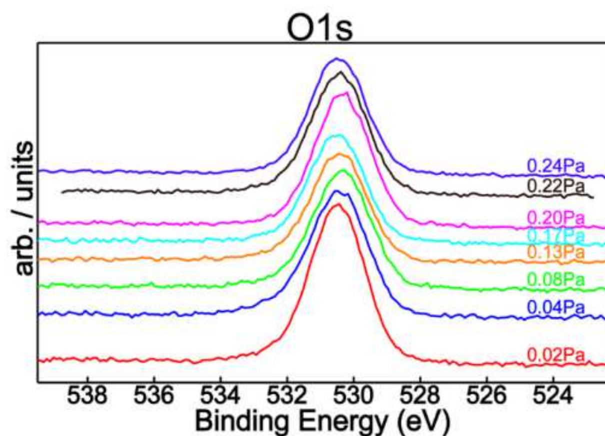

Fig. 2.7. O1s XPS superimposed spectra for different reactive gas partial pressures.

Structural evolution. The influence of the substrate polarization on the structural evolution can be observed by juxtaposing the diffractograms, obtained after XRD analysis, of all samples studied in this experimental program (Series A, Series B, Series C), in figure 2.8, for the crystalline samples, respectively in figure 2.9, for the amorphous samples. X-ray diffraction (XRD) patterns were obtained for the samples deposited onto Si substrates, using for part of the samples a Philips diffractometer (Cu Kα radiation) in a Bragg-Brentano geometry configuration, while for the rest of the samples, measurements were performed using a Brucker D8 diffractometer equipped with a copper electrode (λ = 0.154 nm), as well in Bragg-Brentano geometry, at a working voltage of 40 kV and 40 mA current, respectively. The resulting profiles were fitted with a Gaussian function, and the peak positions were compared to the JCPDS database files for Ta,Ta_xO_y, Ta_xN_y and $Ta_xO_yN_z$ type of compounds.

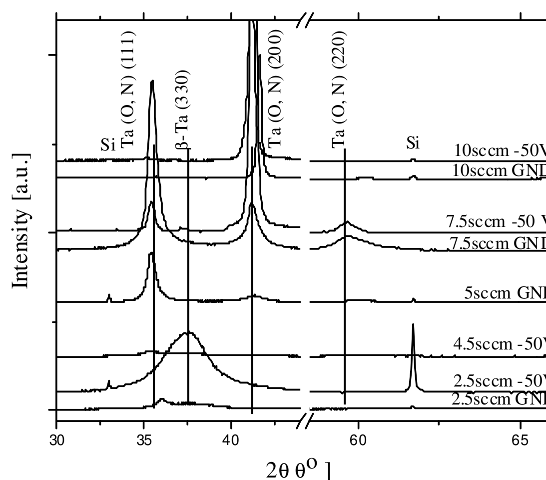

Fig. 2.8. Diffractograms of crystalline samples from Series A, Series B, and Series C, respectively, ordered according to the flow rate of the reactive gas mixture, respectively to the polarization voltage.

The first observation that can be made is that for flows higher than 15 sccm, the samples are amorphous, regardless of the polarization voltage (-50V, -100V). However, the films are considered quasi-amorphous, due to the presence of broad bands in the region 2θ ≈ 25° - 40°, a region where a series of diffraction peaks for tantalum pentoxide are located. This signals the presence of Ta_2O_5 crystallites, included in an amorphous matrix.

Regarding the crystalline samples, a transition of the preferential growth direction can be observed in figure 2.8, from direction (111) to direction (200), observable in the films deposited with the reactive gas mixture flow rate equal to 7.5 sccm ((111) - 7.5 GND, (200) - 7.5 -50V). Moreover, in regards to the quasi-amorphous samples, a shift of the broad band center can be observed, towards lower angular positions in the case of samples obtained with higher flow rates, compared to amorphous films obtained with lower flow rates. This broad band indicates the possible presence of tantalum pentoxide crystallites in the films.

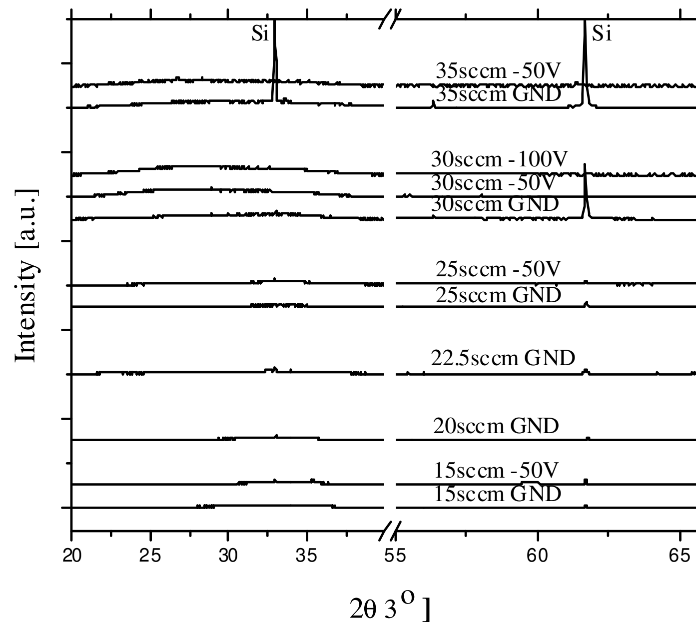

Fig. 2.9. Diffractograms of the quasi-amorphous samples from Series A, Series B, and Series C, respectively, ordered according to the flow rate of the reactive gas mixture, respectively to the polarization voltage.

Furthermore, the density of some of the films, the thickness of the surface contamination layer, respectively the surface roughness, were obtained with the help of XRR curve simulations (X-Ray Reflectivity), obtained with an Empyrean diffractometer. The simulations were performed using the X'Pert Reflectivity software package. These coating characteristics are shown in Table 2.3.

The contaminated layer on the film surface is assumed to consist, in addition to Ta, O, and N, from hydrogen (due to the atmospheric humidity), respectively adventitious carbon. For comparative purposes, the same table shows the density values for a series of tantalum oxides and nitrides with an fcc structure (face centered cube). The first observation that can be extracted from the presented data is that the films obtained with a biased substrate are denser, compared to those obtained with the grounded substrate. This phenomenon can be explained by the supplementary ion bombardment of the growing coating, during the deposition, due to the polarization bias. The second observation is that films obtained with lower partial pressures are denser compared to those obtained with higher partial pressures. This phenomenon could be linked to the relatively higher quantity of gaseous species in the deposition chamber, which can affect the trajectory of the incoming atoms from the target material. The density of the contamination layer is also lower than that of the TaON layer itself.

Table 2.3. Density, thickness of the contaminated layer, respectively the surface roughness; the density of several fcc tantalum oxide or nitride compounds

Sample	Layer	Density (g/cm^3)	Thickness (nm)	Roughness (nm)
A1 (-50V - 0.05Pa)	Contamin.	12.50	3.92	3.05
	Layer	14.79	NA	1.96
A2 (-50V - 0.08Pa)	Contamin.	10.16	0.95	5.03
	Layer	11.25	NA	1.47
A3 (-50V - 0.10Pa)	Contamin.	9.12	2.49	3.02
	Layer	10.88	NA	1.36
B1 (GND - 0.02Pa)	Contamin.	12.24	2.72	2.87
	Layer	13.66	NA	0.63
B2 (GND - 0.04Pa)	Contamin.	11.20	4.97	4.77
	Layer	12.21	NA	1.04
B3 (GND - 0.08Pa)	Contamin.	9.14	4.11	4.60
	Layer	10.10	NA	1.32
98-016-7807 – TaN 4/3		15.13		
98-007-6456 – TaN Delta		15.93		
98-064-7491 – Ta(II)O		15.57		
98-064-4722 – TaN (0.83/1)		13.43		
00-049-1283 – TaN		15.84		
01-089-5196 – TaN delta		15.94		
03-065-9404 – TaN		15.64		
03-065-4090 – OTa γ		15.12		
03-065-6750 – TaO		15.56		
03-065-7449 – $O_{0.9}Ta$		14.82		

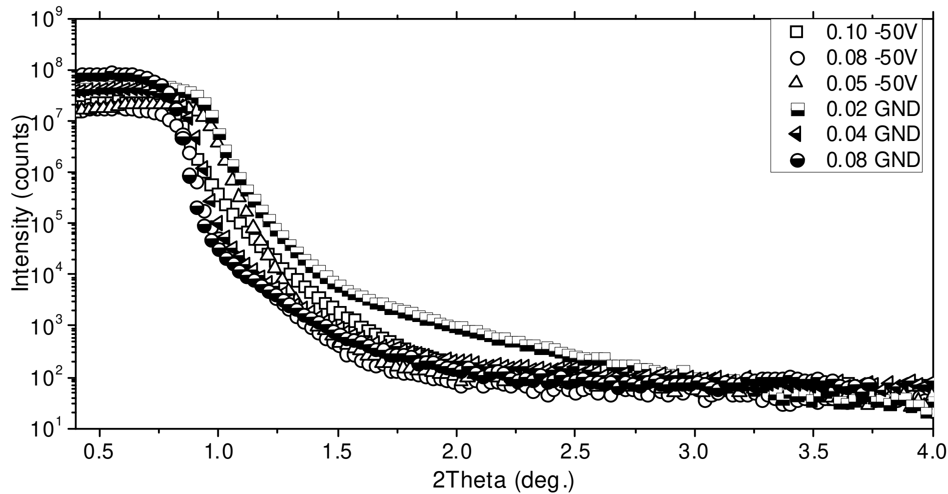

Fig. 2.10. XRR curves obtained for samples deposited with low partial pressures of the reactive gas mixture.

Morphology. The morphology of the tantalum oxynitride thin layers, both of the surface and in cross-section was studied using a ZEISS Supra 55VP scanning electron microscope (SEM). The samples were positioned at a distance of 5mm, and the voltage was 3 KV. To obtain the morphology of the film section, the samples deposited on the silicon substrate were fractured before their introduction into the microscope chamber. Figure 2.11 shows the surface characteristics in the case of samples obtained with substrate bias, with low, mid and high partial pressures (Series A). A relatively fine structure with a grain size of less than 200nm can be observed. The grain size decreases with increasing partial pressure of the reactive gas mixture. This observation confirms the phenomenon of scattering of the sputtered material from the target, due to the increase of the partial pressure (implicitly due to the quantity of gaseous species present in the atmosphere of the deposition chamber). As a result, the energy of the species that reach the substrate is lower and lower. Although in this case the deposition of a ceramic material is discussed, these observations are consistent with the predictions of Thornton's model (Thornton, 1974).

The micrographs representing the cross-sectional area of the films can be seen in Figures 2.13 (for Series A samples) and 2.14 (for Series B samples), respectively. One can observe that the columnar growth, associated with the samples deposited with low partial pressures, becomes more compact, with the increase of the partial pressure. The effect of polarizing the substrate seems to have an effect similar to that of decreasing the partial pressure of the reactive gas mixture. The supplementary ion bombardment promotes the deposition of films with a finer crystalline microstructure, compared to those produced with the grounded substrate.

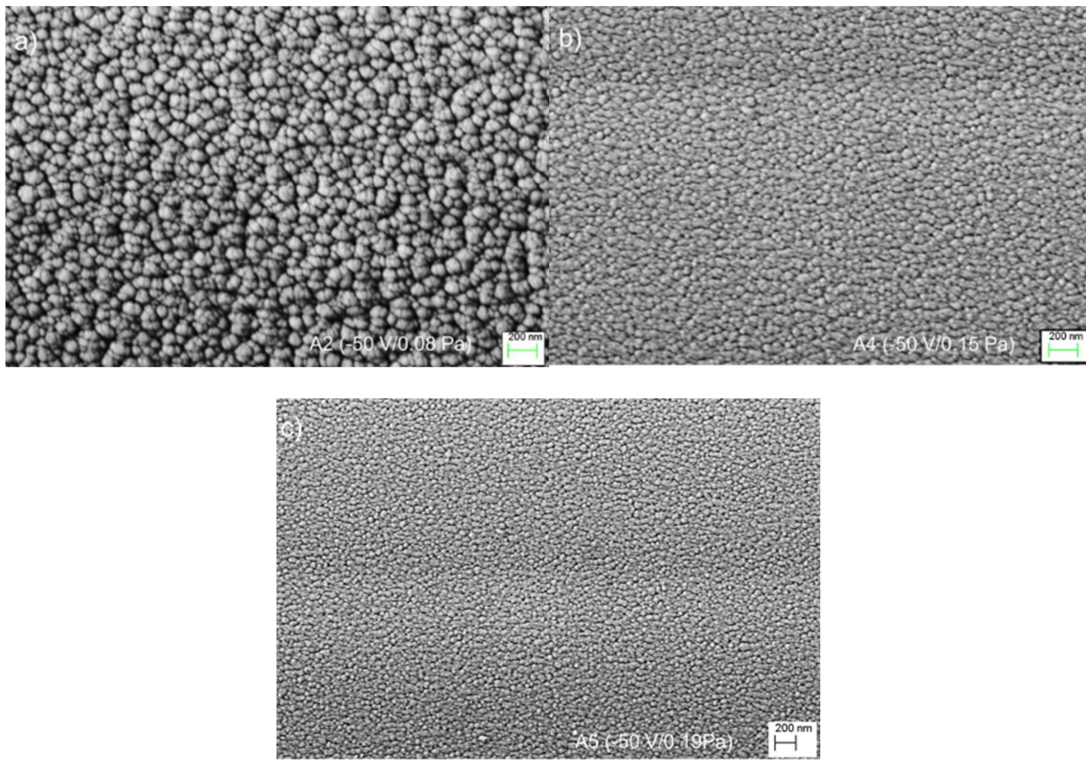

Fig. 2.11. SEM micrographs (surface) obtained for Series A samples.

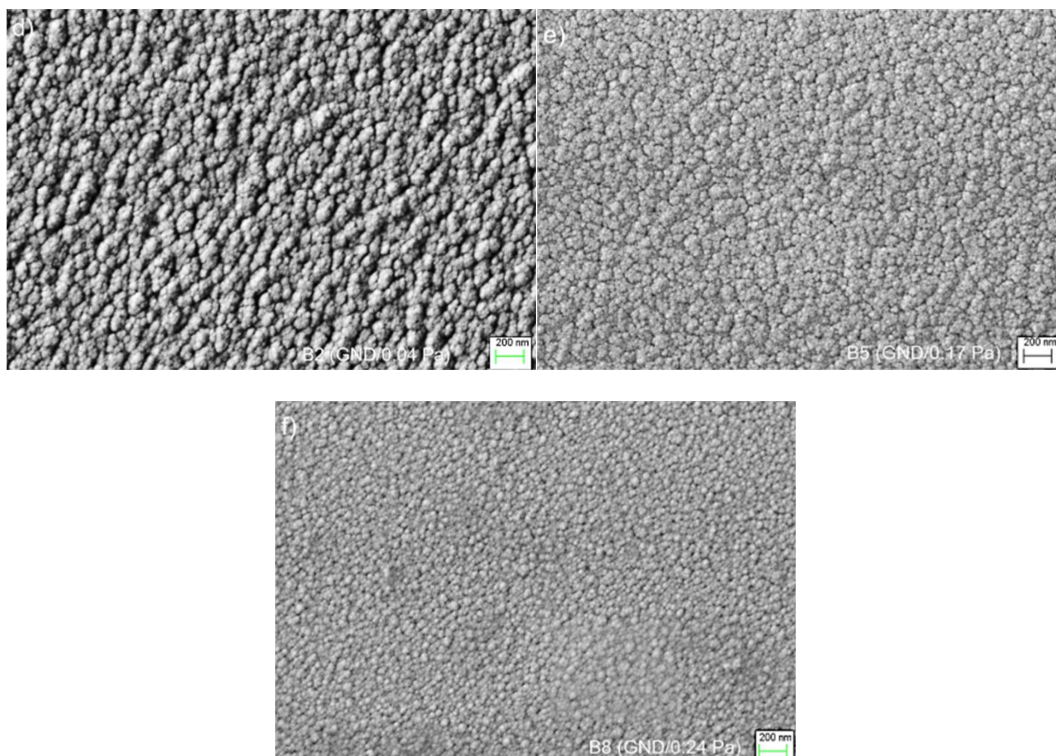

Fig. 2.12. SEM micrographs (surface) obtained for Series B samples, deposited with low, mid, and high partial pressure (grounded).

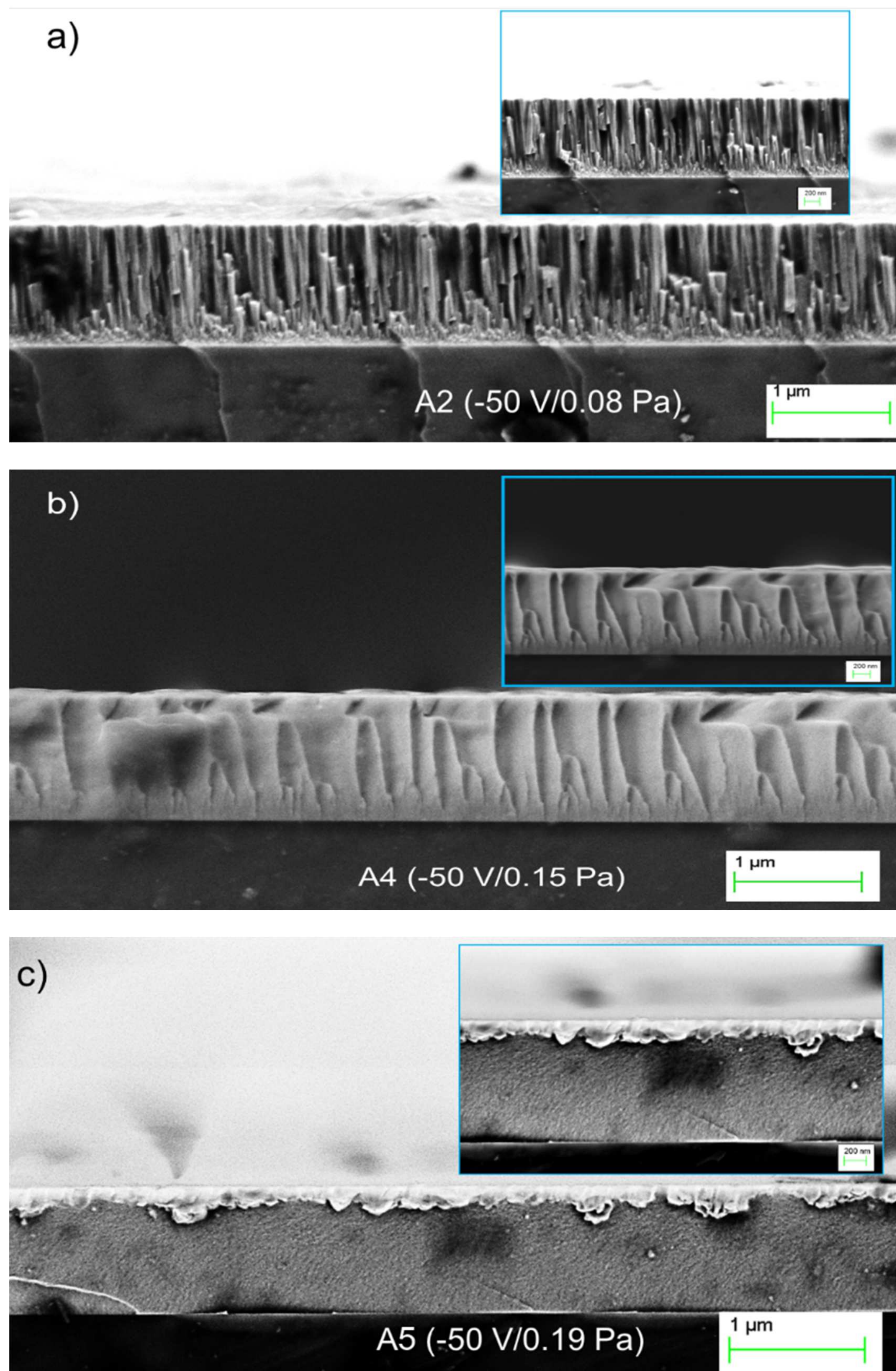

Fig. 2.13. SEM (cross-sectional) micrographs obtained for Series A samples, for the low (a), mid (b) and high (c) partial pressure samples.

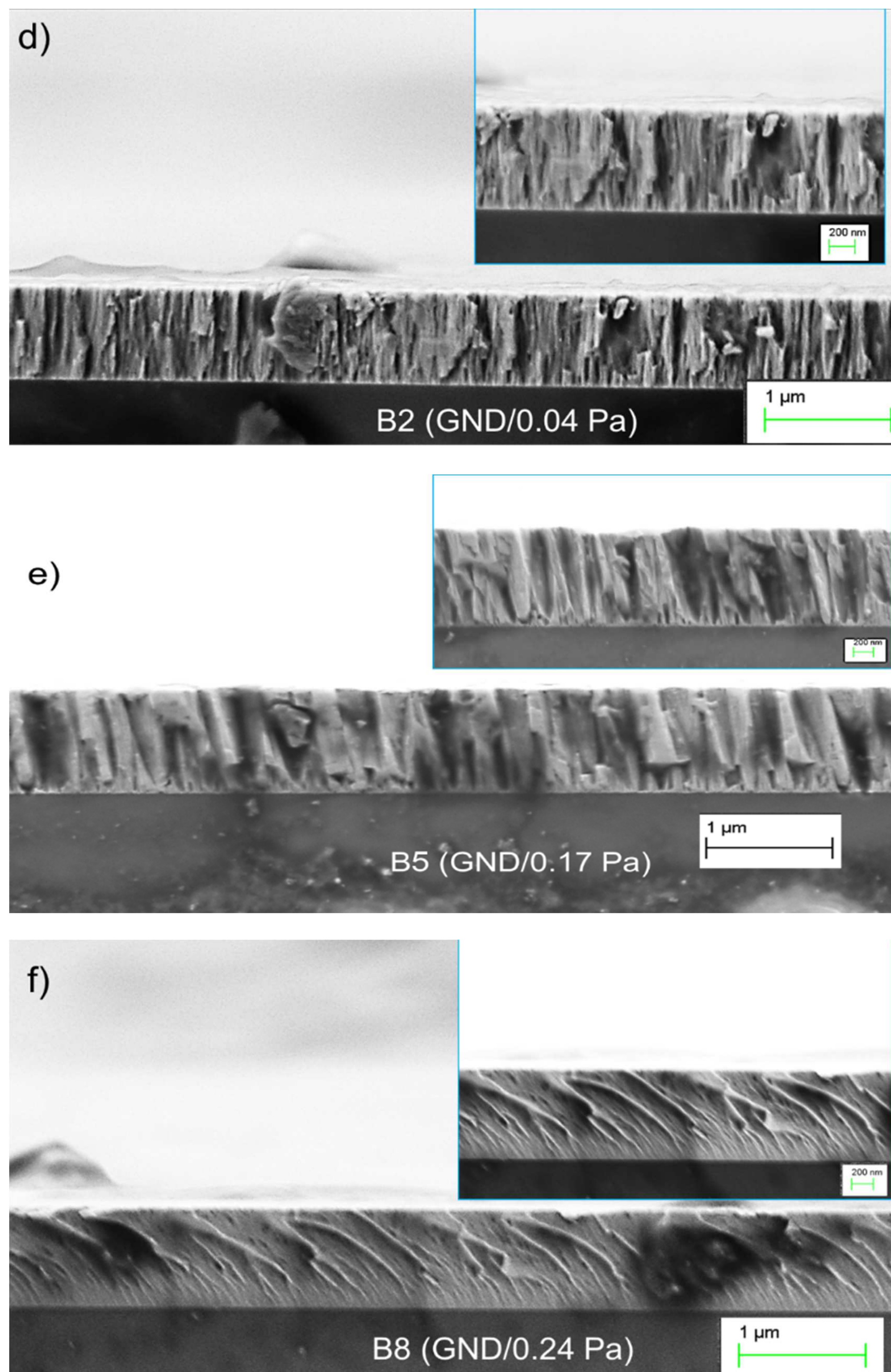

Fig. 2.14. SEM (cross-sectional) micrographs obtained for Series B samples, for the low (d), mid (e) and high (f) partial pressure samples.

Transmission electron microscopy (TEM) analyses were performed on selected samples (coatings deposited on silicon wafers, prepared by erosion of the substrate) using a Tecnai G2 F30 STWIN electron microscope from Thermo Fisher Scientific (Former FEI) operated at an acceleration voltage of 300 kV. The images were obtained in normal BFTEM (Bright Field Transmission Electron Microscopy) mode and HRTEM (High Resolution Transmission Electron Microscopy) mode. The HRTEM micrographs for the two representative samples deposited with a grounded substrate, which showed a good photodegradation ability, (the ones deposited with 0.02 and 0.04 Pa reactive gas mixture partial pressure) are illustrated in figure 2.15. The photocatalytic results will be presented in the next section. These samples show the presence of both metallic Ta (β-Ta) and nitride phases. In the sample obtained at 0.02 Pa, both crystalline and amorphous regions could be seen.

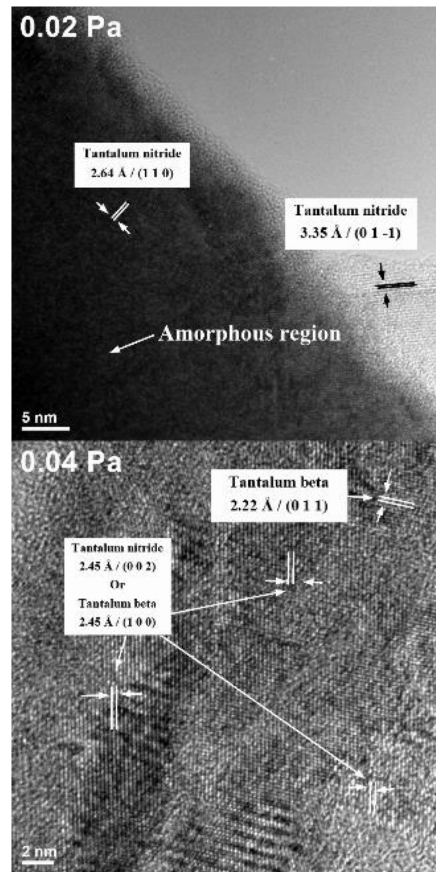

Fig. 2.15. HRTEM images of the samples produced with $P(N_2+O_2)$ = 0.02 Pa and $P(N_2+O_2)$ = 0.04 Pa.

The average spacing between the crystallographic planes is 2.64 to 3.55 Å in the sample produced with $P(N_2+O_2)$ = 0.02 Pa, consistent with the TaN (110) and (01-1) crystallographic planes spacing. In the sample obtained at $P(N_2+O_2)$ = 0.04 Pa, several in-plane randomly-oriented domains could be observed, with possible alternation of crystalline and amorphous phases. In the case of the $P(N_2+O_2)$ = 0.04 Pa sample, the amorphous phase is significantly less present, and some grains correspond to β-Ta ((011) and (100) with 2.22 Å and 2.45 Å interplanar distance.

2.3.2 Electrical, photocatalytic and antibacterial properties.

Electrical properties. The electrical resistance was measured using the four-point probe and the two-point probe methods. The four-point measurement setup consisted of a Keithley 2182A nanovoltmeter, a Keithley 6221 AC/DC current source, and a four-point probe Jandel stand. The four-point probe stand provides a very accurate and constant distance of 1 mm between the electrodes and a controlled load on the sample. Bulk resistivity of the TaON film was calculated as:

$$\rho = R_s \times t_f \tag{2.1}$$

where R_s is the surface electrical resistance in Ω/cm^2 obtained as Rs=4.532U/I, and t_f is the thickness of the thin film, expressed in cm. U and I are the measured values of the voltage and electrical current in the sample.

The two-point probe experimental setup consisted of a Keithley 6487 picoammeter/voltage source and a two-point probe stand. The thickness of the film samples, necessary for the resistivity and relative permittivity calculations, was measured using the ball-cratering method and by spectroellipsometry.

The capacitance of the more resistive samples was determined with an Agilent 4294A Precision Impedance Analyzer, in the frequency range 100 Hz–5 MHz. Gold pads, with an approximate area of 0.22 mm^2, were deposited by magnetron sputtering on top of the films, deposited in turn on the high-speed steel substrate samples, resulting in a capacitor-like structure (conductive steel substrate–dielectric TaON film–conductive gold contacts). The relative permittivity (dielectric constant, ε_r) was calculated from the following formula (Hayt, 2012):

$$\varepsilon_r = \frac{C t_f}{\varepsilon_0 A} \tag{2.2}$$

where C is the measured capacitance, A represents the area of the gold pad, t_f represents the thickness of the dielectric film (or the distance between the capacitor plates), and ε_0 represents the vacuum permittivity ($\varepsilon_0 = 8.854 \times 10^{-12}$F/m (Hayt, 2012)).

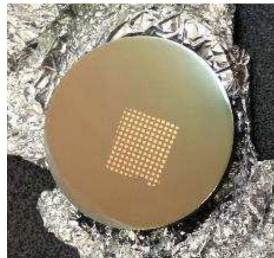

Figure 2.16. Coated sample used for dielectric measurements. Each gold contact represents the upper plate of a capacitor and can be used for analysis.

The variation of the electrical resistivity for the tantalum oxynitride coatings, as function of the flow rate of the reactive gas mixture, is shown in figure 2.17. The resistivity values are spread out in a very wide range, the sample with the lowest resistivity (5.29×10^{-4} Ω · cm) being obtained with a flow rate of 2.5 sccm (GND – grounded substrate), while the sample with the highest resistivity (1.93×10^{6} Ω · cm), being obtained with a flow rate of 30 sccm, respectively a bias voltage equal to -100V. Moreover, it can be seen that the resistivity is influenced by the increase of the reactive gas flow, which means that the resistivity increases with the ratio (N + O) / Ta (Cristea, 2015-1).

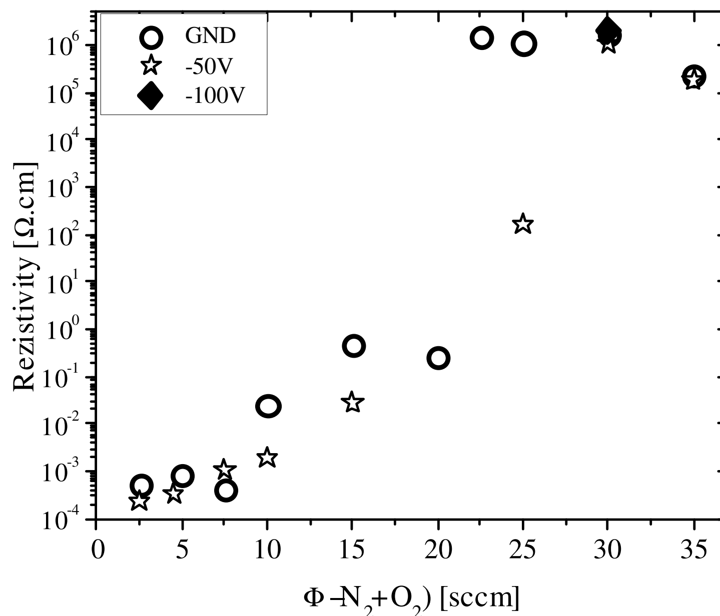

Fig. 2.17. Electrical resistivity of the deposited films as function of the reactive gas flow.

Furthermore, it can be seen that this property increases slowly, until the reactive gas mixture flow reaches the range of values between 8 and 10 sccm, also depending on the polarization voltage. This interval coincides with the one in which the crystallographic structures are either tetragonal β-Ta or fcc Ta (O, N). For flows higher than 10 sccm, the resistivity increases abruptly. In particular, it can be seen that between 15 and 25 sccm, in the case of samples deposited with the biased substrate, the resistivity increases from 2.65×10^{-2} Ω · cm (15 sccm / -50V bias) to 1.69×10^{2} Ω · cm (25 sccm/-50V bias), while in the case of samples obtained with the grounded substrate, the resistivity increases from 4.71×10^{-1} Ω · cm (15 sccm/GND) to 1.10×10^{6} Ω · cm (22.5 sccm/GND). This sudden increase in resistivity, especially for the layers produced with the grounded substrate, is correlated with the increase of the non-metallic content (higher (N+O)/Ta ratio), but also with the decrease of crystallinity.

Given this sudden increase in resistivity, the results will be separated, for a more detailed analysis, as follows: samples obtained with a flow rate less than or equal to 20 sccm (figure 2.18a), and the samples obtained with a flow rate greater than 20 sccm (figure 2.18b). Consequently, studying the variation of resistivity in the graph shown in Figure 18a, a number of observations can be made. First, a faster increase in resistivity is evident for the samples obtained with the grounded substrate.

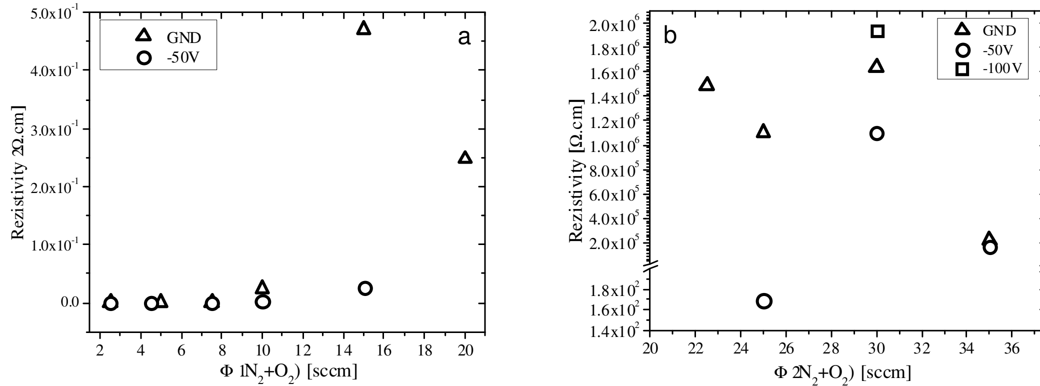

Fig. 2.18. Variation of resistivity for samples obtained with flow rates less than or equal to 20 sccm (a), and with flow rates higher than 20 sccm (b).

This phenomenon could be explained by taking into account the variation of non-metallic elements depending on the gas mixture flow used during deposition (figure 2.19). Thus, it can be observed that up to a flow rate of 15 sccm, in the case of samples deposited with the grounded substrate, the nitrogen content is always higher than the oxygen content. Above this flow rate, the oxygen content is higher than that of nitrogen. However, in the case of the samples deposited with the polarized substrate, this inversion is visible only in the case of a flow rate higher than 25 sccm. This observation seems to suggest that the main criterion influencing the increase in resistivity is the oxygen content.

Figure 2.18b shows the variation of resistivity for samples obtained with flow rates greater than 20 sccm. One observation that should be noted is that for the sample obtained with 25 sccm and -50V bias voltage, a considerably lower resistivity value of $1.69 \times 10^2\ \Omega \cdot \text{cm}$ was measured, both compared to the rest of the samples obtained with flow rates higher than 20 sccm, as well as compared to the sample obtained with the same flow of reactive gases, but with the grounded substrate. An explanation for this phenomenon could be the fact that this sample is the last in the series of samples with a higher nitrogen content than oxygen, visible in figure 2.19. The sample obtained with the grounded substrate shows the following ratios of constituents: O / Ta = 0.93, N / Ta = 0.39, so a significantly higher oxygen content.

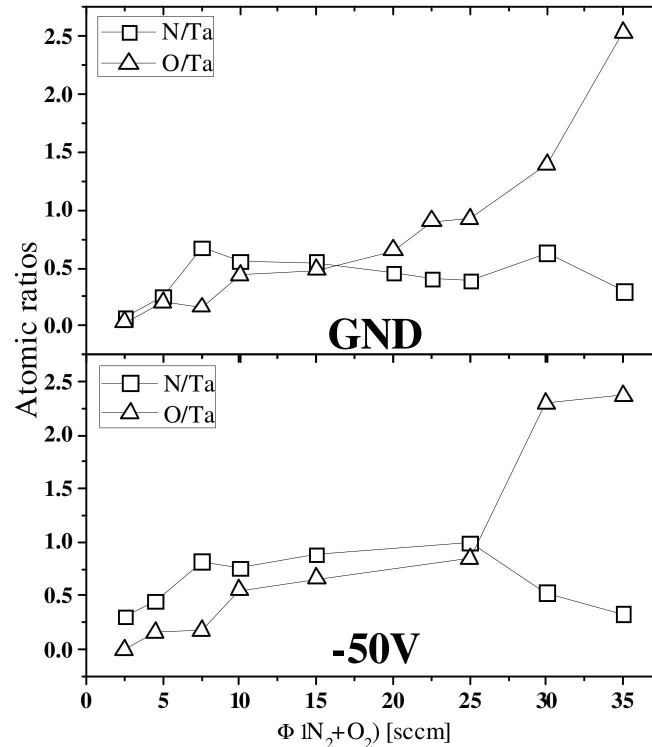

Fig. 2.19. Variation of non-metallic elements content depending on the flow rate of the reactive gas mixture.

Dielectric measurements were performed using an Agilent 4294A impedance analyzer, in the frequency range 100Hz - 5MHz. The starting point for the measurement of the dielectric characteristics was to fabricate some MIM (metal-insulator-metal) type structures, with the following structure: TaON films were deposited on the surface of a copper substrate, and copper layers were deposited on the surface of the films, by sputtering. Due to manufacturing defects (dielectric breakdown), the results obtained from the measurement of these samples were not conclusive regarding the dielectric characteristics. Consequently, new samples were made, with the following configuration: steel substrate, TaON type layer, gold contacts deposited by sputtering, with an area of 0.22mm^2 (figure 2.16). A gold electrode thickness of 100-110 nm was required to achieve good quality ohmic contacts.

The samples that were analyzed in terms of dielectric characteristics were those deposited with flow rates higher than 20 sccm, but with the exception of the samples obtained with 30 sccm and 35 sccm, the character of the remaining films was that of a semiconductor material, with high dielectric losses.

The variation of the dielectric properties (relative permittivity ε_r, dielectric losses tgδ, quality factor Q) depending on the frequency of the applied signal, in the case of samples obtained with flow rates of

30 and 35 sccm, respectively, and different polarization voltages, can be observed in figure 2.20 (30 sccm), respectively figure 2.21 (35 sccm).

Analyzing the evolution of the dielectric parameters in figures 2.20 and 2.21, respectively, it can be concluded that the tantalum oxynitride coatings, obtained in certain configurations, have a high potential to be used in dielectric applications. In the case of samples obtained with a flow rate of 30 sccm, one can observe permittivity values starting with 25 (-50V bias voltage), 28 (GND), up to the value of 41 (-100V bias voltage). These values are stable regardless of the applied signal frequency, over the entire measured frequency range (100Hz - 5MHz). The quality factor reaches a maximum of ~ 70 at 0.30 MHz, followed by a progressive decrease. The sample obtained with a polarization voltage of the substrate of -100V shows a maximum quality factor of 60 at 0.15MHz, followed by a progressive decrease with increasing frequency. The most stable film seems to be the one obtained with a bias voltage of -50V (~ 20 at 0.8 MHz).

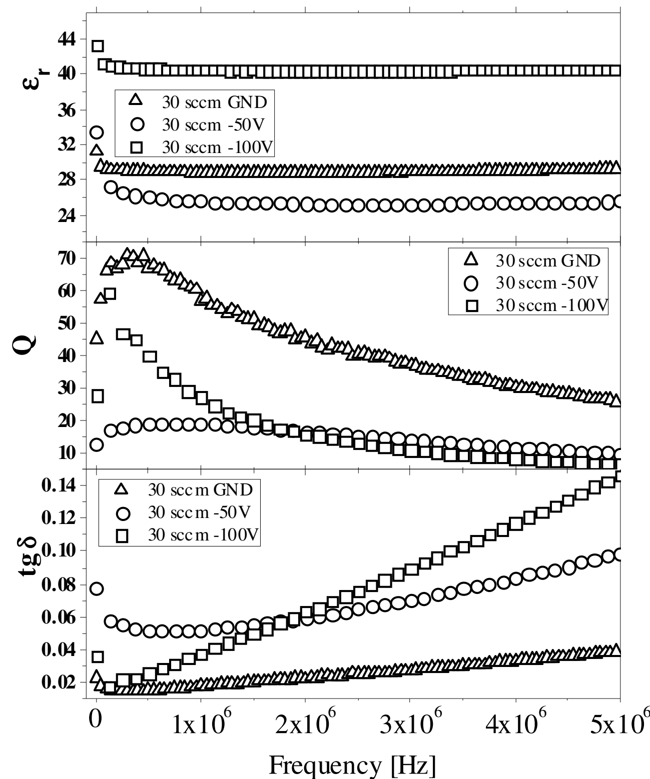

Fig. 2.20. Variation of dielectric parameters as function of the applied frequency, for samples deposited with 30 sccm reactive gas mixture flow and various polarization voltages.

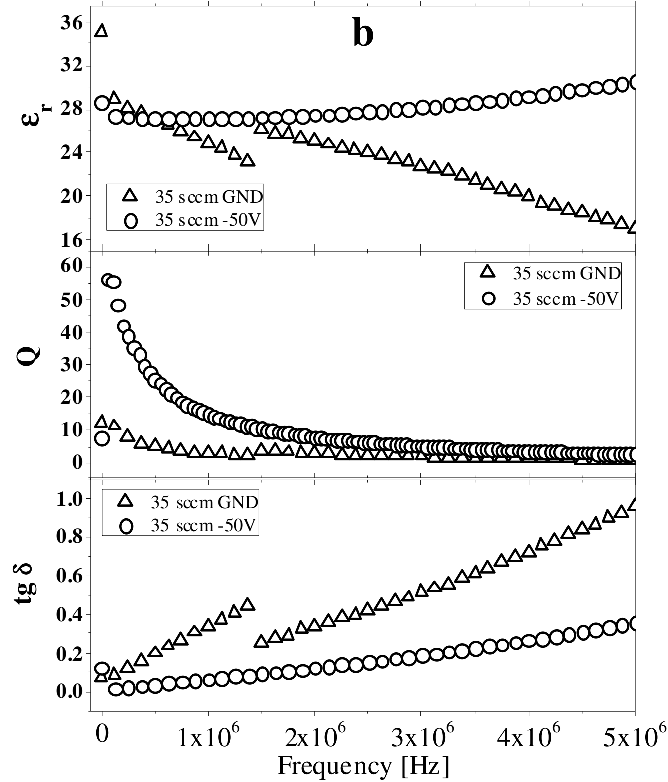

Fig. 2.21. Variation of dielectric parameters as function of the applied frequency, for samples deposited with 35 sccm reactive gas mixture flow and various polarization voltages.

The samples obtained with a flow rate of 35 sccm show slightly weaker dielectric characteristics, compared to those presented previously, especially taking into account their instability depending on the frequency used: $16 \leq \varepsilon_r \leq 29$, $0.5 \leq Q \leq 12$, $0.10 \leq tg\delta \leq 0.97$ (GND), respectively $27 \leq \varepsilon_r \leq 30$, $3 \leq Q \leq 56$, $0.02 \leq tg\delta \leq 0.40$ (-50V). Taking into account the values reported in the literature for relative permittivity, in the case of tantalum-based thin films: $\varepsilon_r = 25$ for Ta_2O_5 (Riekkinen, 2003), $\varepsilon_r = 22$-24 before, and $\varepsilon_r = 34$, after heat treatment, for Ta_2O_5 (McKinley, 1996) , $\varepsilon_r = 23$ for TaON (Le Dréo, 2006) and $\varepsilon_r = 34$ for TaN (Tsai, 1995), it can be said that the films presented herein have high potential for implementation in dielectric applications, especially if the stability of the properties as function of the applied frequency is improved.

Photodegradation capacity. The photodegradation behavior of the TaO_xN_y thin films was tested using two model azo-dyes, namely anionic methyl orange ($C_{14}H_{14}N_3SO_3Na$) (MO) and cationic methylene blue ($C_{16}H_{18}N_3SCl$) (MB). The reason for choosing methyl orange as the photodegradation medium is represented by its high stability to degradation in comparison with other model dyes, such as methylene blue, thus allowing to simulate the photoefficiency response of the thin films to persistent

organic pollutants. Methylene blue, on the other hand, is often used in the reference literature to assess the type of photodegradation kinetic for various photocatalysts, especially under visible light irradiation conditions (Akbal, 2005). The MO photodegradation ability of the eight different TaO_xN_y thin films deposited on glass substrates (grounded substrate), presenting a photoactive area of 2.5 cm^2 was assessed under ultraviolet (UV) and visible (VIS) irradiation conditions by using an open-air photodegradation reactor. The uncoated glass substrate (without any deposited film) was used as reference.

For the UV irradiation experiments, three F18W/T8 black light tubes (Philips) (UVA light, typically 340–400 nm, with peak emission at λ_{max}= 365 nm), placed annularly in relation to the photoreactor stand were used for photolysis. For the VIS irradiation experiments, three TLD Super 80 18 W/865 white light tubes (Philips, λ > 400 nm) were used, annular to the photoreactor stand. The thin film samples and glass substrate reference were submerged in 25 mL of dye solution (MO and MB, respectively) with an initial concentration of c_0= 0.0125 mM, ensuring a constant irradiation power density of 60 mW/cm^2. Before starting the photocatalysis experiments, the films were firstly equilibrated in the dye solution under dark for 5 minutes, to ensure an adsorption-desorption equilibrium of MO or MB on the surface of the samples.

The photo-response of the sputtered samples using MO as model dye was evaluated under four different conditions:

i. ultraviolet (UV) irradiation,
ii. UV irradiation with 100 μl of 30% wt. H_2O_2 added to the volume of MO solution in each flask;
iii. visible (VIS) irradiation;
iv. VIS irradiation with 100 μl of 30% wt. H_2O_2 added to the MO solution in each flask.

The 30% wt. H_2O_2 solution was added as oxidizing agent (electron acceptor) during the photocatalysis reactions. The effective H_2O_2 concentration in each flask, before photocatalysis, was 6.50 mg/L. This concentration was efficient in enhancing MB removal rate, providing also an increased economic efficiency of the process (low amount of hydrogen peroxide), as found in other research (Kaur, 2007; Mitrovic, 2012). The total duration of the photoirradiation experiments has been chosen at 6 hours, considering that, after this period, photodegradation equilibrium occurs in the case of MO. The methyl orange removal efficiency (discoloration efficiency) η has been determined with the help of Eq.2.3, based on the absorption maxima for this dye (λ_{max} = 463 nm, determined with a Perkin Elmer Lambda 25 spectrophotometer):

$$\eta(\%) = \frac{A_0 - A}{A_0} \times 100 \qquad (2.3)$$

where A_0 is the absorbance of the initial dye solutions in contact with the films, and A is the absorbance of dye solutions in contact with the TaO_xN_y thin film samples, determined at λ_{max} = 463 nm, after the 6 h period of illumination. The same formula has been used to determine the removal efficiency for the reference samples.

Moreover, the photocatalytic activity of the TaO_xN_y films deposited onto glass substrates in comparison with the reference (uncoated glass substrate), was evaluated by determining the removal efficiency and type of degradation kinetic for the MB dye under visible light irradiation conditions, without the addition of H_2O_2. The absorbances of the MB solutions at their absorption maxima (λ_{max} = 664 nm, measured with a Thermo Scientific Evolution 300 spectrophotometer) in contact with the samples were measured at determined time intervals until reaching equilibrium (total irradiation time of 2 h). The methylene blue removal efficiency at equilibrium was calculated with the help of Eq.2.3.

The photoactive behavior of the TaO_xN_y thin films and reference glass substrate was also evaluated by water contact angle measurements (θ), under UV irradiation. The measurements were conducted at room temperature, irradiating the samples by a UV lamp (Philips TUV T8) at a power density of 1.8 mW/cm^2 and analyzing the height profiles of small sessile drops (1 μl) of deionized water, deposited on the sample surfaces, with the help of the ImageJ software.

The reflectance of the coatings deposited on silicon was measured on a UV-Vis-NIR spectrophotometer (Shimadzu UV-Vis-NIR 2505) in the spectral range of 250-800 nm. These measurements were used to find the type of energy transition and the optical band gap of the Ta-based phases (Tauc plots), necessary to explain the photodegradation behaviour.

The UV-VIS spectra of the films, shown in figure 2.22, present a reflectance decrease (absorption) at ~408 nm, which could be attributed to a O^{2-} (2p) →Ta^{5+} (5d) charge transfer process (Khemasiri, 2016). These absorption maxima tend to shift to higher wavelengths as the partial pressure of reactive gases increases from $P(N_2+O_2)$ = 0.08 Pa, due to the presence of Ta_2O_5 on the surface of the samples. The samples containing Ta (V) oxide, namely those obtained at partial pressures of 0.08, 0.13, 0.20 and 0.22 Pa, evidence higher reflectance values than the oxynitride-rich samples, as determined also in other research (Hsieh, 2011). The spectra of the films produced with partial pressures in the range 0.20-0.24 Pa show that the coatings are transparent to visible light and show characteristic interference fringes in the visible domain (Cristea, 2019). One of the films containing higher amounts of metallic Ta (produced with partial pressure = 0.04 Pa) presents the highest absorption maximum among all the films, as it was also found elsewhere (Renaud, 2017).

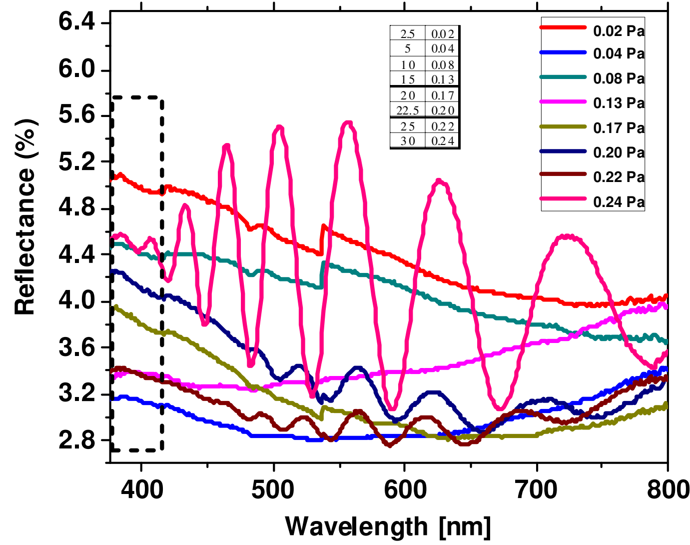

Fig. 2.22. UV-Vis spectra

The UV-Vis spectra were used also to find the type of energy transition and the optical band gap of the Ta species, using the Tauc plots, considering that the optical absorption coefficient α depends on the photon energy (hν) according to Eq. 2.4:

$$ln(\alpha h\nu) = ln\,\alpha_0 + n \cdot ln(h\nu - E_g) \qquad (2.4)$$

where α_0 is the band tailing parameter and n is the power factor of the transition mode (for direct allowed transitions, n = 0.5, for the forbidden transitions n = 1.5, while for indirect allowed transitions, n = 2). To determine the type of transitions for each type of film, ln(αhν) was plotted as a function of n × ln(hν-E_g), giving (for a certain region of the spectrum) a straight line with the slope equal to the power factor n (Perez, 2017). By plotting $(\alpha h\nu)^{1/2}$, or $(\alpha h\nu)^2$, as a function of the photon energy, for indirect or direct transitions, respectively, the resulting dependency will have a linear part, whose intersection with the hν axis gives the values for the optical band gap energy, E_g (eV) (Hassanien, 2015). The valence band and the conduction band edge potentials (E_{VB}, respectively E_{CB}) have been calculated with Eqs. 2.5 and 2.6:

$$E_{VB} = X - 4.5 + 0.5 \cdot E_g \qquad (2.5)$$

$$E_{CB} = X - 4.5 - 0.5 \cdot E_g \qquad (2.6)$$

where X is the absolute electronegativity of the semiconductor species, determined according to Renuka et al. (Renuka, 2017) as 5.47 for TaN and 5.98 for TaON. The results are depicted in Table 2.4.

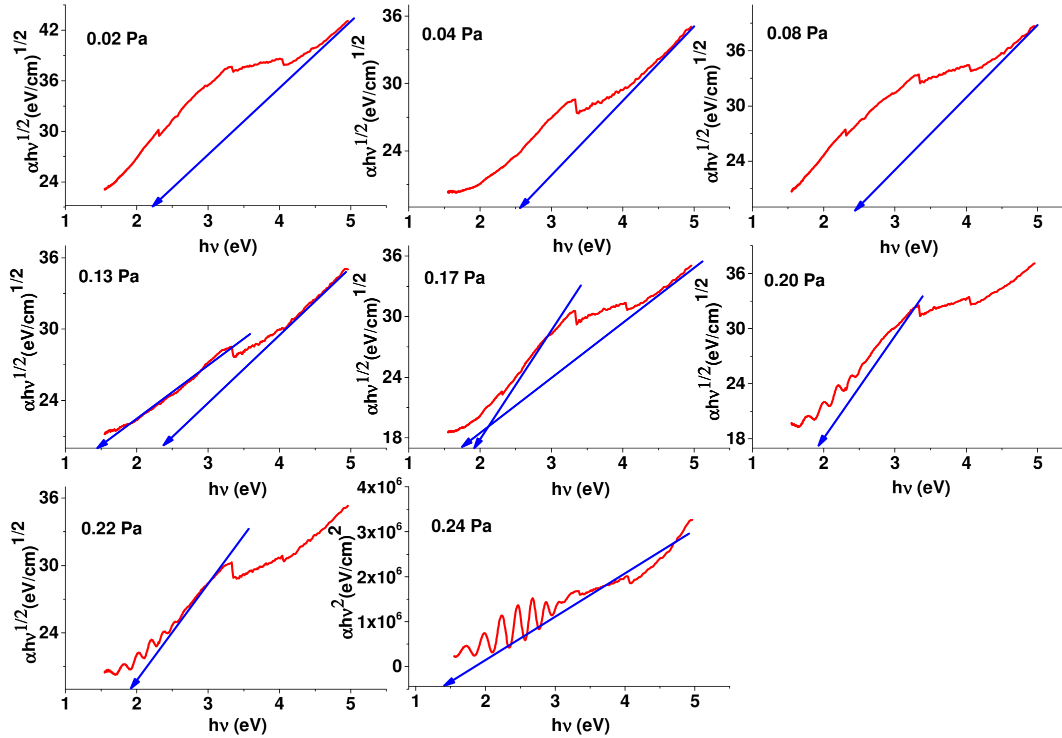

Fig. 2.23. Tauc plots

Table 2.4. Parameters associated to the Tauc plots. The column titled E_U refers to Urbach energy.

Sample	n	R^2	E_g (eV)		E_U (meV)	Edge potentials	
						E_{VB} (eV)	E_{CB} (eV)
0.02 Pa	1.863	0.996	2.265	TaO_xN_y	147.43	2.61	0.35
0.04 Pa	1.947	0.993	2.665	TaO_xN_y	175.67	2.81	0.15
0.08 Pa	1.817	0.964	2.508	TaO_xN_y	259.47	2.73	0.22
0.13 Pa	1.913	0.979	2.411	TaO_xN_y	182.19	2.68	0.27
	1.921	0.962	1.429	TaN		1.69	0.25
0.17 Pa	1.828	0.983	1.979	TaO_xN_y	331.61	2.46	0.49
	1.835	0.967	1.864	TaN		1.90	-0.03
0.20 Pa	2.008	0.997	1.956	TaO_xN_y	485.96	2.46	0.51
0.22 Pa	1.996	0.984	1.951	TaO_xN_y	484.16	2.45	0.50
0.24 Pa	0.501	0.970	1.436	TaO_xN_y	499.97	2.19	0.76

The E_g values of the thin films range from 1.43 to 2.67 eV (Table 2.4). The reported values for E_g of tantalum oxynitrides typically range from 1.9 to 2.5 eV (Xiao, 2017; Murphy, 2006), while tantalum nitrides (TaN_x) present optical band gaps in the 1.88-2.90 eV range. The E_g values for tantalum nitrides (when co-present with TaO_xN_y) tend to be slightly lower than in the case of TaO_xN_y (Zhang, 2014; Harb, 2014).

In the samples obtained at 0.13 and 0.17 Pa, where both the nitride and the oxynitride species are present in a significant amount, two band gaps are observed, the lower value being ascribed for TaN, the higher one being owed to TaO_xN_y. In the samples obtained with 0.02, 0.04, 0.08, 0.20, 0.22, and 0.24 Pa partial pressure, where the oxynitride content is prevalent, only one E_g value has been registered. Nearly all the transitions are of indirect type ($n \approx 2$), while for the sample obtained at 0.24 Pa, a direct type of transition has been registered. The decreasing of the E_g values for these last three samples, as the partial pressure increases, could be due to the presence of lattice defects in the quasi-amorphous structure, promoted by the higher oxygen content, as determined elsewhere (Jones, 2017).

For the chemical systems that present only one value of E_g (other extrapolations of linear domains to the photon energy axis are forbidden, i.e., $n \approx 1.5$), this value could be ascribed to tantalum oxynitride. It may not be ruled out that the nitride/oxynitride phases may form inter-associations (i.e., they may possibly form solid solutions in certain regions of the sample surface, with localized areas of high density of stacking defects, possibly induced by Ta_2O_5) (Jones, 2017).

As localized states extended in the bandgap could be often found in disordered and amorphous materials, the Urbach energy (E_U), i.e., the width of the tail of localized states in the bandgap, has been determined for each film type, through linearly extrapolating the $\ln(\alpha)$ dependence on photon energies to low $h\nu$ values (Valente, 2006). The results depicted in Table 2.4 show an increase in the E_U values with the increase in reactive gas flow, respectively TaO_xN_y content, which could lead to an increase in the disordered atoms and in the defects in the structural bonding (Ristova, 1998; Hassanien, 2018). The lack of a significant rise in the reflectance values of the films above their E_g values may also show a high concentration of defect states in these materials (Balaz, 2013).

The surface morphology has a pronounced effect on the photocatalytic activity. For a high photocatalytic activity, the thin films should have a high effective surface area, thus an increased surface roughness. This increases the number of active sites and the number of defects. An increased surface roughness can be obtained by choosing a substrate with a rough surface, but also can be promoted by generating loosely packed small grains. Quantitative measurements of roughness and surface area, obtained using AFM, suggest that the deposition parameters do not influence significantly the surface roughness of the tantalum oxynitride thin films presented herein. Topological characteristics of both coated and uncoated glass samples were analyzed in terms of root mean square (RMS) surface roughness, by Atomic Force Microscopy (AFM), using a NT-MDT Solver Pro-M system. All the measurements were performed in non-contact mode, under ambient conditions, over multiple random $(10 \times 10)\ \mu m^2$ areas. Figure 2.24 presents the RMS roughness values for some of the as-deposited samples and uncoated substrates. From the RMS roughness values, and also considering the surface features inherited from the substrate, one can conclude that the deposition process

variable parameter (the reactive gas mixture flow) does not have a significant influence on the surface roughness, and, furthermore, that the preparation stage of the substrate could be used, at least in this particular case, to increase the effective surface area of the tantalum oxynitride films, due to the fact that the films follow the irregularities of the substrate surface. However, all the RMS roughness values can be considered to be relatively low, which translates into a relatively small effective surface area of the material. Higher surface roughness values would allow for a better adsorption of dye molecules on the surface of the films and a faster subsequent degradation of the molecules. Thus, the surface roughness would be one of the first parameters to be improved in order to obtain a higher photocatalytic activity for the tantalum oxynitride films deposited using the conditions presented herein.

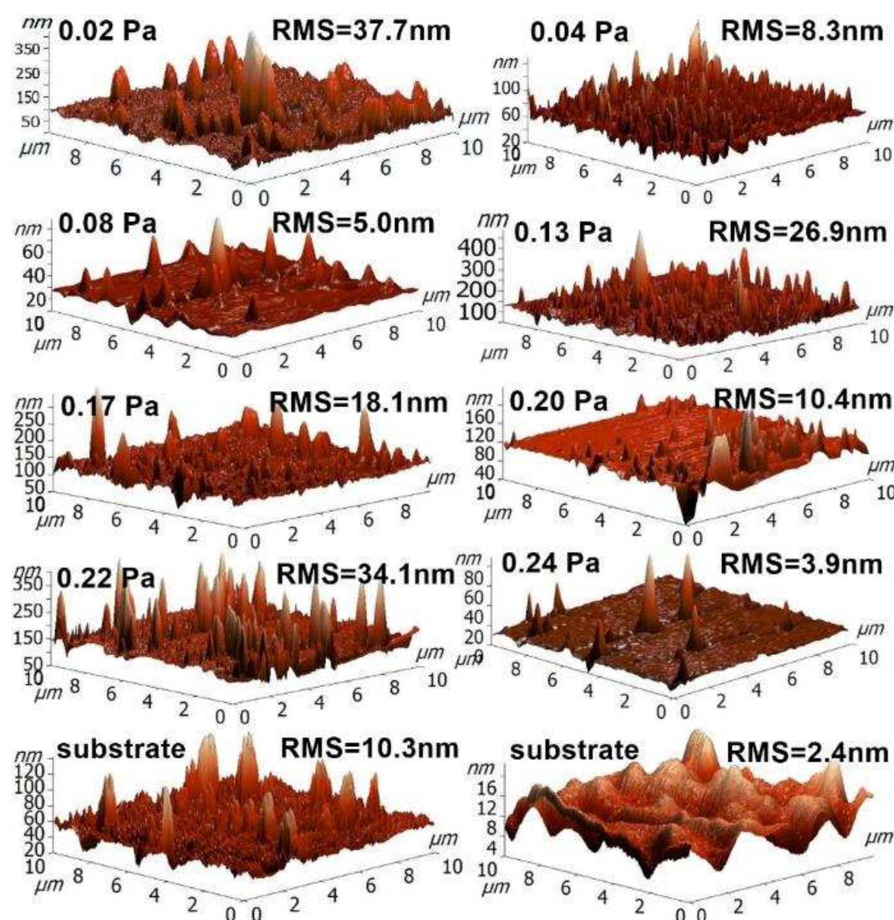

Fig. 2.24. 3D AFM images of TaON deposited on glass substrates, with their respective RMS values.

All the films presented herein could act as visible light harvesters (due to their low E_g values), but, in their as-obtained form, the alignment of their conduction and valence bands are less favorable for degradation of organic compounds (i.e., the conduction bands lie below the oxygen reduction potential

at -0.22 eV, Figure 2.25), or due to fast recombination of the charge carriers (Noguchi, 2003; Zhang, 2013-1).

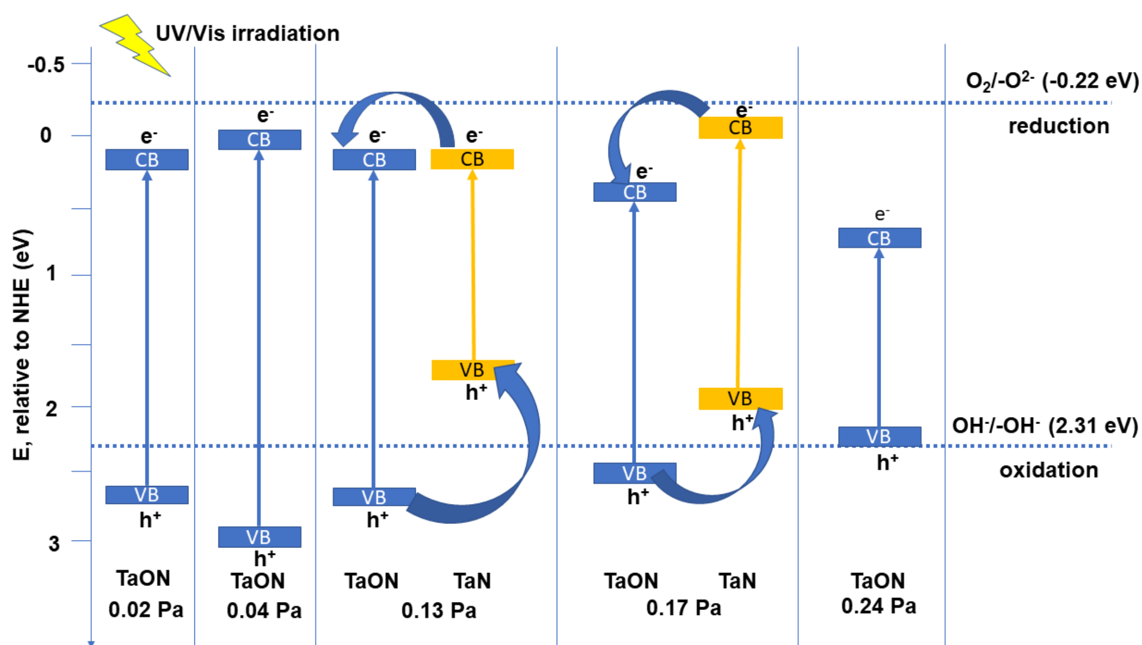

Fig. 2.25. Band edge positions for the thin films.

The main photodegradation mechanism in this case would be the oxidation of the organic dyes with OH· radicals, generated from hydroxyl groups (-OH-) by photoneutralization with holes (h+) at the catalyst-solution interface, or through direct oxidation by reaction with the photogenerated holes (Houas, 2001; Lachheb, 2002):

$(H_2O \leftrightarrow H^+ + OH^-) + h^+ \rightarrow H^+ + OH\cdot$ (free radicals photogeneration)

$Dye + OH\cdot \rightarrow R\cdot + H_2O$ (dye degradation)

$Dye + h^+ \rightarrow R^{+}\cdot \rightarrow$ Degradation products (direct dye degradation)

Figure 2.26 exhibits the methylorange decolorization/degradation efficiency after 6 hours of contact. The MO decolorization/degradation efficiency in the case of UV irradiation (figure 2.26c) ranges from 1.16 to 1.74%, increasing with the amount of oxygen in the reactive gas flow, causing an increase of TaON content of the films. The use of this source of energy for photocatalysis in the case of the TaON films seems inefficient, due to the fast charge carriers' recombination.

However, the films seem to be able to use the visible light in a more efficient manner (figure 2.26d), this observation being inffered from the higher efficiencies (6.67 to 7.94%), per the optical band gaps of each system. The film obtained at 0.24 Pa has the lowest photodegradation efficiency, due to the

unfavorable positioning of TaON valence and conduction band potentials. The highest VIS efficiency for MO degradation is reached for the samples obtained at 0.13 Pa and 0.20 Pa. In the case of the sample obtained with 0.13 Pa partial pressure, a relatively high RMS roughness has been recorded compared to the remaining samples, as determined from the AFM measurements, which determines an increase in the specific surface area of this sample, when in contact with the methyl-orange aqueous solution. Also, a heterojunction between TaON and TaN could be seen (Figure 2.25), which may lead to a more efficient charge carriers separation. After hydrogen peroxide addition (figures 2.26a and 2.26b), the efficiency of the photodegradation process is increased, due to the decrease in the charge carriers recombination (H_2O_2 is an electron acceptor), as well as due to an increased production in hydroxyl radicals (H_2O_2 could be photoreduced by the electrons at the conduction band or it could photocleave by UV radiation) (Dionysiou, 2004).

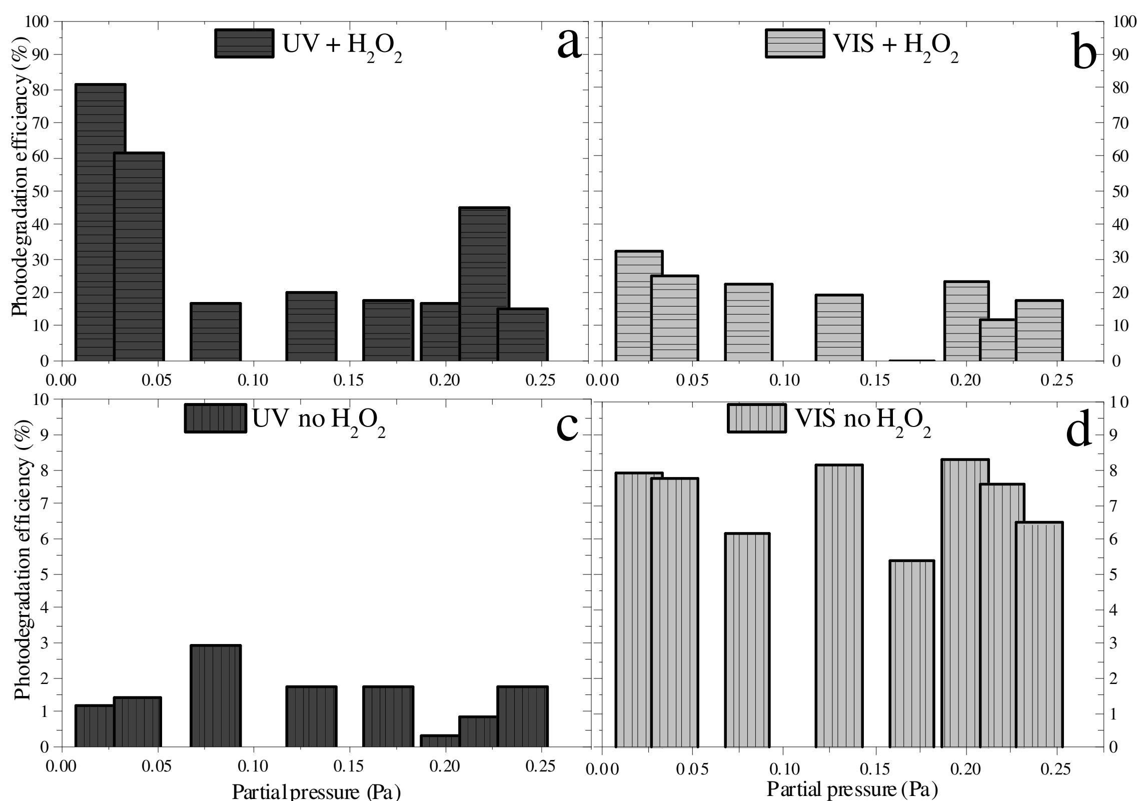

Fig. 2.26. Photodegradation efficiency as function of partial pressure.

The addition of hydrogen peroxide to the aqueous MO solution has a significant influence on the photodegradation efficiency. Photodegradation efficiencies as high as ~82% after the UV irradiation, and close to 34% after VIS irradiation were observed. The highest performance in this case is exhibited by the lower partial pressure samples, namely the ones obtained with 0.02 and 0.04 Pa. For the 0.22 Pa partial pressure sample, the high photodegradation rate could be attributed to the slight increase in

surface roughness (thus a bigger effective surface area), when compared for example with the samples obtained at the next lower and next higher partial pressures: $P(N_2 + O_2) = 0.20$ Pa – RMS = 10.4 nm, $P(N_2 + O_2) = 0.22$ Pa – RMS = 34.1 nm, $P(N_2 + O_2) = 0.24$ Pa – RMS = 3.9 nm (Figure 2.24). The sample obtained with 0.24 Pa partial pressure presents one of the lowest photocatalytic activities, despite its narrow band gap. Being a direct semiconductor, the charge carriers' recombination rate is higher than in the case of the other indirect semiconducting samples (Lin, 2006).

As far as the photodegradation of methylene blue is concerned, the VIS light-mediated methylene blue photodegradation efficiencies of the films range from 29 to 34%, while for the reference the photodegradation efficiency was negligible (figure 2.27a). The dependence of the methylene blue concentration on irradiation time has been modelled against the pseudo-first order kinetic model (simplification of the Langmuir–Hinshelwood mechanism for heterogenous photocatalysis), shown by Eq. 2.7 in linearized logarithmic form (Valente, 2006):

$$ln\frac{c_t}{c_0} = k \cdot t \quad (2.7)$$

where c_0 represents the initial concentration of methylene blue (0.0125 mM), c_t represents MB concentration at different photoirradiation periods "t", and k (min^{-1}) is the pseudo-first-order rate constant.

Table 2.5. MB photodegradation and contact angle kinetic parameters.

	MB photodegradation kinetic		Contact angle kinetic		
Sample	k (min^{-1})	R^2	θ_0 (°)	k_θ (min^{-1})	R^2
0.02 Pa	0.00304	0.998	84.18	0.0303	0.982
0.04 Pa	0.00349	0.998	71.84	0.0185	0.977
0.08 Pa	0.00270	0.991	70.77	0.0062	0.942
0.13 Pa	0.00210	0.993	71.79	0.0054	0.972
0.17 Pa	0.00291	0.998	67.52	0.0030	0.960
0.20 Pa	0.00297	0.999	61.86	0.0032	0.879
0.22 Pa	0.00315	0.999	61.33	0.0017	0.865
0.24 Pa	0.00355	0.996	68.43	0.0101	0.990

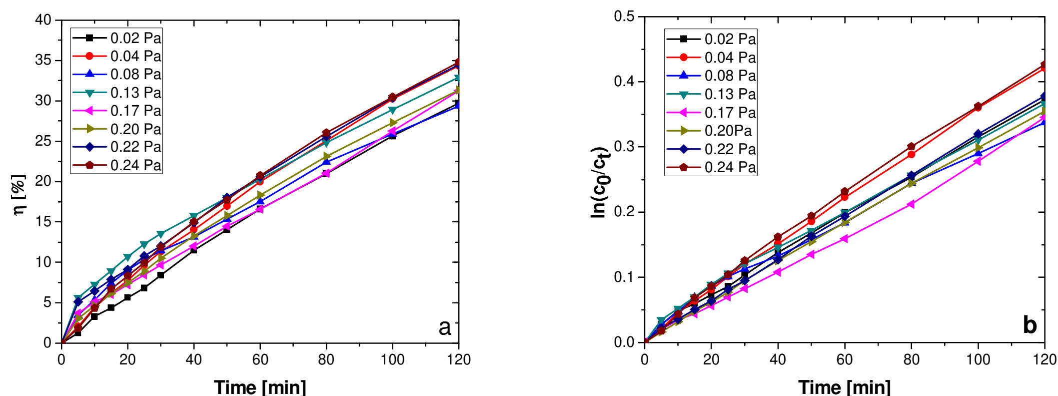

Figure 2.27. (a) Photodegradation efficiencies of the tantalum oxynitride samples; (b) graphical determination of the reaction rate of the photocatalytic degradation of MB.

It can be seen, from Table 2.5 and figure 2.28, that the photodegradation rate depends on the TaN and TaON content and on the surface roughness of the films. The sample obtained at $P(N_2 + O_2) = 0.24$ Pa presents the highest photodegradation rate and highest MB photodegradation/discoloration efficiency from the analyzed sample set, correlated with the highest content in TaON (Fig. 2.28). The samples obtained with $P(N_2 + O_2) = 0.02$ Pa and $P(N_2 + O_2) = 0.04$ Pa also exhibit high k values, due to relatively high roughness, compared to the remaining samples (the former case) or high TaON content (the latter case). The samples with a higher content of Ta_2O_5 present the lowest photodegradation rates and lower photodegradation efficiencies, in accordance with other research (Ullah, 2018).

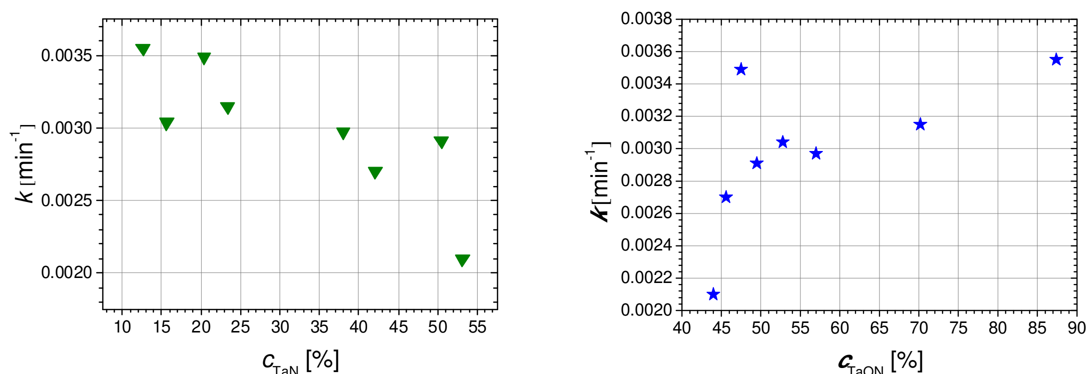

Fig. 2.28. (a) Variation of the rate constant, k, of MB, with the concentration of TaN and (b) TaON phases.

Good wettability (decreased contact angle) is essential for a high photocatalysis reaction rate, ensuring a rapid equilibration of the contact angles at lower values, thus maximizing the contact surface between the photoactive surface and various diluted organic pollutant solutions. As the RMS roughness of the films present low values, the contact angles were not corrected for roughness. All the

deposited films present a hydrophilic character, essential for photocatalysis in an aqueous environment. The initial values of the contact angles (at the beginning of the wetting process) span between 61 and 86°, being significantly higher than in the case of the reference glass substrate (4.3° - not shown on the graph from figure 2.29).

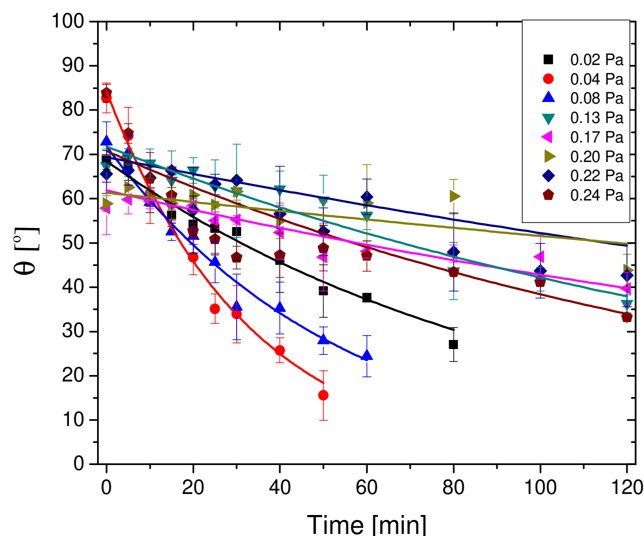

Fig. 2.29. Contact angle kinetic of the films under UV irradiation.

With the increase of the reactive gas flow, the films become less metallic and the contact angles tend to decrease, due to the formation of more hydrophilic oxygen-rich species on the surface of the samples (TaON, Ta_2O_5). The contact angles decrease considerably after UV irradiation (with 40-73%), possibly due to the formation of oxygen vacancies on the surface of the materials, which in turn can photocleave the adsorbed water molecules, leading to transient surface hydroxyl groups, of the Ta-OH type (Sakai, 1998; He, 2016; Cong, 2012; Tezza, 2012). The contact angle kinetic was fitted against an exponential dependency of time, described by Eq. 2.8:

$$\theta = \theta_0 \cdot e^{-k_\theta \cdot t} \tag{2.8}$$

where θ_0 is the contact angle at the beginning of the wetting process (i.e., at t=0) and k_θ is the wetting rate of the surface (related to the drop spreading on the surface of the sample). The fitting parameters are expressed in Table 2.5. The highest wetting rates are recorded for the samples obtained with partial pressures of the reactive mixture of 0.02, 0.04 and 0.24 Pa, for which good photodegradation rates and efficiencies have been registered. This could imply a higher amount of hydroxyl groups formation on the surfaces of these samples, containing a higher amount of metallic Ta (Balaz, 2013; Ahmed, 2016).

<u>**Antibacterial capacity.**</u> The excellent corrosion resistance, fracture toughness and biocompatibility of tantalum-based materials recommend their use as biomaterials, in several applications: vascular clips, flexible vascular stents, dental implants, as well as orthopedic components, as acetabular cups, or other trabecular metal components (Mungchamnankit, 2008; Harrison, 2017).

Bulk Ta is highly unreactive and biocompatible in the body. Ta does not exhibit toxicity to surrounding cells, nor does it inhibit local cell growth of surrounding bone. Moreover, it was found that pure tantalum exhibits a lower or similar *S. aureus* and *S. epidermidis* adhesion when compared with commonly used materials in orthopedic implants (Schildhauer, 2006).

The biocompatibility, antibacterial properties and cytocompatibility characteristics of tantalum-based coatings (mostly oxides) is presented, to date, in a limited number of references. Chang et al (Chang, 2014) report the deposition of Ta and amorphous tantalum oxide coatings by magnetron sputtering. A hydrophilic crystalline β-Ta_2O_5 coating was obtained by rapid thermal annealing of the deposited tantalum oxide coating at 700 °C. It was observed that the antibacterial effect is more obvious for the deposited amorphous Ta_2O_5 coating than for the uncoated and other coated specimens. Moreover, Huang et al (Huang, 2010) reported that tantalum nitride (TaN) coatings with a hydrophobic surface (contact angle = 92.0 ± 1.2°, mean ± SD) exert antibacterial effects against *Staphylococcus aureus*.

The antibacterial/antibioflm capacity of the tantalum oxynitride coatings (deposited with a grounded substrate) was assessed against *Salmonella*. The freeze-dried strain of *Salmonella* was recovered by culturing the bacteria in solid medium, containing 1 g/L yeast extract; 18 g/L agar-agar; 5 g/L sodium nitrate; 0.2 g/L glucose, supplied by Scharlau Chemicals. The third generation of *Salmonella* strain was used for further studies.

With a design to assay the antimicrobial/antibiofilm potential of the TaON coatings, 1 μl of Salmonella strain (1×10^{-9} CFU L^{-1}) was inoculated into 50 mL liquid media, consisting of 0.6 g/L yeast extract; 1g/L sodium nitrate; 3 g/L glucose. The coated samples, deposited on stainless steel, and the control (uncoated stainless-steel disk, mirror polished) were placed in distinct Berzelius beakers. Thereafter the samples were sterilized in an autoclave at 126 °C for 0.5 h to ensure their safe handling in antimicrobial testing.

A volume of 50 μl from the liquid suspension containing bacteria was placed on the surface of each sterile sample, followed by incubation at 33 °C for 48 h. After the incubation period, the samples were washed twice with PBS (phosphate-buffered saline), similarly with the method described by Liu et al. (Liu, 2017). The specimens were subsequently submerged in PBS solution and then exposed to ultrasounds for 0.5 h, using an ultrasonic cleaner to detach the adherent bacteria from the surface of the samples. Simultaneously, Petri dishes containing solid media were prepared in order to inoculate

the solution obtained through ultrasonication. The plates were incubated at 33 °C for 48 h after which the inherent properties of tantalum in antibacterial/antibiofilm activity were evaluated by counting the bacterial colonies and assessing the area of dispersion (Harrison, 2017; Liu, 2017). The antimicrobial/antibiofilm assessment was carried out three times as a verification on the replicability of the experiment.

Figure 2.30 exhibits results obtained on selected samples, concerning the antimicrobial/ antibiofilm capacity of the TaON coatings against *Salmonella*. During the incubation period of the samples covered with liquid media containing *Salmonella*, some of the grown bacterial cells have adhered to the surface of the samples. By rinsing the samples with PBS (phosphate-buffered saline) the non-adherent bacteria were removed. Following ultrasonication the adherent bacteria has also been removed from the surface and immersed in PBS. After inoculation and incubation of the solution containing the adherent bacteria, it could be observed that some bacterial colonies grew on agar plates. The result of interest was the relative surface area of the bacterial colonies, compared to the control sample (uncoated AISI 316L steel). Some researchers have reported that thin film coatings broaden the stainless-steel application field, due to their potential of improving the self-cleaning property of the material. This effect takes place due to a reduction in bacterial adhesion and colonization which are affected mainly by the surface roughness (Evans, 2007; Aiken, 2010). On the other hand, some studies mention that the antimicrobial/antibiofilm potential of thin films could be negatively influenced by the oxide component (Kubacka, 2009; AL-Jawad, 2017). Contrary to this observation, a higher antimicrobial/antibiofilm activity of the coatings was exhibited by the samples deposited with reactive mixture higher partial pressure, as shown in figure 2.31. It has been shown that the antimicrobial performance of tantalum oxide coatings is predominantly exhibited by the amorphous structure, instead of the crystalline alternative, which has also outperformed human skin fibroblast cellular biocompatibility (Chang, 2014).

Chang and his co-authors have argued that there has not yet been developed a certain method which can ensure controlling bacterial adhesion on the coatings, because of the multitude of factors that influence the process, starting from surface properties to bacteria particularities (Chang, 2014). If we consider the observation that tantalum does not have an intrinsic antibacterial activity, as demonstrated elsewhere (Harrison, 2017), the results obtained on the sample deposited with the lowest partial pressure should be as expected. The potential causes for this behavior are the high RMS roughness (RMS = 37.7nm), as well as the high metallic Ta content.

Contrary to the expectations, the dependence between the relative surface area of the bacterial colonies and the contact angle is, in this case, inversely proportional. It was demonstrated that superhydrophobic surfaces (i.e., with higher contact angles) are much more suited to be used as

antibacterial surfaces, due to their anti-adhesive capacity (Liu, 2004). Anti-adhesive surfaces should reduce the adhesion force between bacteria and a solid surface to enable the easy removal of bacteria (Zhang, 2013).

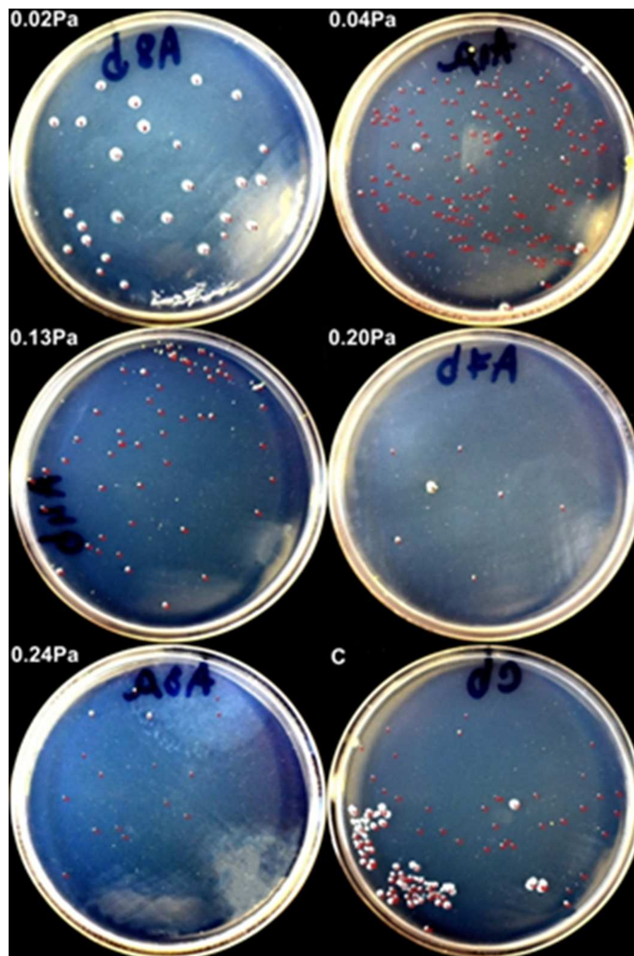

Figure 2.30. Bacterial colonies grown on agar plates.

When discussing about the surface roughness, higher values for Ra or RMS roughness do not necessarily mean better adhesion of the bacterial colonies, hence poorer antibacterial capacity. Cells are easily removed from lower roughness surfaces, but they may be retained within features approximating in size to that of the cells. In larger features, the cells may again be relatively easily removed. Hence, the distance between surface features plays an important role. Micron-sized features may favor bacterial adhesion, whereas nano-sized features may create difficult surface conditions for attachment of the bacterial cells (Adlhart, 2018).

These observations are implying that there are more factors governing the antibacterial/ antibiofilm activity. Even if the mechanism related to the antibacterial capacity is not entirely understood, tantalum-based (oxides) thin films have been tested, and they own antimicrobial potential against

several microorganisms, such as, *Staphylococcus aureus*, *Staphylococcus epidermidis*, *Actinobacillus actinomycetemcomitans*, *Streptococcus mutans* (Mungchamnankit, 2008; Chang, 2014). The research in this area is necessary due to the reported high potential of tantalum to stimulate osseointegration. Moreover, if trabecular structures coated with Ta-based materials would be used, their geometry makes difficult the adhesion of microorganisms to the surface (Harrison, 2017).

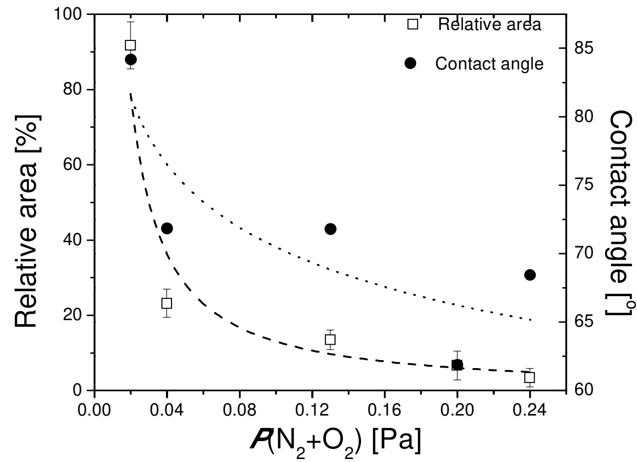

Fig. 2.31. Relative surface area of the bacterial colonies and contact angle, as function of the partial pressure.

2.3.3 Thermal treatment structural effects.

The potential of refractory metal compounds as thin films to be used in high temperature applications is significant. Several publications can be found where the behaviour of tantalum and tantalum nitride films under annealing is studied. Applying a heat treatment to a material can significantly modify its structure, hence its properties.

Generally, concerning the structural stability with the temperature of any material, most of the studies follow the same pattern: annealing execution, generally in vacuum, followed by structural evaluation, normally by XRD, at room temperature. Only a few studies refer to the study of the structure evolution, obtaining the XRD patterns at specific temperatures, simultaneously with the annealing process. In this subchapter, the differences concerning the structural evolution of magnetron sputtered TaN_xO_y films are discussed, after vacuum annealing, in two conditions: the diffraction patterns were captured at room temperature, after vacuum annealing, and compared to in-situ annealing and structural evaluation by XRD.

TaN_xO_y thin films were deposited onto silicon (100) substrates by DC reactive magnetron sputtering. Before being inserted in the deposition chamber, the substrates were cleaned with ethanol. Prior to the etching process and subsequent deposition, the chamber was evacuated to a base pressure of

$1.1 \div 1.3 \times 10^{-3}$Pa. The substrates were plasma etched for a period of 500 s, using pure argon with a partial pressure of ~0.3 Pa (60 sccm) and a pulsed current of approximately 0.6 A. The gas atmosphere during deposition was composed of argon as plasma gas, injected from a bottle (99.999% purity) and a mixture of nitrogen + oxygen, as reactive gas, injected from a bottle with composition 85% ± 2% of N_2 and 15% ± 2% of O_2. The argon flow (70 sccm) was kept constant during all depositions, while the N_2+ O_2 gas mixture flow was varied from 2.5 to 35 sccm, corresponding to a partial pressure of the reactive gases ($P(N_2+ O_2)$) varying from 0.02 Pa to 0.24 Pa.

The structural stability of the TaN_xO_y films as function of the applied heat treatment temperature, deposited with varying reactive gas partial pressures, was studied under two different situations:

i) Annealing, followed by ex-situ XRD: The vacuum annealing of the as-deposited samples was done using a vacuum furnace, with a base pressure of 10^{-4}Pa and a thermal treatment cycle with three steps: a) an increase of the furnace temperature, with a heating rate of 5 °C/min, up to the programmed temperature (T_{max} = 800 °C); b) isothermal period of 1 h at the programmed temperature; c) free cooling until reaching room temperature. X-ray diffraction patterns were obtained after the annealing process, at room temperature, using a Philips PW diffractometer (Cu-Kα radiation) in a Bragg-Brentano geometry configuration. From this point forward, this process is called "ex-situ annealing" or "ex-situ process".
ii) Annealing with in-situ XRD: The annealing was performed during High Temperature X-ray diffraction (HT-XRD) measurements, using a Bragg-Brentano geometry XRD diffractometer and Cu Kα radiation (λ = 0.154 nm). The device operated at a working voltage of 40 kV and 40 mA current, respectively. The annealings were performed in a specially designed oven (Anton Paar HTK 1200) coupled to the diffractometer. The experiments were performed at low pressure (~10^{-2} Pa). The samples were fixed on an Al_2O_3 plate and heated from room temperature gradually, to 500°C, followed by 100°C steps up to 800°C. The heating rate was 30 °C/min with 60 min isothermal periods, at each temperature, for annealing and thermal stabilization. The XRD acquisition took 20 minutes at each selected temperature. At the end of the experiments the pressure reached in the oven was ~10^{-2} Pa. XRD diffraction patterns were obtained until the maximum in-situ annealing temperature of 800 °C, in order to compare with the ex-situ process results. From this point forward, this process is called "in-situ annealing" or "in-situ process".

The samples were divided into three gropus, based on previous analysis and observations regarding their chemical composition, structural development, and deposition parameters (Cristea, 2015-2). Firstly, the results observed in the case of the tantalum oxynitride film produced with $P(N_2+ O_2)$ = 0.02 Pa will be discussed. Figure 2.32 reveals the XRD pattern of the as-deposited sample and of the samples that suffered ex-situ annealing at 400°C, 600°C and 800°C. The XRD pattern of the as-

deposited samples evidences a quasi-amorphous structure with signs of poorly developed β-Ta or Ta_2N crystallites, revealed by a broad peak, in the range 33°< 2θ< 42°. The peak detected at 2θ = 36.1° may be assigned to the (410) planes of the β–Ta structure or, more probably, to (002) planes of a hexagonal phase of tantalum nitride (Ta_2N). The main difference detected on the XRD pattern of this sample, at the ex-situ annealing temperature of 400 °C is a shift of the diffraction peak position towards the unconstrained position of the (002) peak of Ta_2N, probably due to stress relaxation induced by the thermal treatment helped by the eventual segregation of atoms in interstitial positions of the crystallites.

A significant structural development is detected after the annealing at temperatures above 600 °C (Cunha, 2018). Two new peaks appear (2θ = 34.1° and 2θ = 50.9°) and the broad peak detected in the as-deposited sample, still detected at T = 400 °C, develops to a sharp peak at 2θ = 38.8°. The set of four peaks observed in the XRD pattern can only be attributed to a hexagonal structure of tantalum nitride. They are close to angular positions of several peaks of hexagonal TaN_x structures, with x ≤ 0.5 (e.g., Ta_2N (ICDD 26-0985), $TaN_{0.5}$ (ICDD 089-4764), β-$TaN_{0.43}$ (ICDD 071-0265) and $N_{0.86}Ta_2$ (ICDD 031-1370)).

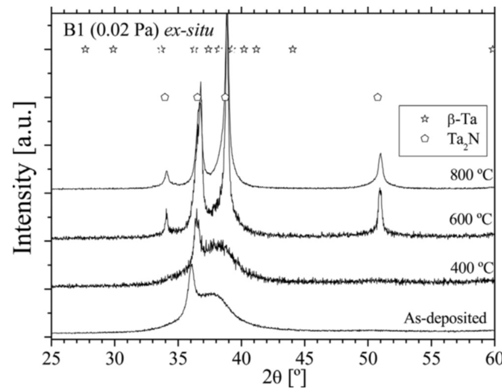

Fig. 2.32 XRD patterns: as-deposited and ex-situ annealed at 400 °C ≤ T ≤ 800 °C.

In figure 2.32, besides the XRD patterns at different temperatures, only the unconstrained angular positions of the XRD peaks of the Ta_2N and β–Ta phases are shown. The unconstrained positions of the remaining hexagonal TaN_x structures are not shown to avoid overloading the figure with excess of information, however, the angular positions of the peaks of the different tantalum nitride hexagonal structures are very close to those of Ta_2N.

Regarding the films produced with $P(N_2+O_2)$ = 0.04 Pa, the XRD pattern (figure 2.33) of the as-deposited film presents peaks that have to be assigned to a face centred cubic (fcc) structure. Taking into account the film composition, the detected crystallites can be attributed to structures of type TaN or/and γ-TaO (Fig. 2.33). The peaks are assigned to planes of the fcc structure: (111), (200) and (220).

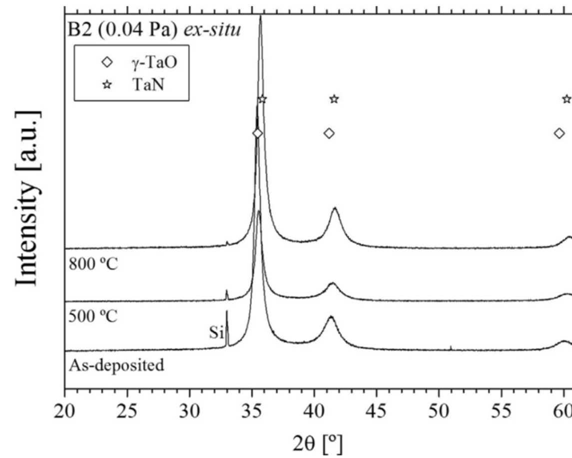

Fig. 2.33 XRD patterns: as-deposited and ex-situ annealed at T = 500 °C and T = 800 °C).

The structural stability of this film was also observed during the in-situ process. This is particularly important, taking into account that during the in-situ annealing the pressure was two orders of magnitude higher, compared to the ex-situ process. This could provoke oxidation, but this film revealed to be oxidation resistant enough. Figure 2.34 depicts the variation of the lattice parameter of the fcc-Ta(N,O) crystallites, as function of the annealing temperature, obtained from the most intense peak: (111). The dashed lines represent the unconstrained lattice parameter of the fcc TaN and γ-TaO structures. The experimental lattice parameter of the as-deposited sample for both processes should be the same, but the XRD patterns were obtained from different equipment. All things considered, the results are still inside a margin of error of 1%. For both annealing processes, a decrease of the lattice parameter is observed until 800 °C, becoming closer to the unconstrained lattice parameter of TaN. When the temperature increases, some of these atoms may be segregated to the boundaries, inducing a decrease of the lattice parameter, becoming closer to the TaN unconstrained lattice parameter.

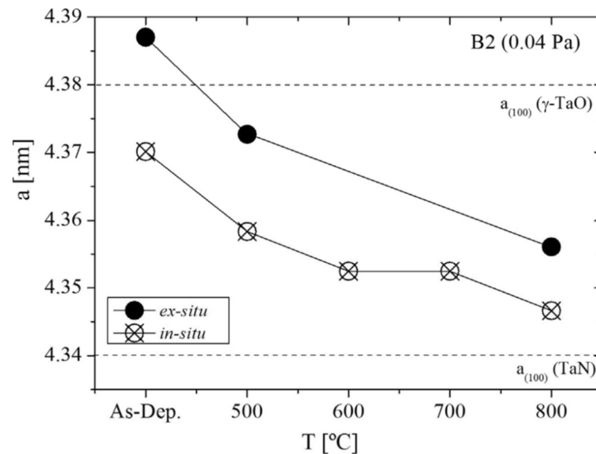

Fig. 2.34 Variation of the lattice parameter of fcc crystallites, as function of the annealing temperature, calculated from the (111) peak.

All the films produced with $P(N_2+O_2) \geq 0.13$ Pa exhibit an amorphous structure and very high structural stability after ex-situ thermal treatments up to 800 °C. In the region 25°< 2θ < 40°, a broad band is observed, coincident with the angular position of peaks belonging to Ta_2O_5 phases. These films reveal excellent structural stability, maintaining the amorphous condition, during the in-situ annealing process, but differently: in the case of samples B3 and B4, until T = 700 °C; in the case of sample B5 until T = 800 °C (Fig. 2.35). For the remaining temperatures, no noticeable changes were observed. At T = 800 °C, for samples B3 and B4, several diffraction peaks are identified and they can be clearly assigned to the monoclinic phase of tantalum oxynitride (m-TaON). There are several ICDD charts registering m-TaON structures with similar lattice parameters (e.g., 20–1235; 70–0178; 70–1193). In figure 2.35 are registered the unconstrained peaks positions of the m-TaON of ICDD 20–1235. The processing conditions seem to be able to promote the formation of the m-TaON phase if the temperature is high enough and the accumulated duration of in-situ annealing is long enough. In addition, a certain degree of oxidation during the in-situ annealing, which cannot be prevented, may facilitate the formation of this phase, not observable during the ex-situ annealing.

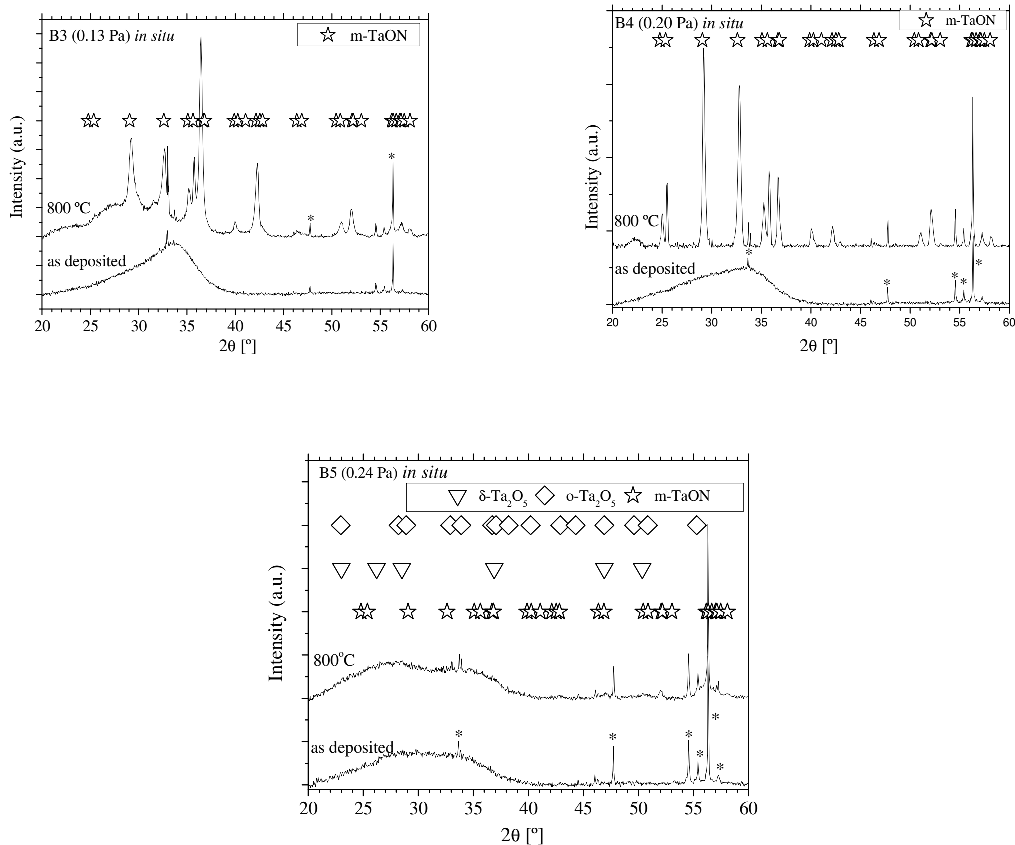

Fig. 2.35 XRD patterns of samples B3, B4, and B5 (– peaks due to the Si substrate): as-deposited and in-situ annealed at 800 °C.*

Chapter 3 - Ceramic composite thin films

3.1. Motivation and theoretical aspects.

In all tribological applications, the use of coatings deposited on a portant surface is an effective and relatively economical way to reduce friction and to protect the substrate surface from wear. However, selecting the appropriate deposition method and deposition coating materials for a particular tribological application is still difficult due to the fact that the tribological response of the system to the coating method depends on several factors, such as: the mechanical and tribological characteristics of the coating; the properties of the substrate and its opposite part (friction counterpart) and the working conditions of the friction couple. Tribological coatings must improve the wear resistance of the surfaces, consequently to ensure the extension of the friction couple life.

In recent decades, numerous coating methods have been successfully developed and used in tribological systems to reduce friction and protect surfaces from damage. Obtaining new and complex materials for tribological coatings is done today using deposition technologies, either with vacuum or at atmospheric pressures.

Most of the research in the field of tribological coatings is done nowadays using PVD methods, in particular standard or reactive magnetron sputtering using direct current, pulsed direct current, or radiofrequency sources.

The first generation of hard PVD coatings (with increased wear and corrosion resistance and a relatively small reduction in the coefficient of friction) was represented by metal nitrides, such as TiN, CrN, ZrN and ZrCN. These coatings have been commercially exploited since the early 1980s in cutting applications due to their high hardness compared to high-speed steel and for their decorative purpose due to their attractive appearance. TiN has a distinct golden-yellow color, CrN has a shiny-gray (silver-like) appearance, ZrN has a golden-green color, and ZrCN has a very similar appearance to gold, being therefor used in decorative applications (for watch cases, ornaments, etc.).

The second generation of PVD coatings was developed by introducing other elements, such as: Al, Cr, C, Y in the TiN crystal lattice: TiAlN, TiCrN, TiCN, TiAlYN, or using multilayers, such as: TiN/TiAlN; TiN/TiCN, TiAlN/CrN, TiAlYN/VN, etc. Through the addition of these elements, the characteristics of the PVD coatings (hardness, wear, coefficient of friction, adhesion to the substrate, corrosion resistance and oxidation resistance at high temperature, etc.) have been significantly improved.

The third generation of PVD type coatings has recently appeared and is aimed at diversifying the applications of vacuum deposited thin layers and improving their functional properties by:

- using the latest and most efficient methods of vacuum deposition;
- the use of new materials with complex structures and compositions.

For example, a nanocomposite coating consists of at least two immiscible phases, of which at least one has at least one dimension in the nanoscale (a nanocrystalline phase which can act as a reinforcing agent, and an amorphous phase (which takes the role of the matrix phase) or two nanocrystalline phases (one as the matrix phase). The nanocrystalline phase can be chosen from a myriad of materials: nitrides, carbides, borides and oxides of metals of group III, IV or V of the periodic table of elements, while the matrix phase may include metals, diamond-like carbon (DLC), hBN (hexagonal boron nitride) or $Si_{1-x}N_x$, and others (Erdemir, 2006).

Furthermore, a coating with a superlattice structure is obtained when two or more successive layers with thicknesses of less than 10 nm are deposited on top of eachother. It was reported that TiN/NbN multilayers with a superlattice structure, deposited by HiPIMS, can exhibit significantly higher hardness compared to their non-superlattice counterparts (Long, 2003). Recent research has shown that there is the possibility of creating hybrid layers, i.e., multiple thin layers with nanometric thickness (superlattice structures) whose cumulative properties (wear, corrosion, oxidation resistance, etc.) are significantly improved due to a synergistic effect (Kuznetsov,1999; Ehiasarian, 2002; Ehiasarian,2007; Christie, 2005; Clapa, 2006; Erdemir, 2006; Long, 2003; Veprek, 2008).

To expand the range of working temperatures for PVD coatings, considerable effort has been made to obtain complementary-cumulative properties for new coatings. Some of the first coatings which addressed this issue (high temperature resistance) were the solid lubricating compounds obtained from oxides and chalcogenides (PbO/MoS_2; ZnO/MoS_2; ZnO/WS_2) which can work in a wide range of temperatures (Voevodin, 2000).

Moreover, in recent years, a new concept called "chameleon coatings" has been developed by using new nano-composite structures, consisting of crystalline carbides (for example TiC) and transition metal chalcogenides (for example WS_2 or MoS_2) embedded in a matrix, for example hydrogen-free diamond-like carbon (DLC), using a hybrid deposition technique by combining pulsed laser deposition and magnetron sputtering (Voevodin, 2000).

Solid lubricants have been used in the aerospace industry for decades. Solid lubricants include lamellar solids, such as: transition metal chalcogenides (ex: MoS_2 and WS_2) and graphite, soft metals (ex: Pb, Au, Ag, In), and polymers (such as: polyamides and polytetrafluoroethylene = PTFE). There are certain industrial processes that take place in extreme lubrication conditions: high (or very low) temperatures, high pressures, very high speeds, etc. Due to the fact that in the above-mentioned conditions fluid lubricants cannot be used, the need to develop new deposition technologies that use new deposition materials with new coating structures, which will ensure as little wear as possible and therefore a longer life, becomes obvious.

As mentioned previously, ceramic materials, such as titanium nitride, titanium carbide, zirconium nitride, hafnium carbide, vanadium carbide, tungsten carbide, niobium nitride, tantalum nitride and many more, have been used successfully as coatings due to their good mechanical, refractory, corrosion resistance and electrical properties, including wear resistance. However, some drawbacks still exist. For example, titanium diboride (TiB_2) exhibits excellent physical and chemical properties such as high hardness, high melting point, good oxidation resistance and good corrosion resistance (Wang, 2014; Song, 2012-1). However, it has a very low fracture toughness and flexural strength (Gu, 2006-1), which severely limits its application as a structural material. This drawback is caused by its poor sintering capacity and densification (Song, 2012-2). The densification of monolithic TiB_2 requires a high sintering temperature (up to 2100 °C) and a long holding time due to the predominant covalent bonding and low self-diffusion coefficient (Mukhopadhyay, 2009; Raju, 2009). However, due to its superior properties, TiB_2 has already been studied as a material for wear components and cutting tools, among others (Gu, 2008). Tungsten carbide (WC) is another material that has been studied and used for hard coatings (Srivastava, 1986; Jhi, 2001) and electrochemical sensors (Nikolova, 2000), among other applications. The relevant properties for wear resistant applications are its high melting temperature (2870 °C), high hardness, relatively low thermal conductivity and excellent chemical stability (Beadle, 2008).

However, not disregarding the remarkable properties exhibited by the monolithic ceramics, in the recent years a new trend has emerged, that of ceramic composites (Jinga, 2015-1). These types of compounds exhibit many advantages over monolithic ceramic materials (Gu, 2006-1). Their main attribute is the possibility to tune the composition and structure in order to obtain optimal properties for the desired application. For example, in order to improve the mechanical properties of TiB_2, a number of metallic (nickel, cobalt, molybdenum, etc.) (Gu, 2006-2), and ceramic additives (TiC, Al_2O_3, etc.) (Bhaumik, 2000; Gu, 2006-1) can be used. The addition of these materials can positively alter the microstructure and mechanical properties of the TiB_2 ceramic, improving its strength, sintering capacity and toughness (Deng, 1998). Titanium has also been reported to be often used as matrix in composites reinforced with TiB_2 (Ma, 2002; Jeong, 2002). The wear resistance of the nanocomposite coating is improved due to the presence of TiB_2, while Ti (used as an interlayer) strengthens the adhesion between the composite coating and the substrate (Gebretsadik, 2011). Furthermore, the hardness of the TiB_2–Ti composite coating was reported to be enhanced over the rule-of-mixture value by 5–10 GPa (Ranade, 2012). The anti-frictional effect of TiB_2 was also observed for TiB_2–Ni composites (Zhu, 2013). Following this promising path, multiple component composites have been developed and studied (Mateescu, 2015). Ti/TiB_2/MoS_2 graded-composite coatings deposited by pulsed-dc magnetron sputtering exhibit improved wear properties for low Ti/Mo and S/Mo ratios (μ = 0.015–0.47) (Bidev, 2013). For TiB_2/TiC/WC composite coatings (Song, 2012-2), when the WC content is more

than 20 wt. %, the mechanical properties are improved, with flexural strength and Vickers hardness values of 955.71 MPa and 23.5 GPa, respectively.

This chapter presents results concerning the composition, morphological and mechanical characteristics (wear, adhesion to the substrate, hardness) for ceramic composite magnetron sputtered (Ti + TiB_2 + WC) coatings. The films were obtained by simultaneous standard/reactive magnetron sputtering from three targets (Ti, TiB_2 and WC).

3.1.1 Compound characteristics

Tungsten carbide (WC), which can be used as a tribological coating, due to its hardening and lubricating properties, is an inorganic chemical compound with the chemical formula WC (in which the number of W atoms is equal to the number of C atoms). This compound belongs to the family of transition metal carbides based on groups IV (Ti, Zr, Hf - with a hexagonal close-packed crystalline structure), V (V, Nb, Ta - with a body-centered cubic crystalline structure) and VI (Cr, Mo, W - with a body-centered cubic crystalline structure), characterized by:

- high hardness (which can translate to a high abrasion resistance);
- high elasticity/Young's modulus (which expresses the resistance to elastic deformation);
- very high melting temperatures (hence the name of refractory carbides);
- thermal stability (including thermal shock resistance) over a wide range of temperatures;
- very low chemical reactivity (at room temperature they are attacked only by acids or bases with very high concentrations and in the presence of an oxidizing agent);
- high thermal conductivity (facilitates the transfer of heat produced in the contact area).

In the phase equilibrium diagram of the WC system there are two types of chemical compounds, namely WC (higher tungsten carbide) and W_2C (lower tungsten carbide) with several polymorphic systems, which occur at different temperatures and concentrations of C.

Tungsten carbides (WC and W_2C) have very high hardness (8.5 ... 9 on the Mohs scale) and are used in the production of glass cutting alloys or in the manufacture of drilling tools as well as extra hard alloys. These carbides alloyed with Co (5%) are used for cutting tools, in which cobalt is used as a binder element of the carbide particles to the steel support and as a matrix for incorporating WC crystals. Some of the essential properties of WC are listed below:

- Melting temperature: 2785-2830 °C
- Vickers hardness: 2100
- Young's modulus: 550 GPa

Tungsten carbide deposited by magnetron sputtering fits perfectly into the family of non-stoichiometric interstitial compounds, i.e., chemical compounds with an elemental composition that cannot be represented by integers, which means that the correct chemical formula of a transition metal carbide obtained by magnetron sputtering is MC_{1-x} (and therefore the chemical formula of the non-stoichiometric tungsten carbide is WC_{1-x}), even though the sputtering target is stoichiometric. The cause of the non-stoichiometric character is represented by crystallographic defects, as well as due to the much smaller diameter of carbon atoms compared to the diameter of the transitional metals.

The carbides of transition metals from subgroups IV (Ti, Zr, Hf) and V (V, Nb, Ti), form carbides with a face-centered crystalline structure (Space group: Fm3m, Pearson symbol: cF8), exemplified by the reference crystal structure of NaCl.

Titanium diboride (TiB_2) is a refractory intermetallic compound of Ti and B with excellent properties: high hardness, high thermochemical stability, corrosion resistance, electrical conduction, etc. The properties of this material make it very attractive for certain applications: as an abrasive material, as a corrosion resistant material or refractory material.

TiB_2 crystallizes in a hexagonal structure (type C32), in which the planes of Ti, in rhomboidal (trigonal) structure and the planes where B resides, in hexagonal structure, alternate along the c (respectively z) axis, so that in the horizontal projection of the crystalline structure, two Ti atoms are inside the hexagonal network of B (on the large diagonal of the rhombus).

Significant attention is currently devoted to several characteristics of TiB_2 in thin film form, such as: morphological, structural, compositional, electrical, thermal and mechanical properties. The desired purpose for titanium diboride would be to manufacture hard coatings, wear resistant coatings, corrosion and oxidation resistant films, etc. Recent studies have shown that thin layers of TiB_2 have a low adhesion to stainless steel substrates, due to the high stresses that occur in the structure of the deposited layer. To eliminate these inconveniences, it is recommended to use an intermediate adhesion layer (usually Ti) or to apply a heat treatment to the substrate-coating system. Some of the essential properties of TiB_2 are listed below:

- Melting temperature: 2970 °C
- Young's modulus: 510-575 GPa
- Oxidation resistance up to 1000 °C
- Knoop hardness: 1800

3.2 Sample preparation.

For the deposition of the films presented in this chapter, a laboratory sized magnetron sputtering chamber was used. Three targets are placed at the top of the chamber, facing downwards, toward the substrate surface. The magnetrons positioned behind the targets are supplied independently by three DC (direct current) power supplies, with a maximum power of 600 W each. The sample substrate holder can be used either in static or in rotation mode. The targets were positioned at 12 cm above the substrates and have the following characteristics: a diameter of 50.8 mm (2 in.), 99.5% purity for the TiB_2 and WC targets, 99.99% purity for the Ti target. The TiB_2 target contains up to 0.12% carbon and 0.32% oxygen. The substrates (stainless steel and polycrystalline Si wafers), were polished, followed by ultrasonic and glow discharge cleaning. During the deposition process, the substrate holder was in rotation mode (20 rpm). The magnetrons were positioned in such a way to ensure a confocal deposition, to improve the homogeneity of the deposited films. The substrates were heated at 550 °C during the entire deposition period (150 min) and the polarization voltage on the substrate holder was set at 0.5 kV. Several trial runs were made before obtaining improved coating characteristics. Hereinafter the results concerning the samples with the best performance will be presented. These samples have been deposited with the following protocol: simultaneous sputtering deposition using all three targets, using different sputtering powers on each target; the chamber was evacuated to a base pressure of 9×10^{-6} mbar; a flow of argon of 150 sccm, corresponding to a partial pressure of 3.5×10^{-3} mbar was used as the plasma gas. The main difference between the two sets consists in the addition of N_2 as reactive gas during one of the deposition sessions, with a flow of 40 sccm, corresponding to a partial pressure of 5×10^{-3} mbar. The thickness of the coatings was estimated using an Inficon Controller (SQC 300) with crystal quartz microbalance equipped with four quartz crystals. The controller is capable of measuring in real time the deposition rate, by measuring changes in mass detected by a quartz crystal sensor. The sensor area and change in mass are used to calculate the deposition rate of the film deposited on the sensor. However, for complex materials with unknown densities in film form, such as the ones presented herein, a calibration factor must be used. According to previous calibration tests, in order to obtain the estimated thickness of the coatings, the measured thickness by the controller must be reduced by a calibration factor (between 3 and 6). The estimated coating thickness, obtained by multiplying the sputtering rate with the deposition period, was divided by a calibration factor of 6. The reasoning behind choosing this factor was to obtain an underestimated film thickness value, which would later on be used while setting the mechanical analysis protocols. If the estimated thickness would have been larger, the penetration depth used during nanoindentation would have been too large and therefore, the substrate would have influenced the measurement results. However, the estimated thickness was verified by ball cratering and the estimated results are in good agreement with the experimentally obtained data.

3.3 Results and discussions.

3.3.1. Composition and morphology

The chemical composition of the samples was assessed by Rutherford Backscattering Spectrometry (RBS) at the 3 MV Tandetron™ accelerator from "Horia Hulubei" National Institute for Physics and Nuclear Engineering using 4.47 MeV $^4He^{2+}$ ions. The measurements were performed in IBM geometry using normal incidence and a laboratory scattering angle of 165°. Scattered particles were registered with an AMETEK type BU-012-050-100 charged particle detector, having a solid angular acceptance of 1.641 msr, connected to a standard spectrometric chain and acquisition system. The typical energy resolution of the spectrometer was 18 keV. The RBS spectra were evaluated using SIMNRA code.

The Rutherford Backscattering Spectrometry (RBS) technique can be used to determine the chemical composition and areal density (atoms/cm^2). Since the density of the deposited samples is not known and it may differ from the bulk's one, the areal density cannot be correctly converted into nanometers (Malinsky, 2012). In case of the sample which was deposited using N_2 as a reactive gas, by assuming the bulk mass densities of 17.8, 2.56 and 7.54 g/cm^3 for WN, TiB_2N and WCN, the following thickness was determined: 1240 nm, corresponding to an areal density of 1.08 × 10^{19} atoms/cm^2. The mean composition for this sample was $W_{0.16}C_{0.02}Ti_{0.07}B_{0.2}N_{0.45}O_{0.1}$. Furthermore, assuming the bulk mass densities of 15.63, 4.52 and 4.5 g/cm^3 for WC, Ti and TiB_2, in the case of the sample deposited in standard DC sputtering mode (without reactive gas), the following thickness was estimated: 1380 nm, corresponding to an areal density of 1.75 × 10^{19} atoms/cm^2. The mean composition for this sample was $W_{0.31}C_{0.3}Ti_{0.16}B_{0.15}O_{0.08}$. In both cases, after reactive or non-reactive sputtering from the three targets, oxygen was present in the surface layer (8–10% concentration). The presence of oxygen can be due to several factors: firstly, as a residual gas in the deposition chamber; secondly, oxygen existent as an impurity in the TiB_2 target (0.32%); thirdly, oxidation in open atmosphere, after the deposition process. Comparing the estimated thicknesses calculated using the crystal quartz microbalance results, to the estimated thicknesses calculated from the RBS measurements, a significant difference was observed, especially for the sample obtained with reactive sputtering (with the addition of nitrogen in the deposition chamber). This sample exhibits an increase of almost 40% in thickness, while in the case of the non-reactive sputtered sample, a slight decrease, of ∼100 nm is noticed. The significant difference might be due to the initial assumption that the simultaneous deposition from three targets will result in stoichiometric films. However, the obtained coatings are nonstoichiometric compounds, as can be observed from the mean compositions. The RBS patterns can be observed in Fig. 3.1. A good agreement between the experimental data and simulation results is evident.

The roughness was analyzed using a MultiMode NanoScope IIID Controller microscope (Digital Instruments Veeco Metrology Group, Santa Barbara, CA, USA) equipped with a 125 m piezoelectric

scanner. Images were obtained in tapping mode in air using a TESP (0.01–0.025 Ωcm Antimony (n) doped Si) tip at a scan speed of 1 Hz at 512 pixels per line scan. Tapping mode is the most popular atomic force microscopy (AFM) technique which allows high resolution topographic imaging of sample surfaces, including surfaces that are easily damaged or otherwise difficult to image by other AFM techniques. Acquisition and offline analyses were performed using SPIP 6.0.9 and 531r1 NanoScope software. Images were processed by first order flattening to remove any background tilt. The topography of the coatings deposited on stainless steel was qualitatively investigated after the wear tests by profilometry using a DEKTAK 3030 surface profilometer.

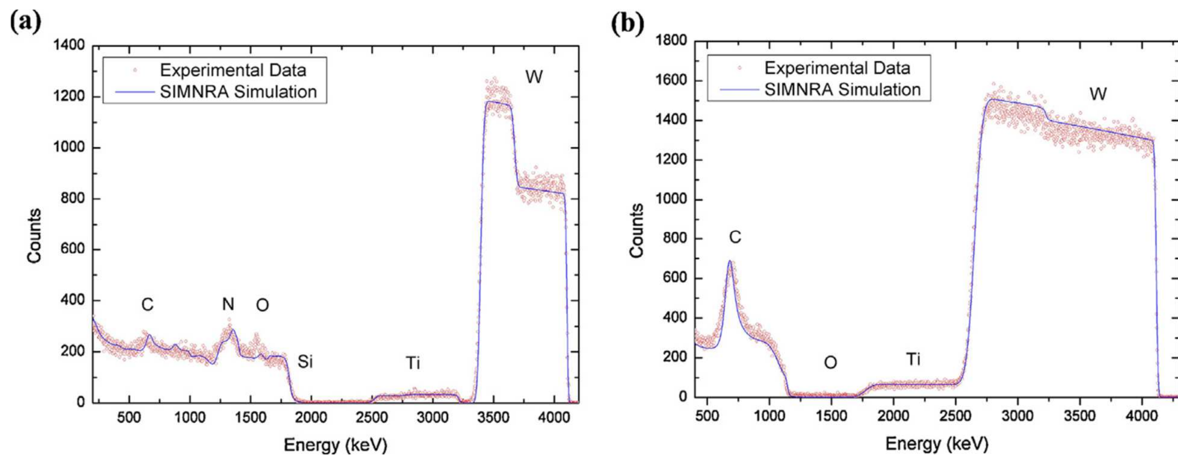

Fig. 3.1. 4.47 MeV $^4He^{2+}$ back scattered at 165° from a single layer structure ((a) – reactive deposited sample and (b) – standard sputtered sample, deposited on silicon (dots – experimental data, solid lines – simulation).

The morphology of the films, deposited on Si and steel substrates, was assessed by AFM. Figures 3.2a and 3.2b show topographical images of the two samples deposited on polycrystalline Si wafers. The results are showing a granular structure for both types of compounds, with a RMS (root mean square) roughness value of 6.79 nm for the sample (Ti + TiB_2 + WC + N_2), and of 10.4 nm for the sample (Ti + TiB_2 + WC). Both values can be considered to be low, although a significant increase (53%) for sample (Ti + TiB_2 + WC) is noticed.

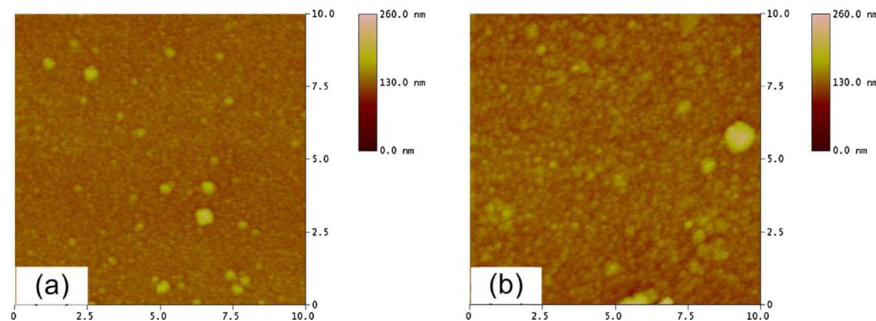

Fig. 3.2. Tapping mode AFM images of: (a) (Ti + TiB_2 + WC + N_2) and (b) (Ti + TiB_2 + WC), deposited on silicon.

In figure 3.3(a–d), one can observe the comparison between the topography features corresponding to the two samples deposited on stainless steel plates, before and after the wear tests. The Ti + TiB_2 + WC sample exhibits a smoother surface after the wear test and a significant decrease of roughness on the wear track, from RMS = 41.6 nm to RMS = 15.9 nm. The Ti + TiB_2 + WC + N_2 sample, however, exhibits an increase in roughness on the wear track, from RMS = 38.8 nm before the wear test, to RMS = 55.5 nm after the wear test. The same z scale was used for direct comparison. The roughness of the coatings deposited on stainless steel is much higher than the roughness of the coatings deposited on polished Si due to the initial higher roughness of the stainless-steel plates (before deposition).

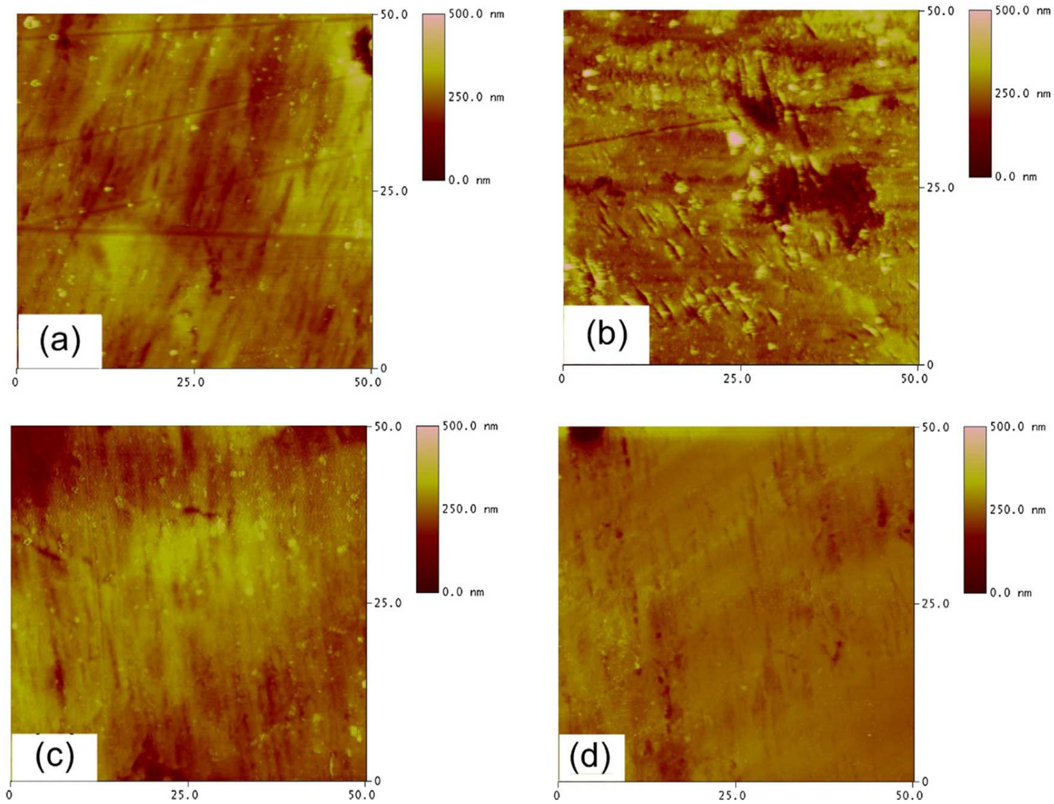

Fig. 3.3 Tapping mode AFM images of: sample (Ti + TiB_2 + WC + N_2) deposited on steel plates, before (a) and after the wear test (on the wear track) (b); sample (Ti + TiB_2 + WC) deposited on steel plates, before (c) and after the wear test (on the wear track) (d).

The topography of the samples deposited on stainless steel was investigated also after the wear tests by profilometry. A single trace was scanned on the diameter of the wear track for both samples. The resulting profiles can be observed in Fig. 3.4 (a - sample (Ti + TiB_2 + WC + N_2), b - sample (Ti + TiB_2 + WC). One can notice that the wear track on sample (Ti + TiB_2 + WC + N_2) is clearly visible. The depth of the wear track is greater than the estimated film thickness, which means that the film was removed in its entirety.

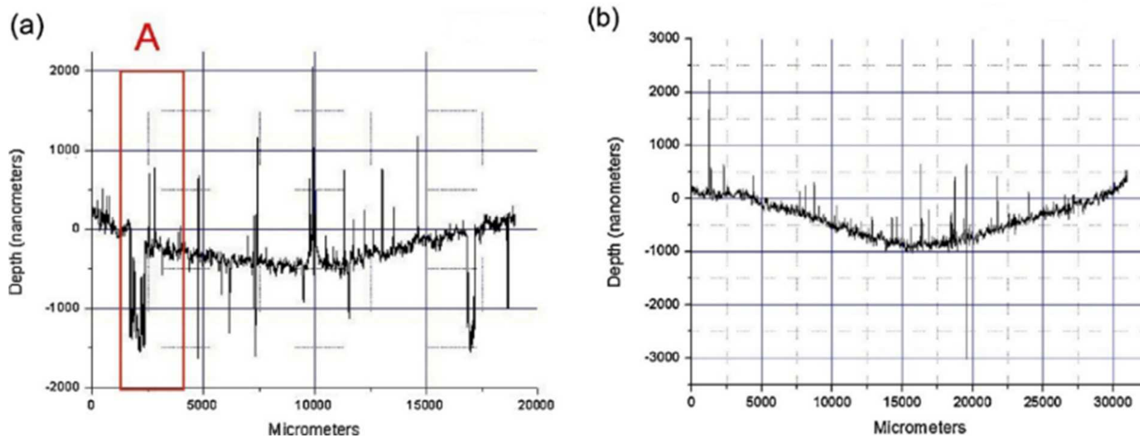

Fig. 3.4. Surface profile of sample (Ti + TiB_2 + WC + N_2) (a) and sample (Ti + TiB_2 + WC) (b), after the wear tracks were made.

3.3.2 Mechanical characterization.

The mechanical characterization was assessed by instrumented indentation, to measure the indentation hardness and indentation elastic modulus; by scratch tests, to determine the critical adhesion loads between the deposited coatings and the substrates; and by wear tests, to measure the friction coefficient.

Nanoindentation measurements were performed on a device produced by CSM Instruments (NHT-2) equipped with a Berkovich diamond tip. To minimize substrate contributions the indentation experiments were performed controlling the depth penetration of the indenter. This parameter was set at values lower than 10% of the estimated film thickness. The hardness and indentation elastic modulus were determined following the model of Oliver and Pharr (Oliver, 1992). On each series of samples, for statistical relevance, at least 15 measurements have been made, with the following protocol: linear loading, loading rate = 400 nm/min, unloading rate = 800 nm/min. The load resolution of the apparatus is 40 nN, with a usable indentation load range between 0.1 and 500 mN. The thermal drift, which can influence the measurements with indentation depths lower than 100 nm, is countered with the use of a zirconium reference ring. This ring is in contact with the sample surface and acts as a local environmental enclosure to passively protect the measurement location from air currents, sound waves and changes in humidity and temperature. For comparison purposes, nanoindentation measurements have been performed also on the steel substrate material and on the pin material, which was later-on used for the wear tests.

The scratch tests, used to assess the adhesion of the coatings to the substrate, were performed on a Micro Scratch Tester (CSM Instruments) using a diamond tipped indenter with a Rockwell geometry

(tip radius = 100 μm). The load was applied progressively with a speed of ~5 N/min. The length of the tests was set at 4 mm. Three tracks were made on each sample.

Mechanical wear tests were carried out at room temperature, in air atmosphere using a pin-on-disk tribometer from CSM Instruments, in rotation mode. The variation of the dynamic friction coefficient against a 6 mm diameter pin, positioned at a 45° angle relative to the sample surface (point-on-flat contact), without lubricant, was observed. Both the samples and the pins were ultrasonically cleaned in an ethanol bath prior to the wear tests. The mechanical characteristics of the counter-body (pin – AISI 100Cr6 steel) are presented in Table 3.1. The normal load applied on the pin and therefore on the sample surface, was 1 N. The stop condition was set at different distances, in order to observe the friction variation as function of distance.

The mechanical characteristics of the (Ti + TiB_2 + WC) composite coatings, deposited with or without nitrogen as a reactive gas, (indentation hardness, indentation elastic modulus, dynamic friction coefficient and critical adhesion loads) can be observed in Table 3.1. For comparison purposes the indentation hardness and elastic modulus for the steel substrate and wear pin are presented as well. A first look at the nanoindentation results shows slightly better characteristics for the sample that was deposited without the presence of N_2 in the sputtering chamber. It was reported elsewhere, for TiB_2/N compounds, that the incorporation of nitrogen has adverse effects on the mechanical characteristics, due to the formation of the soft BN phase in the film (Rupa, 2014). If this is the case, then the deposition conditions along with the nitrogen incorporation could play an important role in influencing the hardness of ((Ti + TiB_2 + WC) + N_2) – type composite films.

Table 3.1 Nanoindentation, wear and adhesion results for the (Ti + TiB_2 + WC) composite thin films.

Sample	Nanoindentation				Adhesion			Wear
	H_{it} [GPa]	E_{it} [GPa]	H/E	H^3/E^2	Lc1 [N]	Lc2 [N]	Lc3 [N]	Friction coefficient
Ti + TiB_2 + WC + N_2	20.53 ± 9.18%	247,31 ± 5.60%	0.08	0.14	-	0.4 ± 12.5%	6.61 ± 5.95%	0.18 ± 27%
Ti + TiB_2 + WC	22.9 ± 9.67%	300,38 ± 7.44%	0.07	0.13	0.63 ± 3.72%	1.24 ± 3.23%	7.61 ± 4.6%	0.23 ± 6.78%
Substrate (steel)	3.43 ± 5.31%	232.24 ± 5.18%	-	-	-	-	-	-
Pin	4.62 ± 12.07%	209.36 ± 6.50%	-	-	-	-	-	-

The variation of the loading–unloading curves as a function of the penetration depth for the (Ti + TiB_2 + WC) films is presented in Fig. 3.5. One can observe that the load necessary to obtain the same

penetration depth (100 nm) is around 4.5 mN for sample Ti + TiB_2 + WC, compared to ~4 mN for sample Ti + TiB_2 + WC + N_2 (the one deposited with N_2 as a reactive gas). However, the rest of the loading–unloading curve parameters are relatively similar: the plastic deformation and therefore the elastic deformation for this penetration depth are comparable for the two samples. Moreover, using the hardness and elastic modulus values, it is possible to evaluate other important key parameters, which can predict the wear behavior of the films. The H/E ratio can provide information about the wear of the films (Oberle, 1951), while the H^3/E^2 ratio gives information about the resistance to plastic deformation. Observing the values for these two ratios (Table 3.1), the sample deposited without nitrogen should, in theory, behave slightly better during the wear tests. The film adhesion to the steel substrate was determined by scratch tests. The critical load values were obtained after optical analysis of the wear tracks, and these are defined as follows: Lc1 – the load necessary for the emergence of the first cracks (fissures) in the film, Lc2 – the load corresponding to the first delamination of the film (the substrate should be visible), Lc3 – the load responsible for the delamination of more than 50% of the film from the scratch track. In the case of sample Ti + TiB_2 + WC + N_2, the optical Lc1 critical load was not observed, even with higher magnifications.

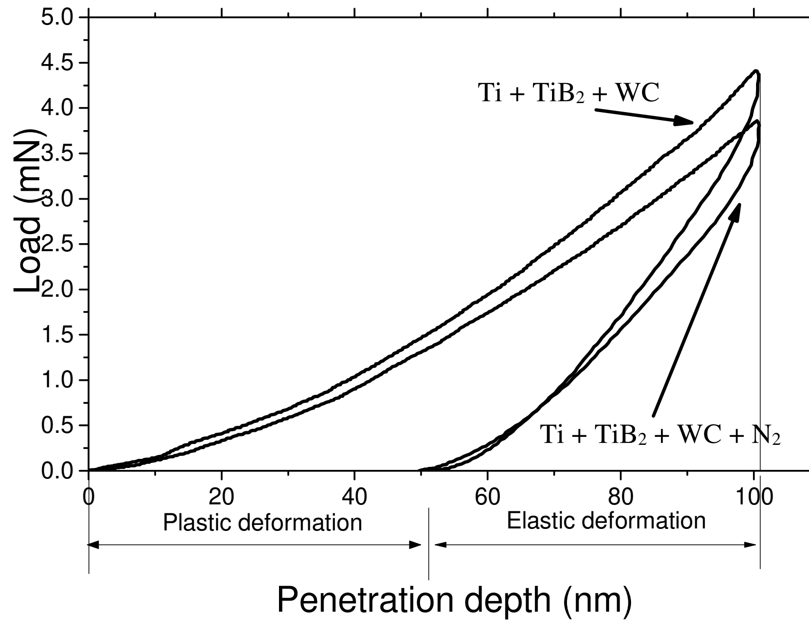

Fig. 3.5. The representative load/displacement curves for the (Ti + TiB_2 + WC) films, deposited on steel.

Overall, the films exhibited poor adhesion to the steel substrate. The first failures were observed for loads smaller than 1 N (Lc2 for sample Ti + TiB_2 + WC + N_2 and Lc1 for sample Ti + TiB_2 + WC). A combination of several factors can influence the adhesion to the substrate, such as: toughness, stiffness, strength under shock, hardness and others, for both the substrate and coating material. In this particular case one of the main reasons for the very low critical loads is the discrepancy between

the film and substrate mechanical characteristics, especially the very large difference in hardness. Considering the low hardness of the substrate (H_{it} ~ 3.5 GPa), it can be said that the substrate is easily deformed under the load applied by the indenter, especially plastically, and the coating is no longer supported by the substrate. This observation is confirmed by the analysis of the failure features for the (Ti + TiB_2 + WC) coating, presented in Fig. 3.6. According to reference (Bull, 1991), the shape (chevrons) and orientation of the cracks (open to the direction of the scratch) observed in the image corresponding to Lc1 for sample Ti + TiB_2 + WC, are characteristic to the process called through-thickness cracking. This phenomenon is usually followed by recovery spallation (as it can be observed in the images corresponding to Lc2 for both samples), where the coating is delaminated due to the elastic recovery which occurs behind the stylus as it travels over the coated surface. Moreover, the stiffness for sample Ti + TiB_2 + WC is significantly higher in relation to the one exhibited by sample Ti + TiB_2 + WC + N_2 (deduced from a higher value for the elastic modulus), this parameter contributing to the slightly better adhesion to the substrate. Even if the Lc3 loads are some-what comparable, the films are already considered compromised starting with Lc2.

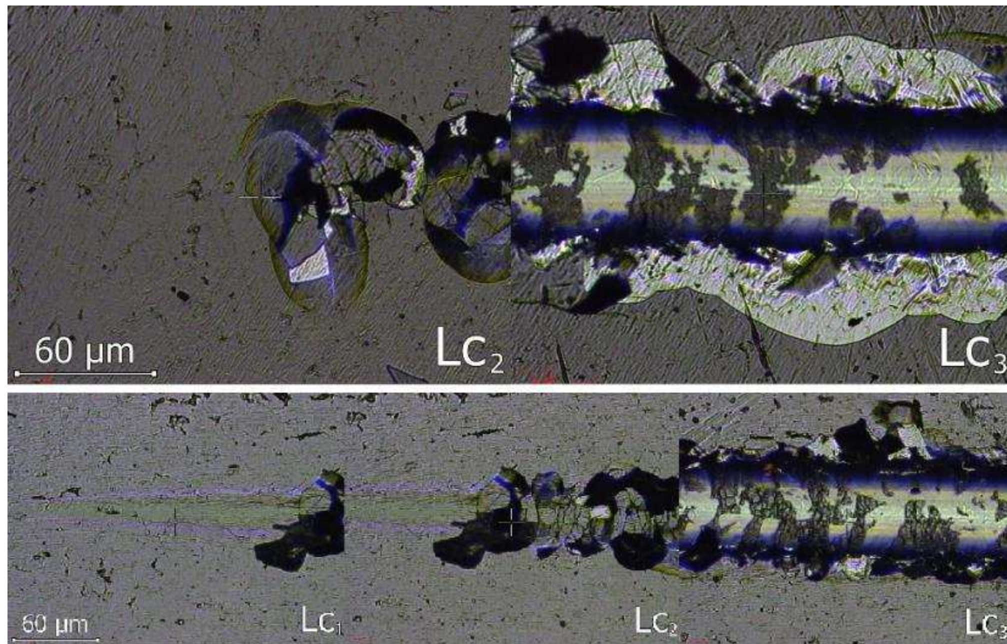

Fig. 3.6. Thin film failure features, observed on the scratch tracks for sample Ti + TiB_2 + WC + N_2 (a), and sample Ti + TiB_2 + WC (b).

The variation of the dynamic friction coefficient as a function of sliding distance for two of the test runs done on sample Ti + TiB_2 + WC + N_2, as well as one representative test done on sample Ti + TiB_2 + WC, can be observed in figures 3.7a and 3.7b, respectively. If one analyzes the graphs presented in these two figures certain observations can be made: firstly, both samples exhibit a low friction regime signified by $\mathbf{t_1}$, followed by a high friction regime, marked with $\mathbf{t_2}$. The average friction coefficients,

presented in Table 3.1, were calculated only for the low friction regimes, due to the fact that the high friction regime has origin in the partial (sample Ti + TiB_2 + WC) or total (sample Ti + TiB_2 + WC + N_2) film failure; secondly, a much better wear behavior can be observed in the case of sample Ti + TiB_2 + WC + N_2, deduced from the longer distance until the high friction regime is reached. If one analyzes the sample surface profiles presented in figure 3.4, one can notice that the film failure in the case of sample Ti + TiB_2 + WC + N_2 is total, due to the negative peak situated below the estimated film thickness for this sample. One factor contributing to this increased abrasion could be the rise in roughness, as observed after the AFM analysis, from 38.8 nm (before the wear test) to 55.5 nm (on the wear track). The wear tracks on the surface of sample Ti + TiB_2 + WC cannot be observed on the profile from figure 3.4, which would lead to two observations: firstly, the film, at least in these test conditions, is wear resistant; secondly, the change in friction regime could be attributed to material buildup in front of the pin. If the dislodged material is naturally removed, a drop of the friction coefficient is noticed (in the 300–400 m region).

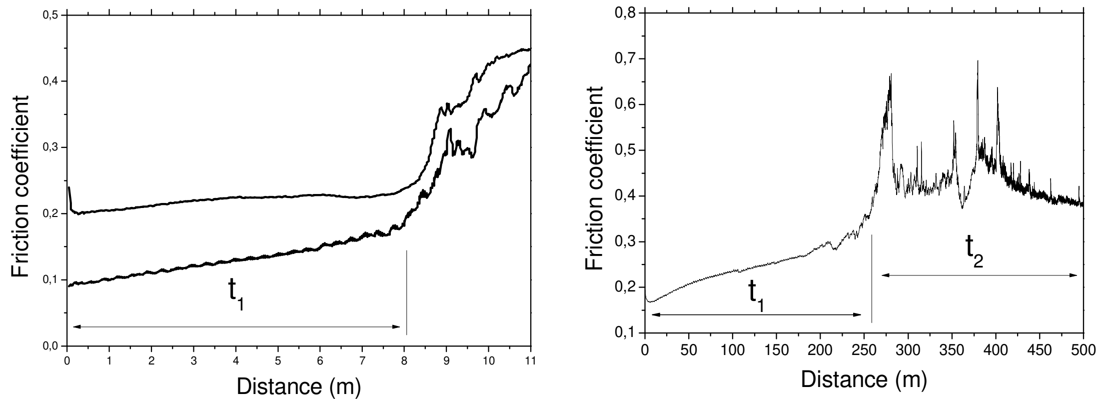

Fig. 3.7. The variation of the friction coefficient as function of the distance for sample Ti + TiB_2 + WC + N_2 (left), and for sample Ti + TiB_2 + WC (right).

However, one has to consider the relatively low normal load applied on the pin during the wear tests. Considering the lack of adhesion, due to the significant difference in hardness measured on the substrate and on the films, it would be expected that the films would fail much more quickly if higher normal loads would be used on samples using a substrate with the same characteristics. The failure of sample Ti + TiB_2 + WC + N_2 can be attributed to the lower hardness, compared to sample Ti + TiB_2 + WC, meaning that the film was not able to withstand for a long period of time the normal load applied on the pin. If certain precautions would be taken, such as a significantly harder substrate and considering the other mechanical characteristics of the films presented in this chapter, (Ti + TiB_2 + WC) composite films could potentially be used as wear resistant coatings (Jinga, 2015-2).

Chapter 4 – Magnesium-based ternary nitride thin films

4.1 Motivation and theoretical aspects.

Corrosion protection is one of the most important applications of thin solid films, both in terms of total surface coated area and economical value. Hence, improving the corrosion resistance of corrodible parts by applying proper surface coatings and surface modifications can lead to significant economical benefits as well as the preservation of resources. Corrosion protection requires a suitable coating material and a suitable coating structure for this particular application. Generally, an appropriate surface finishing (e.g., a mechanical pretreatment or a thermochemical treatment) can be necessary to prepare the surface of the parts to be protected, before the deposition of the thin film. The coating material must be either cathodically protecting or inert and defect-free.

Most wear resistant and hard coatings possess also a high corrosion resistance. However, when deposited on less noble (more easily corodable) materials like steel, brass, Al or Mg alloys, the coated parts, when exposed to a corrosive medium, suffer significant corrosive damage due to inherent defects or inhomogeneities in the thin film (cracks, pores, transient grain boundaries), mostly due to inadequate deposition conditions (Park, 1990; Jehn, 1992; Jehn, 1993; Creus, 2000; Fenker, 2006). These surface defects are causing the appearance of channels, through which the corrosive media can reach the substrate. Consequently, galvanic corrosion at the substrate will occur if a less noble substrate material was used. This kind of corrosion, namely galvanic corrosion, is localized to the defect area and is characterized by the anodic dissolution of the substrate material with a high anodic current density at the defect site. If pores and pinholes are the type of surface defects, pitting corrosion occurs. If the coating material does not cathodically protect the steel substrate, the corrosion behavior depends on the number and size of pores and/or on the chemical composition of incorporated particles (e.g., droplets or foreign particles). These kinds of defects strongly depend on the deposition technique used for coating application.

To suppres or minimize the occurance of surface defects which can lead to poor corrosion performance, several coating or surface treatment technologies can be employed sequentially. Duplex processes (duplex treatments or duplex surface engineering) involve the sequential application of two surface technologies to produce a surface composite with combined properties which are unobtainable through the individual surface technology (Bell, 1998). An example of a duplex treatment consists of plasma nitriding plus deposition of a hard PVD coating. Another example of a duplex process consists in ALD (atomic layer deposition) sealing of a hard PVD coating. A third example of a duplex process is the already established duplex treatment of depositing a very thick electroplated coating and subsequently applying a hard PVD coating.

Another promising approach in terms of corrosion protection of a less noble substrate is to consider the coating as a sacrificial agent, while trying to maintain as much as possible the mechanical characteristics (high hardness, high wear resistance, etc). Several reports from the literature mention the use of Mg, Al, or other elements as the dopant in an already known hard coating, for example TiN, thus obtaining for example a TiMgN coating (Balzer, 2018). The hypothesized corrosion protection mechanism is divided into several components, as follows:

1. In the beginning a temporary cathodic protection of the low-alloyed steel will prevail by the preferred anodic Mg dissolution.
2. Related to this is the alkalization of the adjacent electrolyte up to about pH 10 by formation of $Mg(OH)_2$, which causes the steel to passivate and achieve some tolerance towards chloride ions. The relatively large amount of dissolved Mg in the electrolyte of the defects probably leads to a buffering effect, which extends the protective effect in time.
3. The third mechanism is the attraction of chloride ions to the places of anodic dissolution of Mg from the TiMgN, thus reducing their concentration on the steel substrate.

However, the main drawback of this proposed method is a significant loss in terms of mechanical properties (significantly lower hardness, for higher Mg contents). Therefor, a balance between the corrosion protection capacity and the mechanical properties should be found. Building on the foundation started by other researchers (Fenker, 2014; Fenker, 2019; Balzer, 2018), the objective of the research presented in this chapter was to observe whether the hypothesis of doping with Mg other transitional metal nitrides leads to the same results, i.e., improved corrosion behavior, coupled with adequate mechanical properties. The underlying scope is to develop a surface treatment technology which adequately protects a less noble material, in a single processing step (unlike the duplex processes).

O. Banakh et al. (Banakh, 2004) mention the fabrication of TiMgN thin films, by reactive magnetron sputtering from Ti and Mg metallic targets in a mixed Ar/N_2 reactive atmosphere. The Mg content in the coatings was adjusted by the target power and by partial shuttering of the Mg target. It was observed that, with the increase in Mg content, from 2.5 at.%, to 16 at.%, the color of TiMgN coatings changes from golden (TiN) through a brownish–yellow (2.5 at.% Mg) to violet (4 at.%) and grey (16 at.%), while the oxidation resistance of the TiMgN coatings is much higher as compared to TiN (the higher the Mg content, the higher the oxidation resistance of the coating). Similar findings were reported elsewhere, both in terms of color variation, and oxidation resistance (Hodroj, 2011). Moreover, increasing the Mg content up to 35 at. %, it was observed that the morphology of TiMgN coatings is columnar up to a Mg content of 24 at. %, with no columnar structure observed in coatings with higher Mg content. Increasing the Mg content in TiMgN coatings over 17 at. % leads to a decrease in hardness

(Fenker, 2005). Sakip Onder et al. reported that the addition of Mg equivalent to x = 0.064 in TiMgN coatings did not form separate Mg or magnesium nitride phases, instead, Mg incorporated in the TiN structure. The Mg-doped TiN structure acted as a magnesium source promoting the Mg-substituted hydroxyapatite formation in simulated body fluids, potentially allowing improved tissue integration, in biomedical applications (Onder, 2013; Onder, 2015). In terms of corrosion protection, Balzer et al. (Balzer, 2018) found that a 2.5 µm thick TiMgN monolayer, containing 34 at. % Mg and 41 at. % N, deposited by co-sputtering on substrates rotating in front of Ti and Mg targets could protect steel substrates for at least 24 h in NSS tests with no red rust visible on the sample surface, independent of the number of growth defects. Compared to TiN, the TiMgN (34 at.% Mg) coating has a strongly reduced hardness, but also a reduced friction coefficient and wear depth against Al_2O_3 balls.

However, with the exception of TiMgN, reports on other types of RM-Mg-N compounds could not be found. Reckeweg et al. observed that Mg in general seems to form many fewer ternary nitrides compared with those of Ca, Sr and Ba. However, from the development of quaternary Ba-Mg-M-N materials (Reckewe, 2001), where M = Nb or Ta, it can be inferred that the ability of Mg to share the same crystallographic site with Nb or Ta in nitride compounds could lead to potentially interesting Nb/Ta,MgN-type compounds. In the case of NbN or TaN, when some of the Nb or Ta atoms are substituted by Mg ones, new compounds (NbMgN or TaMgN) might form. Since NbMgN or TaMgN are derived compounds from NbN, TaN and MgN, they should incorporate the advantages and characteristics of these species. The atom substitution of Nb or Ta by Mg may distort the lattice constant, for the former (Nb atomic radius = 215 pm, Ta atomic radius = 220) are bigger than the latter in diameter (Mg atomic radius = 173 pm). As a result, the NbMgN or TaMgN films may possess different expected hardness values than NbN, TaN and MgN films.

The purpose of the research presented herein was to study the chemical, structural, morphological and, consequently, property variation concerning RM-Mg-N (RM – refractory metal) multiple component nitride-type thin films, obtained by simultaneous sputtering of two metallic targets (high purity RM and Mg), with the addition in various proportions of reactive gas (N_2). The RM candidate was chosen after preliminary tests in respect to the corrosion behavior of RM-N-type coatings, where RM = Zr, Hf, V, Nb, Ta, Cr, Mo, or W.

4.2. Experimental details and results.

The coatings presented herein were deposited by reactive DC magnetron sputtering. The depositions of the samples were done in a vacuum plant Leybold L560 UV (base pressure < 1.5×10^{-3} Pa) using a special magnetron arrangement. It consists of three circular 2" magnetrons (US Inc.) arranged in a triangle all facing a one-fold rotating flat substrate holder, positioned at a distance of 4.5 cm from the magnetron surface.

In the first phase, binary nitrides of transitional metals were deposited with varying nitrogen contents, in order to assess which configuration exhibits the lowest and most stable OCP potential. For the RM-Mg-N samples (Phase II), two cathodes were used for each deposition, one equipped with a Me (99.9 at.% purity) and one with a Mg-target (99.95 at.% purity). A suitable high rotation speed of the substrate holder (100 rpm) ensured that no complete atomic layer could grow per turn.

The desired Mg-contents of the MeMgN films were realized by adjusting the power fed to the Mg-target while keeping a constant target power for the Me magnetron. All coatings were deposited at a bias voltage U_{bias} = -50 V and a total pressure of p = 0.4 Pa. Prior to the depositions the substrates were plasma etched at U_{bias} = -1000 V at p_{Ar} = 2.6 Pa with cathode support.

The first choice for substrates was Si, since it is smooth, flat and has a single crystal structure, with clearly known diffraction peak positions. All investigations required to understand the structure, composition and properties could be easily performed on films deposited on Si substrates.

For mechanical properties measurements, especially adhesion and wear rates, and also for corrosion resistance, films were also deposited on 100Cr6 and high-speed steel (polished to a mirror–like finish, and sand blasted) and polished and partially sand-blasted or etched glass. Since when depositing hard coatings on smooth surfaces, without interlayers, adhesion problems and delamination can occur, using sand-blasted substrates was the chosen method to improve the adhesion.

a. Phase I

The aim of Phase I was to create a database for electrochemical properties of coatings from up to 8 RM-N systems (RM: refractory metal), from groups IVb, Vb, and VIb of the periodic table. The coatings were deposited by magnetron sputtering in Ar/N_2 atmosphere with medium and high N_2 flux. The results were compared to former investigations on the Ti-N system.

The selection was made on the basis of the electrochemical measurements in NaCl solution (0.8 M) by means of the open circuit potential, E_{OCP}, of the RM-N coatings. Considering that the aim is to reduce the amount of magnesium from the samples deposited in Phase II, necessary to receive an excellent corrosion behavior (Balzer, 2018), the RM-N coatings with the lowest E_{OCP} were sought after. The closer E_{OCP} of the coating is with respect to the E_{OCP} of the low-alloyed substrate steel, the lesser Mg will be needed to shift the E_{OCP} below the one of the low-alloyed steel.

Table 4.1 - Deposition parameters for Phase I samples

Target material	N2 flux	
	medium	high
Zr	1	1
Hf	1	1
V	1	1
Nb	1	1
Ta	1	1
Cr	1	1
Mo	1	1
W	1	1
Total number of depositions:		**16**

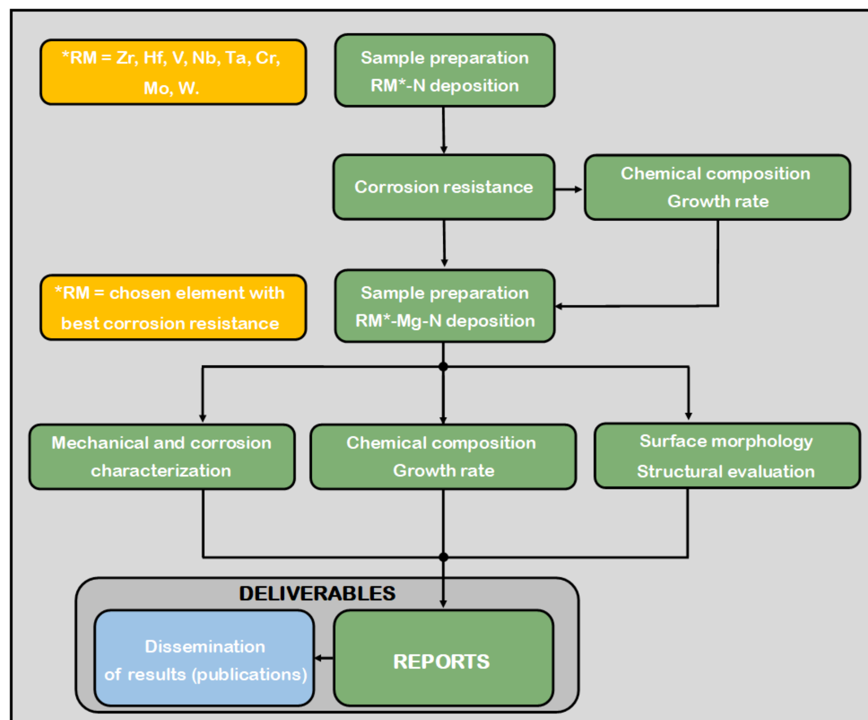

Fig 4.1 Research activities workflow.

The reactive gas flow, namely nitrogen, was chosen based on the hysteresis curves obtained for each target material (the variation of the target voltage as function of the applied nitrogen flow). The following graphs present these hysteresis curves, and the nitrogen flow used for each deposition (marked with a vertical line).

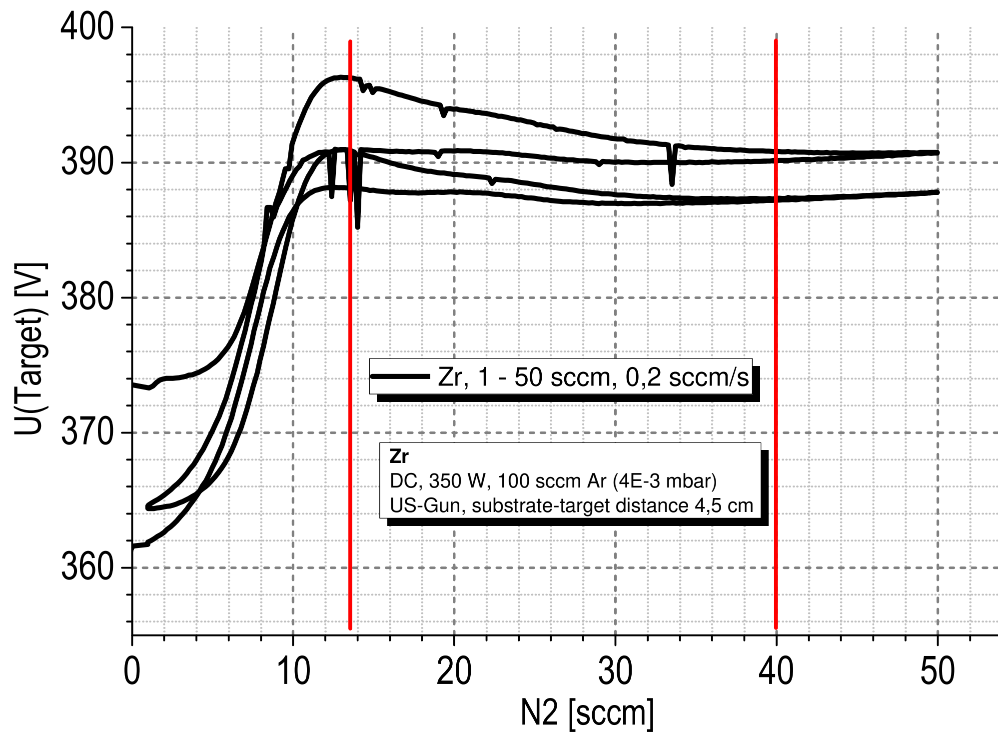

Fig 4.2 Hysteresis curve (the variation of the target voltage as function of the applied nitrogen flow), for the Zirconium target. The nitrogen flows used for the depositions were 13 sccm and 40 sccm.

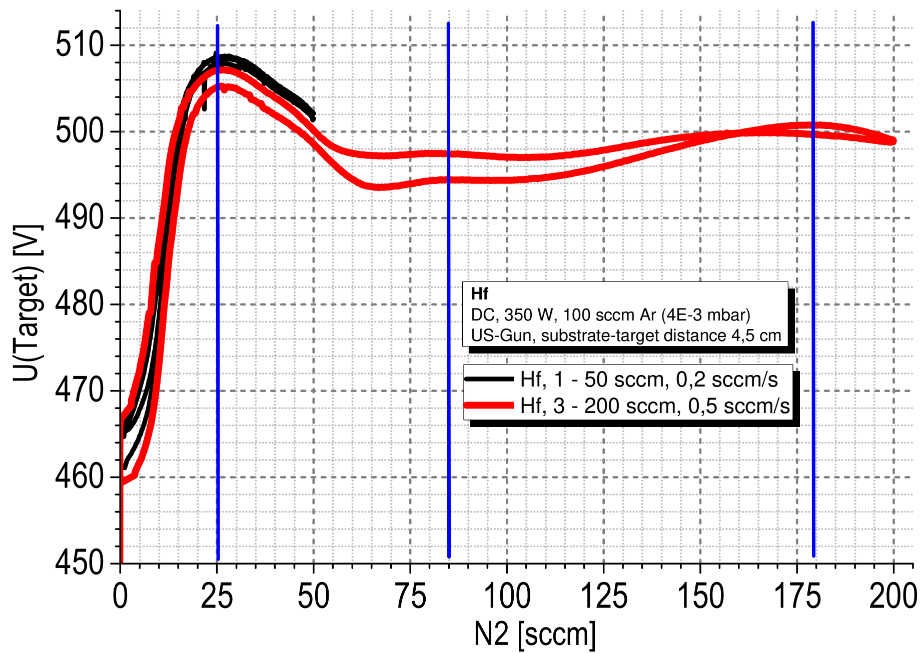

Fig 4.3 Hysteresis curve (the variation of the target voltage as function of the applied nitrogen flow), for the Hafnium target. The nitrogen flows used for the depositions were 25 sccm, 85 sccm and 180 sccm. Hafnium is the only material where three nitrogen flows were used.

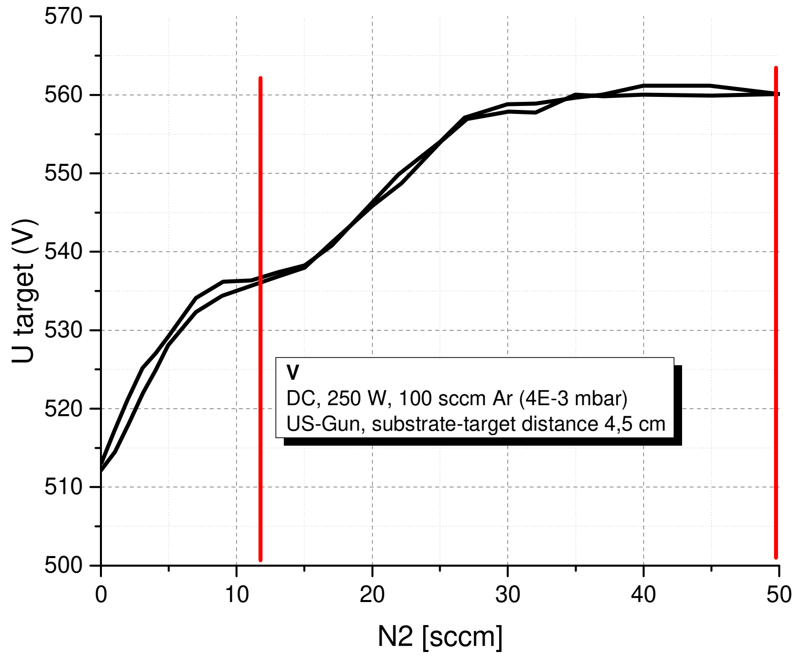

Fig 4.4 Hysteresis curve (the variation of the target voltage as function of the applied nitrogen flow), for the Vanadium target. The nitrogen flows used for the depositions were 13 sccm, and 50 sccm.

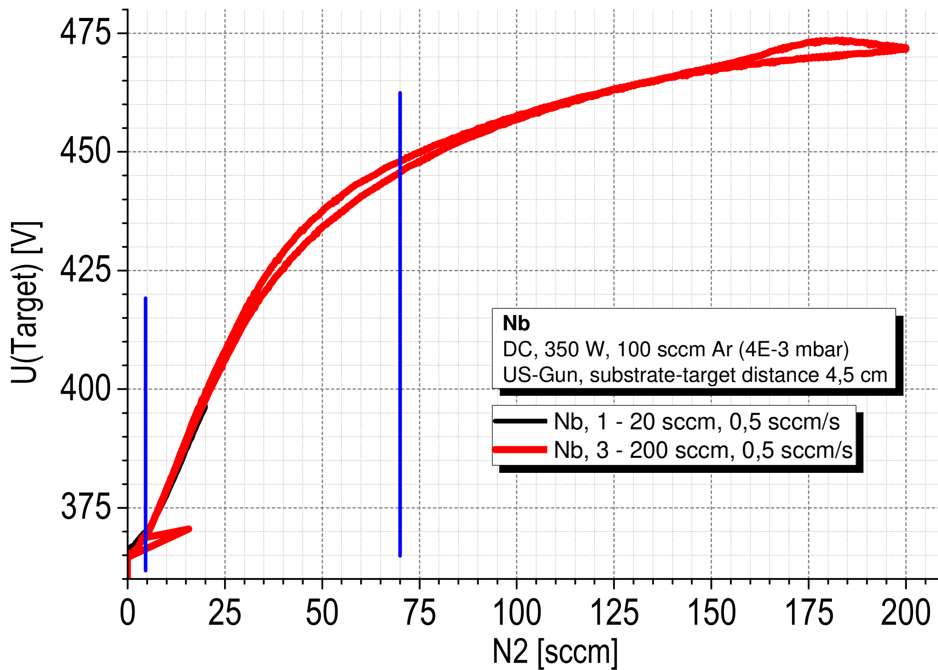

Fig 4.5 Hysteresis curve (the variation of the target voltage as function of the applied nitrogen flow), for the Niobium target. The nitrogen flows used for the depositions were 5 sccm, and 70 sccm.

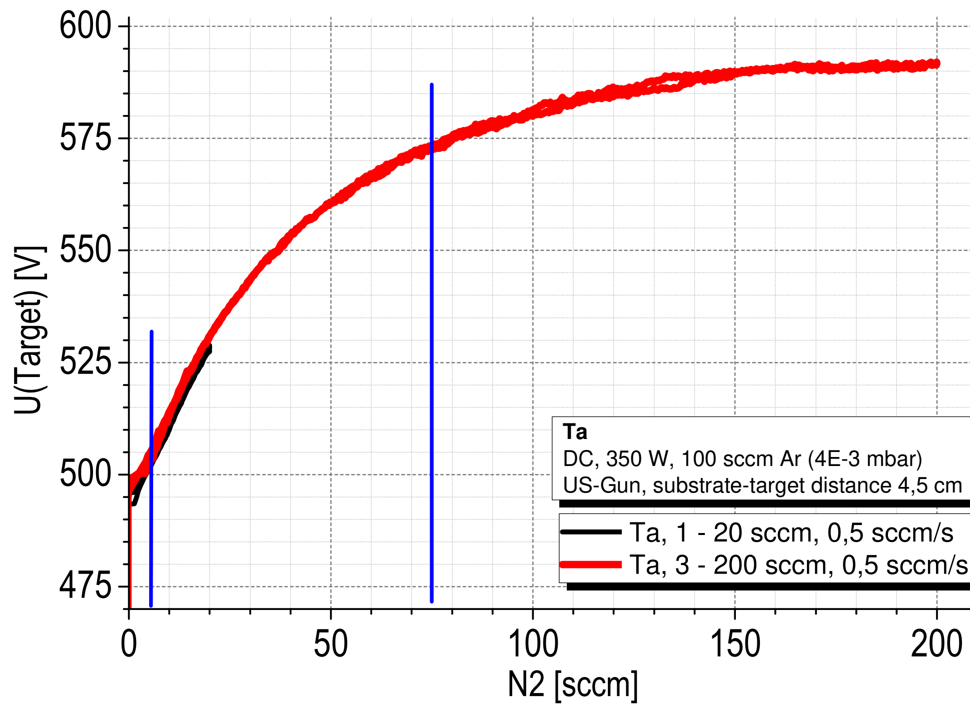

Fig 4.6 Hysteresis curve (the variation of the target voltage as function of the applied nitrogen flow), for the Tantalum target. The nitrogen flows used for the depositions were 5 sccm, and 70 sccm.

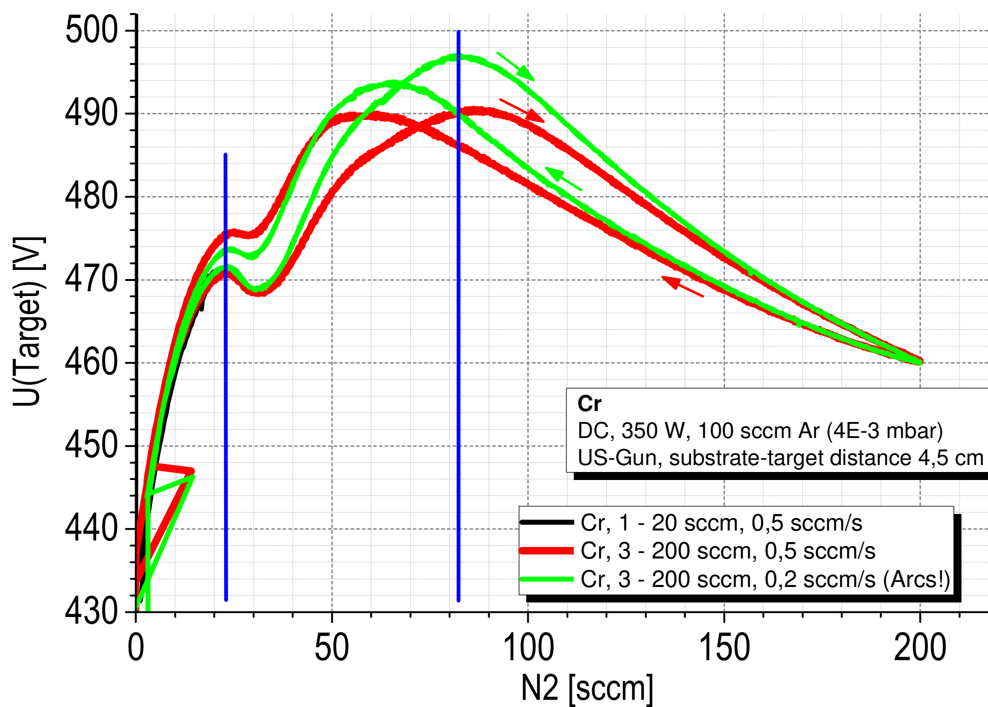

Fig 4.7 Hysteresis curve (the variation of the target voltage as function of the applied nitrogen flow), for the Chromium target. The nitrogen flows used for the depositions were 22 sccm, and 82 sccm.

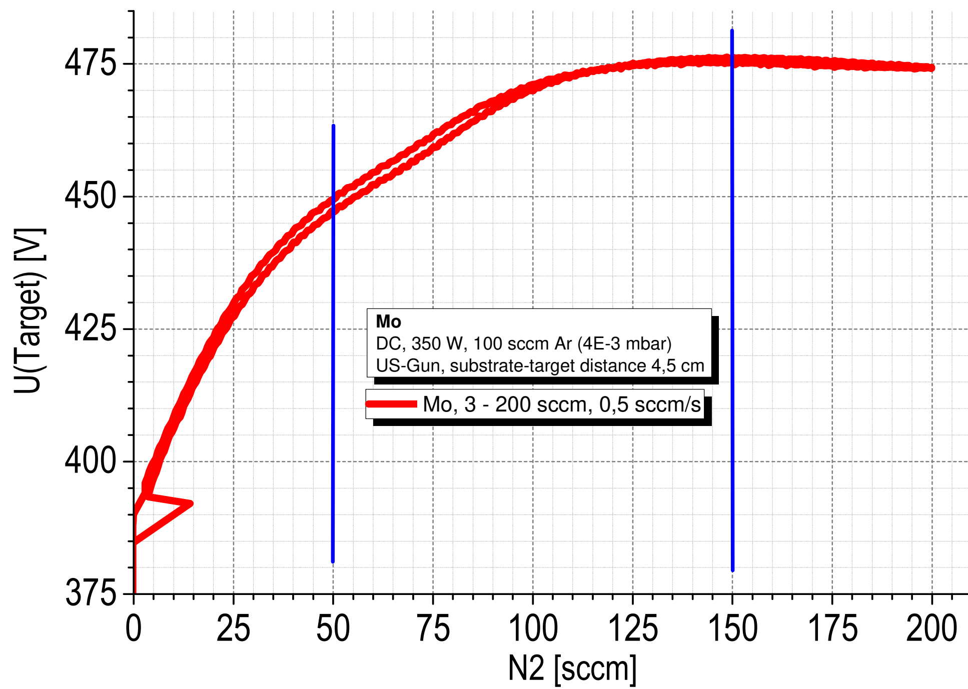

Fig 4.8 Hysteresis curve (the variation of the target voltage as function of the applied nitrogen flow), for the Molybdenum target. The nitrogen flows used for the depositions were 50 sccm, and 150 sccm.

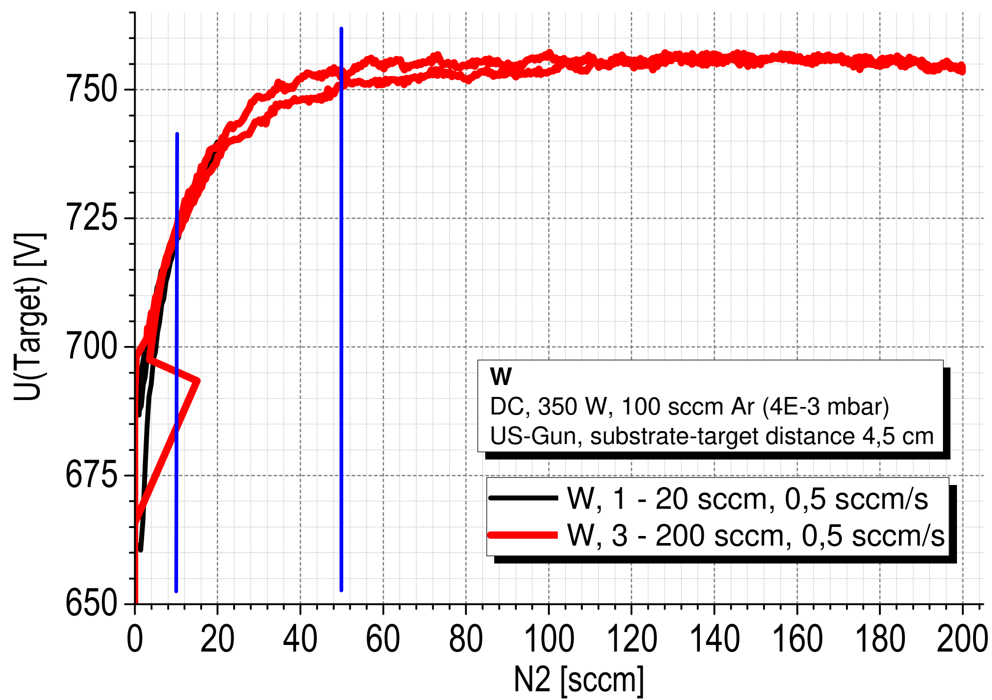

Fig 4.9 Hysteresis curve (the variation of the target voltage as function of the applied nitrogen flow), for the Tungsten target. The nitrogen flows used for the depositions were 10 sccm, and 50 sccm.

After the deposition of the MeN samples, the open circuit potential (OCP) or open circuit voltage (OCV) was used to assess which nitride variant exhibits the lowest potential. The open circuit potential is the potential where no current is flowing, because the circuit is open. Between two metals in the same solution the OCP is the highest potential difference possible without applying a potential from the outside. Measuring the OCP is also non-invasive, because no current is flowing. For most applications the OCP and other potentials will be measured versus a reference electrode. Due to the fact that potentials are additive, one can easily calculate what the potentials would be versus other reference electrodes. There is no absolute potential, but electrochemists consider that the standard potential of the standard hydrogen electrode (SHE) is by convention 0 V. This makes it easy to identify noble metals. The corrosion potential is the potential a sample has, when no external current is applied. A current can still flow to enable two reactions, one oxidation and one reduction, at the sample. For example, a steel sample in contact with an acid solution will oxidize (depending on the steel composition) and protons will be reduced at the surface. Observing the OCP or corrosion potential allows one to monitor corrosion processes as well. High corrosion potentials signify that the materials are noble, less likely to corrode. If the corrosion potential is dropping, it means that the sample is oxidizing and negative charges are accumulating in it.

The setup for the OCP measurements consisted in a PCU 100-PCR potentiostat, a saturated calomel reference electrode (Hg/HgCl), and NaCl 0.8 M solution as the electrolyte. The OCP variation as function of time was recorded for each sample, in at least 4 points, for 30 minutes each. The open circuit potential was measured on the glass coated samples, both polished and sand blasted. The open circuit potential values after 30 minutes of immersion for all the nitride variants is shown in figure 4.10.

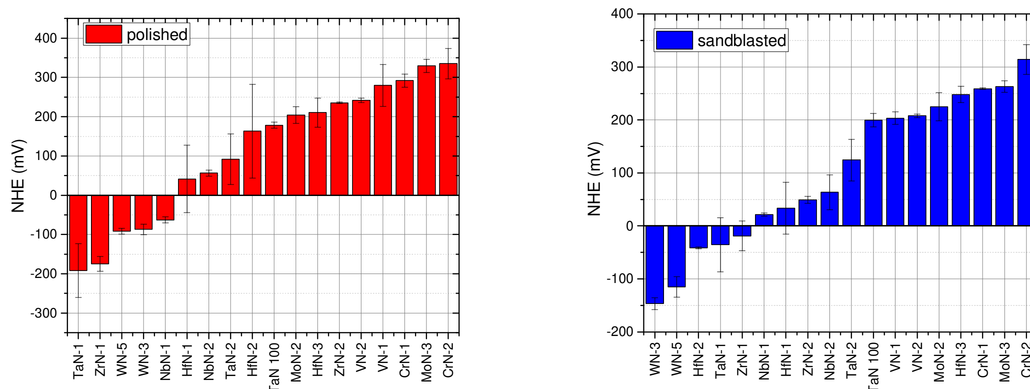

Fig 4.10 The open circuit measured average potential for each nitride variant.

Examining the information presented in figure 4.10, one can observe that the nobler variants of these nitrides are the ones based on chromium, molybdenum, and vanadium, while the less noble nitrides

are the ones based on zirconium, tungsten, tantalum, and niobium. The rather large error bars for certain samples are related to surface defects which significantly influence the corrosion response. Regarding the samples deposited on polished glass, one could observe that the coatings which exhibit the lowest open circuit potential are variants based on tantalum and zirconium, followed by the tungsten nitrides. However, upon further inspection of the samples with a Keyence VHX 7000 microscope, after the corrosion analysis was performed, surface defects and partial delamination of the coatings were observed in case of the TaN and ZrN polished glass samples, shown in figure 4.11, which were not observed before their immersion in the electrolyte. Consequently, for the Phase II of the research, namely the deposition of MeMgN type coatings, the chosen element for Me was tungsten.

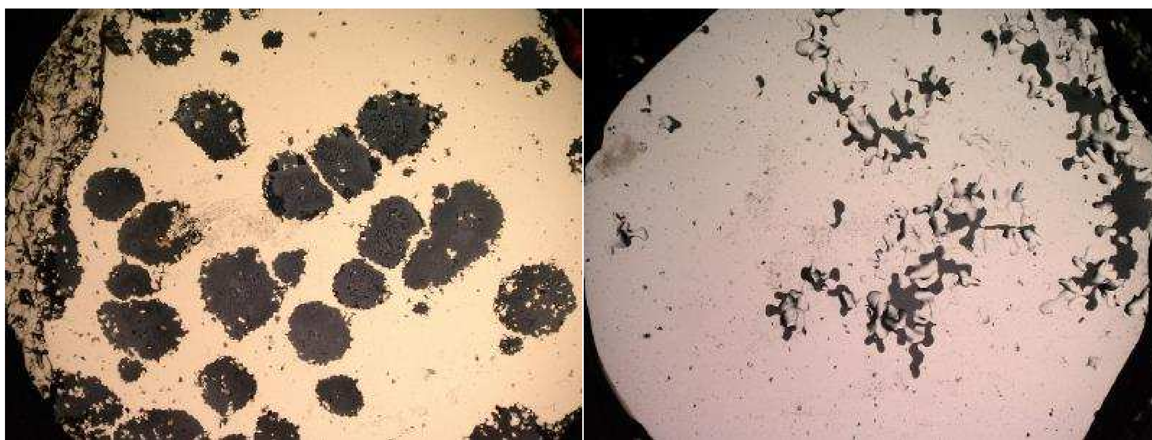

Fig 4.11 Surface defects and partial delamination observed after the open circuit potential corrosion analysis on the ZrN sample (left) and on the TaN sample (right).

b. Phase II.

Phase II of the research consisted in the deposition and analysis of WMgN-type nitrides. The depositions were performed on polished and sandblasted glass (corrosion analysis), on silicon wafers (structural analysis), on polished 100Cr6 steel rectangular substrates (mechanical properties: hardness, elastic modulus, scratch resistance, and wear behaviour), and on sandblasted high-speed steel (corrosion analysis: neutral salt spray tests and water vapours+sulphur dioxide tests).

The variables between the depositions were chosen to be the applied power on the magnesium target, to observe the influence of the magnesium content on the coating properties, and the nitrogen flow, to observe the effect of the absence, presence and quantity of nitrogen on the coating properties. The experimental matrix is shown in table 4.2. The deposition parameters, including the deposition period, were modified to be able to deposit relatively thick coatings (tf > 1μm), without any delaminations and as few as possible surface defects.

Table 4.2 contains the hardness values, obtained through instrumented indentation, and the coating thickness, obtained through surface profilometry (the samples were deposited with masking on a small portion, and the height difference was measured. The instrumented indentation was performed with a Fischer H100 XYp indenter, following the protocol according to DIN EN ISO 14577-1, while the surface profilometry was measured with a Mahr surface profiler, controlled by the MarWin software.

Table 4.2 Experimental matrix, thickness, and hardness for the samples from Phase II.

Sample	N_2 flow [sccm]	Mg power [w]	Thickness [μm]	Hardness HV
W	0	0	1.6	1880±70
WMg50	0	50	1.3	1800±15
WMg100	0	100	1.3	1940±60
WMg150	0	150	1.4	1840±60
WN10	10	0	1.3	2540±220
WN10Mg50	10	50	1.2	2520±200
WN10Mg100	10	100	1.2	2530±140
WN10Mg150	10	150	2.0	1110±12
WN50	50	0	1.2	1900±50
WN50Mg50	50	50	1.0	2700±250
WN50Mg100	50	100	1.2	3000±200
WN50Mg150	50	150	1.6	2700±130

Figure 4.12 presents the variation of the deposition rate, as function of the nitrogen flow, as well as in relation to the sputtering power applied on the magnesium target. One can observe that the deposition rate increases with the increase of the sputtering power, a phenomenon which was expected, considering the significantly higher sputtering yield of the magnesium target compared to the tungsten target (200 Å/s versus 80Å/s). A second observation which can be made regarding the variation of the deposition rate for the samples presented herein is the fact that the deposition rate is decreasing for the higher reactive gas flow samples, compared to the ones deposited with 10 sccm of N_2. This phenomenon could be explained by the fact that, generally, the sputtering/resputtering yield rate of compounds is lower, compared to the one of the elemental targets. Considering that in the deposition chamber a higher quantity of reactive gas is added, the target poisoning phenomenon could occur relatively faster. This observation is confirmed if one observes the values for the deposition rate for the samples which were deposited without applied power on the magnesium target, namely W, WN10 and WN50, the latter two exhibiting lower deposition rates compared to the elemental coating (nitrogen flow = 0 sccm).

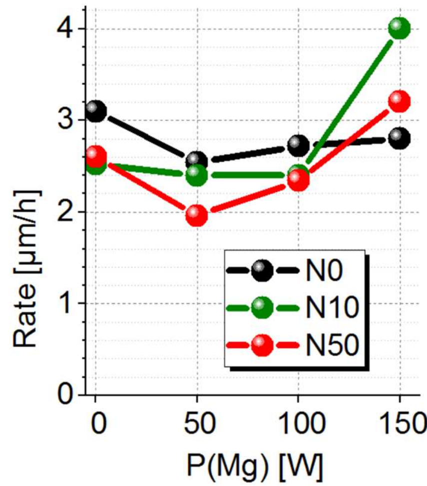

Fig 4.12 The variation of the deposition rate as function of the applied power and of the reactive gas flow.

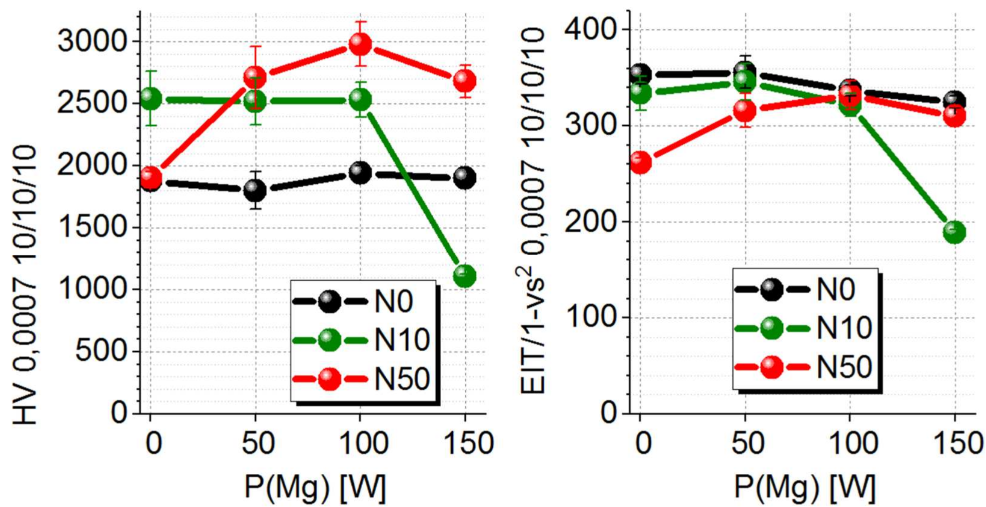

Fig 4.13 The variation of the hardness and elastic modulus as function of the applied power and of the reactive gas flow.

As mentioned previously, the scope of this research was to find a certain coating configuration that answers in the same time to both needs of high hardness and corrosion protection capacity. Figure 4.13 represents the variation of some mechanical characteristics, namely the indentation hardness and elastic modulus, as function of the applied power on the magnesium target, and as function of the reactive gas flow. It can be observed that the hardness of the reactively deposited samples (N_2 addition) is generally significantly increased than the samples deposited without reactive gas. The highest hardness for the N10 and N50 samples is obtained for 100W of magnesium target sputtering power. Increasing the sputtering power on the magnesium target further leads to a significant and sudden drop in the mechanical characteristics. The reason for this behaviour needs to be further investigated.

The second characteristic which was highly desired for these samples was a low enough open circuit potential value, in order to shift the corrosion sites towards the coating and away from the high-speed steel substrate. As for the nitride samples from Phase I, the samples based on tungsten were immersed in NaCl 0.8 M solution for 30 minutes, and the open circuit potential was measured against a saturated calomel reference electrode. The variation of the OCP as function of time for the tungsten-based samples is shown in figure 4.14. The lowest values of OCP are exhibited by the samples deposited with 100 and 150W Mg applied power, and without reactive gas, as well as the ones deposited with 10 sccm of nitrogen gas. As expected, a lower Mg content, inferred from a lower applied power (50W) leads to relatively high OCP values. Curiously, the coatings deposited with 100 and 150W of Mg applied power, but with 50 sccm of nitrogen, exhibit the highest OCP values. Without a thorough structural and chemical analysis of the coatings, which will be performed at a latter date, the reason for this behaviour is unclear.

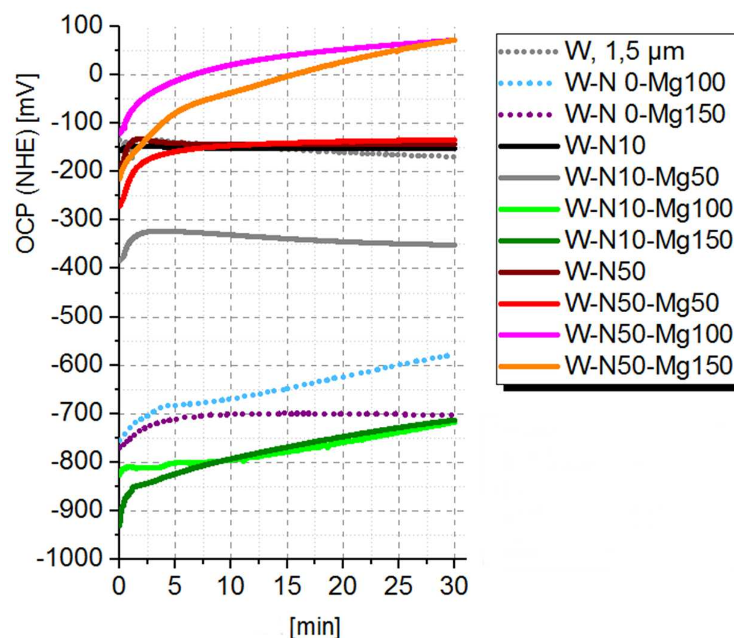

Fig 4.14 The variation of the open circuit potential as function of time, for the tungsten-based coatings.

To further assess the corrosion protection capacity of these WMgN coatings, the samples were subjected to a neutral salt spray (NSS) environment, for several hours. Firstly, the samples were sealed with a protective resin, thus allowing only the surface of the coating to be subjected to this corrosive medium. The sample were analyzed every 60 minutes. The results are presented in Tables 4.3 and 4.4 (detailed images). As mentioned previously, a balance between high hardness and good corrosion protection capacity was sought after. The samples which exhibited the highest hardness (HV > 2700) are the ones deposited with 50 sccm of nitrogen gas and 50, 100 and 150W of power on the

magnesium target. Unfortunately, their corrosion protection capacity is not optimal, considering that the surface exhibits signs of corrosion after only one hour of NSS exposure. Furthermore, the samples deposited with 10 sccm of nitrogen exhibit slightly better corrosion protection capacity. The WN10Mg100 coating seems to show the optimal configuration of characteristics, namely HV 2530 and corrosion resistance up to 4 hours.

Table 4.3 Neutral salt spray test results for the samples from Phase II.

		0 h	1 h	2 h	4 h	24 h	48 h	
L200 225a	W							HV1880 ±70 1,6 µm
L200 224a	W Mg50							1800 ± 150 1,3 µm
L200 224b	W Mg100							1940 ± 60 1,3 µm
L200 224c	W Mg150							1840 ± 60 1,4 µm
L200 214a	W N10							2540 ± 220 1,3 µm
L200 214b	W N10 Mg50							2520 ± 200 1,2 µm
L200 217a	W N10 Mg100							2530 ± 140 1,2 µm
L200 218a	W N10 Mg150							1110 ± 12 2 µm
L200 213b	W N50							1900 ± 50 1,2 µm
L200 214c	W N50 Mg50							2700 ± 250 1 µm
L200 217b	W N50 Mg100							3000 ± 200 1,2 µm
L200 218b	W N50 Mg150							2700 ± 130 1,6 µm

Table 4.4 Neutral salt spray test results (detail) for the samples from Phase II.

		0 h	1 h	2 h	4 h	24 h	48 h	
L200 225a	W							HV1880 ±70 1,6 µm
L200 224a	W Mg50							1800 ± 150 1,3 µm
L200 224b	W Mg100							1940 ± 60 1,3 µm
L200 224c	W Mg150							1840 ± 60 1,4 µm
L200 214a	W N10							2540 ± 220 1,3 µm
L200 214b	W N10 Mg50							2520 ± 200 1,2 µm
L200 217a	W N10 Mg100							2530 ± 140 1,2 µm
L200 218a	W N10 Mg150							1110 ± 12 2 µm
L200 213b	W N50							1900 ± 50 1,2 µm
L200 214c	W N50 Mg50							2700 ± 250 1 µm
L200 217b	W N50 Mg100							3000 ± 200 1,2 µm
L200 218b	W N50 Mg150							2700 ± 130 1,6 µm

Moreover, the coatings were subjected to a water vapour + sulphur dioxide atmosphere, in a Liebisch KBEA 300 Corrosion Diagnostic Chamber, in accordance to the DIN 50018 standard (Testing in a saturated atmosphere in the presence of sulfur dioxide). The samples were analyzed optically every 60 minutes. One can observe from the results presented in figure 4.15 that the water vapour + sulphur dioxide environment is significantly more corrosive, all samples exhibiting corrosion products on the coating surface after only one hour of exposure.

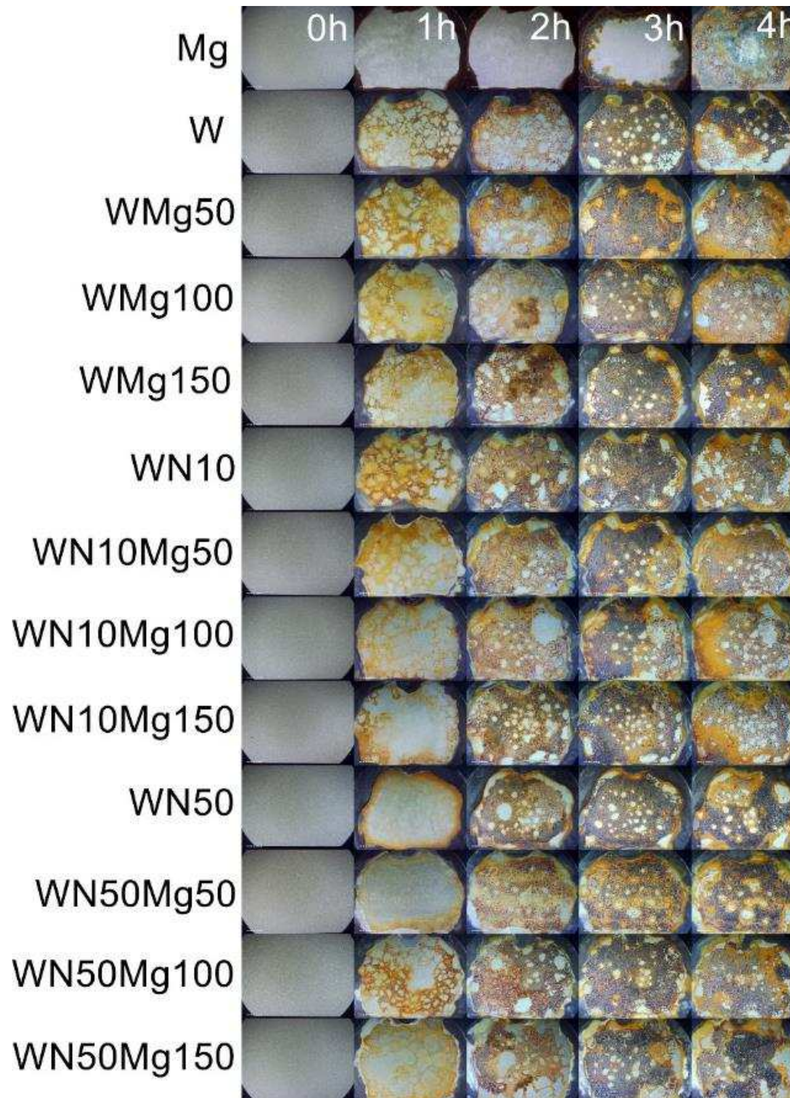

Fig 4.15 Images obtained after water vapour + sulphur dioxide exposure, for the tungsten-based coatings.

The corrosion behavior of hard Physical Vapor Deposition coatings depends strongly on the number of growth defects (Balzer, 2018). The corrosion behavior of the samples presented herein was somewhat expected as due to the sand-blasting a very rough surface was generated and a highly porous coating can develope on such kind of surfaces. The steel surface is heavily disturbed by the sand-blasting procedure. Therefore, the coating microstructure could be highly defective with many large open pores, which allow the transfer of the electrolyte to the substrate material. The protection effect of magnesium is observed in figure 4.15, the magnesium coated sample being the only sample which exhibited corrosion effects only after 3 hours of exposure. However, the mechanical characteristics of this pure magnesium coating are insufficient for the desired application. Further analysis on these samples is needed, in terms of structural development, surface chemistry, morphology, roughess, etc, in order to elucidate the reasons for such behaviours.

Conclusions

The scope of this habilitation thesis was to show that reactive magnetron sputtering is a powerful technique which is able to obtain complex thin solid films, with multifunctional properties, that can be tailored to suit the desired application.

Chapter one contains relevant information regarding the theoretical aspects of sputtering, some information on the role of the applied magnetic field, and key information regarding the reactive sputtering process, with emphasis on some factors that govern the stability and reproducibility of the reactive magnetron sputtering deposition. It was shown that when dealing with complex coatings, the control of the process is relatively difficult, if several factors related to the deposition process are not entirely understood and adequately controlled.

Chapter two presents results obtained after the completion of my PhD program, on optimized tantalum oxynitride TaO_xN_y thin solid films, regarding certain possible applications:

a) **Photocatalytic behavior.** The photodegradation of some solutions of methylene blue, respectively methyl-orange, with or without hydrogen peroxide, under the action of the ultraviolet spectrum, respectively of the visible spectrum, in the presence of the tantalum oxynitride thin solid films, had the following results:
    - Photodegradation of a solution of methylene blue (+ 100µl H_2O_2) under the action of ultraviolet radiation: efficiencies between 43 and 57%.
    - Photodegradation of a methyl-orange solution (+ 100µl H_2O_2) under the action of ultraviolet radiation: efficiencies between 15 and 81%.
    - Photodegradation of a methyl-orange solution (+ 100µl H_2O_2) under the action of visible radiation: efficiencies between 11 and 32%.
    - Photodegradation of a methyl-orange solution (without H_2O_2) under the action of visible radiation: efficiencies between 5.5 and 8.2%.
    - Photodegradation of a methyl-orange solution (+ 100µl H_2O_2) under the action of visible radiation: efficiencies between 3 and 65.2%.

b) The results obtained from the measurements on some **electrical properties** of tantalum oxynitride thin solid films can be summarized as follows:
    - The electrical resistivity increases with increasing partial pressure, starting from characteristic values of metallic compounds to characteristic values of oxides. The range of values is wide, the sample with the lowest resistivity ($5.29 \times 10^{-4}\ \Omega \cdot cm$) being obtained with a flow rate of 2.5 sccm (GND), while the sample with the highest resistivity (1.93 ×

10^6 Ω · cm), being obtained with a flow rate of 30 sccm, respectively a bias voltage equal to -100V.

- Samples with high resistivity were subjected to measurements to determine the dielectric character. Permittivity values up to 41 were determined, significantly higher than those for other tantalum-based films found in the literature.

c) The tantalum oxynitride thin solid films presented herein exhibit adequate **antibacterial/ antibiofilm** capacity against *Salmonella*, thus implying that one potential use for these coatings could be in the biomaterials sector.

Chapter three presents results concerning the composition, morphological and mechanical characteristics (wear, adhesion to the substrate, hardness) for ceramic composite magnetron sputtered (Ti + TiB_2 + WC) coatings. The films were obtained by simultaneous standard/reactive magnetron sputtering from three targets (Ti, TiB_2 and WC). The chemical composition was measured by RBS and showed that the films are nonstoichiometric. The film surface morphology was measured by AFM. When measured on the films deposited on silicon, there are no significant differences concerning the surface roughness between the samples. However, the quality of the substrate surface seems to be very important, as observed on the steel substrate samples. For the set of samples deposited with nitrogen as reactive gas the roughness increases on the wear track, when compared to the as-deposited film surface, while for the other set of samples, it decreases. The films are hard (instrumented indentation hardness values between 20 and 22 GPa), but if they are deposited on softer materials, they exhibit poor adhesion to the substrate. However, the (Ti + TiB_2+ WC) films show promising results concerning their wear resistance, especially if the films would be paired with an appropriate substrate material.

Chapter four presents preliminary results concerning the development of single stage deposition ternary hard coatings with improved corrosion properties. The purpose of the research presented herein was to study RM-Mg-N (RM – refractory metal) multiple component nitride-type thin films, obtained by simultaneous sputtering of two metallic targets (high purity RM and Mg), with the addition in various proportions of reactive gas (N_2). The RM candidate, where RM = Zr, Hf, V, Nb, Ta, Cr, Mo, or W, was chosen after preliminary tests in respect to the corrosion behavior of RM-N-type coatings. The second stage of the research was to deposit WMgN-type coatings, and to analyze them in terms of corrosion protection capacity, but coupled with as high as possible mechanical properties. It was observed that the mechanical properties exhibit a drop when the magnesium content exceeds a certain threshold. However, when the magnesium content is situated below this threshold, it contributes to improved mechanical properties, compared to the binary nitride obtained in identical conditions. The surface defect density needs to be controlled in order to improve the corrosion protection capacity.

(B3) The evolution and development plans for career development

My evolution and development plan for career development is based on the two main pillars of academia, namely teaching related activities and research activities.

B3.1 Teaching activities

The estimated didactic activity associated with the position of Professor involves conducting classes and practical activities on the following topics: nanomaterials; surface engineering; advanced materials for renewable energies, etc. In order to obtain the best results from a didactical point of view, I will use modern teaching methods that will have video and audio support, accompanied by a rich bibliography and I will present in real time the data available on the faculty website.

A real support for carrying out teaching activities at the highest level, both in terms of teaching courses and in terms of laboratory activities is the experience gained by participating as a team member in numerous research contracts. Based on the knowledge and experience acquired in the field of materials science and engineering, in the future I intend to publish a specialized book on Surface Engineering, and a guide of applications on materials analysis techniques, in order to support the education and activity process and the practical training of students.

I will maintain the novelty of the courses by adapting them every year to the new discoveries that appear in the field, by continuously studying the specialized literature (Journal of Materials Science, Applied Surface Science, Surface & Coatings Technology, Thin Solid Films, etc.). I also intend to continue my contribution to the development of new didactic laboratory works for fundamental and applied research, and to involve the bachelor's and master's students in practical activities from an early stage of their studies.

After the admission in the doctoral school, the main intention is to attract possible candidates for the PhD program, and to build a research team which will be able to attract funding through project proposals. A good relationship between the teaching staff and the students (bachelor's, master's or PhD levels) is the basis for a good performance in science and a way to promote collaboration and the success of all the members in an academic group.

B3.2 Research topics

The research topics planned for the forseeable future are building on the experience gained during and after the completion of my PhD program, and are related to the development and analysis of complex (multiple component) thin solid films, deposited by magnetron reactive sputtering. The theoretical aspects, motivation of research and expected results are presented in the following sections. These

activitities will be carried out in partnerships within new or already established collaborations, at both national and international levels.

B3.2.1 Complex oxynitride coatings.

Complex oxynitride-type compounds ($Me_1Me_2O_xN_y$, where Me_1, Me_2 = Ti, Al, Sr, Nb, Mg, Mo, etc.) have received attention in recent years due to their original properties compared to their oxide or nitride parents. For example, the decrease of the band-gap consecutive of the nitrogen substitution for oxygen in the perovskite ($Me_1Me_2O_3$) structure leads to an absorption in the visible domain, with potential applications as pigments and visible photocatalysts, for instance, in overall water splitting reactions (Le Paven, 2017). Other applications which have been proposed are mostly related to high-temperature solar selective absorbing coatings for parabolic trough concentrated solar power (CSP) photo-thermal conversion: NbTiON (Liu, 2012); WAlON (Atasi, 2016), NbAlON (Harish, 2008), NbMoON (Yongxin, 2015), all with the same purpose (absorbing layers). Furthermore, NbAlON was proposed as a superconductive material (Shinichi, 2009). TiAlON films were reported to be potentially used as corrosion resistant films (Kazuki, 2001), as dark decorative coatings (Luthier, 1990), as oxidation and wear resistant dry cutting tool coatings (Tönshoff, 1998; Schalka, 2016), as high temperature miniaturized strain gauges (Zarfl, 2015), as absorber layers for photo-thermal conversion multilayers (Harish, 2014; Rebouta, 2012). The multitude of possible applications for $Me_1Me_2O_xN_y$-type materials stems from the numerous types of structures that can arise, controllable through the processing parameters. However, the scarcity of reports concerning these types of compounds is staggering, shown also in the reduced reference list and in the large interval of publication year.

To the best of my knowledge, there are no reports in the scientific literature concerning the deposition and characterization of $TaTiO_xN_y$-type thin films. Regarding the $ZrTiO_xN_y$ system, one report presents their potential use as an interlayer in a solar spectral selective absorbing coating (Liu, 2014). The main difference compared to dual magnetron sputtering, which is the deposition method that I will use in future research, is the fact that the authors used a compound target (Ti:Zr = 1:1 at%), thus greatly limiting the compositions and properties which could have been obtained. However, a limited number of reports can be found in the literature, concerning TaTiO and TaTiN-type compounds, from which a number of properties could be inferred for $TaTiO_xN_y$ thin films.

In the case of TiN, when some of the Ti atoms are substituted by Ta ones, a new phase (TaTiN) will form. Since TaTiN is a derived compound from TaN and TiN, it should incorporate the advantages and characteristics of the two species. The atom substitution of Ti by Ta may enlarge the lattice constant, for the latter (Ta atomic radius = 200 pm) is bigger than the former in diameter (Ti atomic radius = 176 pm). As a result, the TaTiN film may possess higher expected hardness values than TiN or TaN films

(Feng, 2010). The same phenomenon could appear in the case of $ZrTiO_xN_y$ system, where Zr would substitute Ti atoms, or vice versa, resulting in expected property changes.

The majority of the limited number of reports concerning TaTiO-type thin films (Lukosius, 2011-2; Rouahi, 2012; Chiang, 2005; Rouahi, 2016; Lukosius, 2011-1; Rouahi, 2013; Salimy, 2013) are recommending their use as a potential high-k dielectric thin film, in structures like: MIM capacitors (metal – insulator – metal), MOS capacitors (metal – oxide – semiconductor), gate for transistors and memory applications. Other candidates for these types of applications are Ta_2O_5 and TiO_2 films. Ta_2O_5 films have been considered to be used in Dynamic Random-Access Memories (DRAM). At temperatures lower than 700 °C, Ta_2O_5 is amorphous and has a dielectric constant of ~25, and a band gap of 4.5 eV (Chiu, 2000). However, its poor leakage current density still limits its use in mobile applications. On the other hand, TiO_2 displays a very high-k value of ~80 (tetragonal phase) but the small band gap (3.5 eV) and the corresponding small (1.2 eV) conduction band directly correlate with high leakage currents. Another factor that causes high leakage currents is the crystallization of TiO_2, which starts at low temperatures. TiTaO thin films have been shown to exhibit intermediate dielectric characteristics which allow overcoming the critical issue of high leakage currents. For example, it was reported that TiTaO MIM capacitors showed lower leakage currents of about 12×10^{-3} $A\times m^{-2}$ which are ~5-7 orders of magnitude smaller than those of TiO_2 devices (Lukosius, 2011-1).

The scope of future research is to study the chemical, structural, morphological and, consequently, property variation concerning Me_1/Me_2-based multiple component oxynitride-type thin films, where Me_1 = Ta, Zr and Me_2 = Ti (e.g. $TaTiO_xN_y$, $ZrTiO_xN_y$), obtained by simultaneous sputtering of two metallic targets (high purity Ti, Ta, Zr), with the addition in various proportions of reactive gases (N_2 and O_2). The elements were chosen as function of their atomic radius, in order to obtain distorted crystalline networks, possibly leading to properties variation (e.g. hardness increase). The objectives that are considered for this class of thin films are related to the properties that will be investigated: **i)** chemical, structural and morphological variation; **ii)** mechanical characteristics (hardness, wear resistance); **iii)** electrical characteristics (resistivity, dielectric characteristics) and thermal stability; **iv)** corrosion resistance, photocatalytic and antibacterial activity.

Considering that the oxides, nitrides and single-Me (Me = Ti, Ta, Zr) oxynitride classes of coatings are already demonstrated to be reliable candidates in terms of multifunctional coatings, I intend to use these building blocks to study $TaTiO_xN_y$ and $ZrTiO_xN_y$ coatings. The research directions are relatively limitless, considering the myriad of possible structures that could be obtained.

In order to test the hypothesis concerning the usability of complex oxynitride type films, and their property variation, dependent on the deposition conditions, I already performed a small number of

preliminary depositions and tests on $TaTiO_xN_y$ films. A batch of five samples was deposited, with the following identical deposition conditions: base chamber pressure < 1.2×10^{-6} Pa, Ar flow 70 sccm, substrate bias voltage -50V, fixed proportion reactive gas mixture (15% O_2 + 85% N_2) with a flow of 15 sccm, 1h deposition period. The variable parameter was the target current, in the following configuration: 1) Ta target = 1A, Ti target = 0A (TaO_xN_y film); 2) Ta target = 0.75A, Ti target = 0.25A ($TaTiO_xN_y$ film); 3) Ta target = 0.5A, Ti target = 0.5A ($TaTiO_xN_y$ film); 4) Ta target = 0.25A, Ti target = 0.75A ($TiTaO_xN_y$ film); 5) Ta target = 0A, Ti target = 1A (TiO_xN_y film). The variation in perceived color was clearly noticeable, which would indicate the possibility of using the films as optical coatings (filters) or decorative coatings.

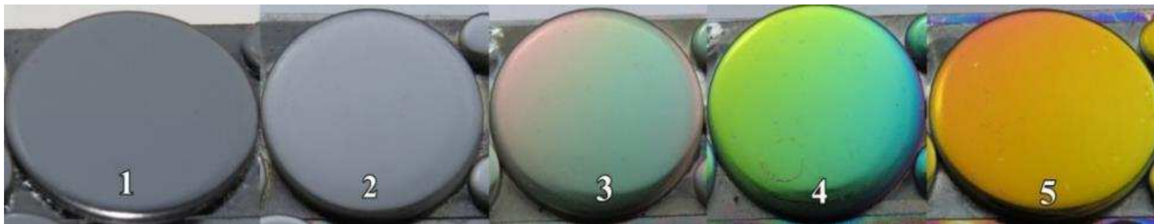

Variation of perceived color for $TaTiO_xN_y$-type film, as function of target current.

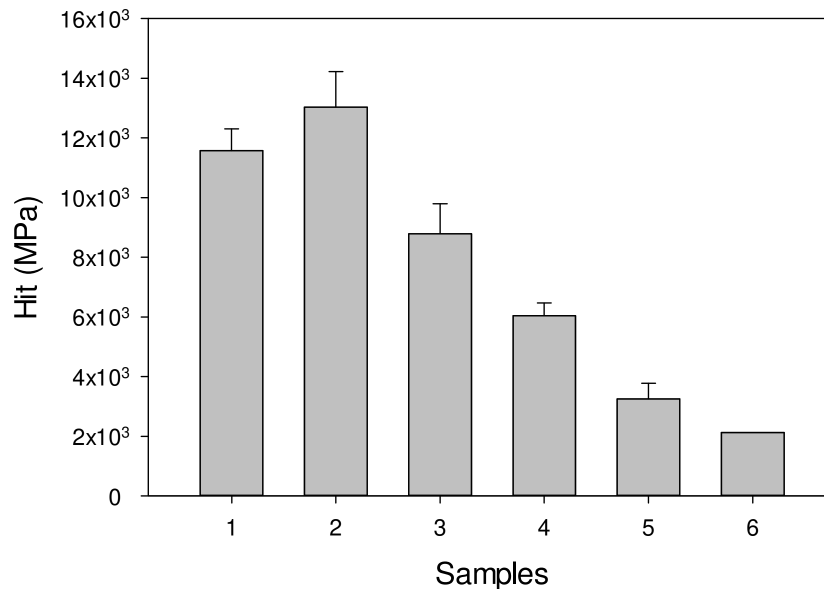

Hardness variation as function of the target current.

The variation in hardness, obtained by nanoindentation, on the same five samples, can be observed in the previous histogram. Sample 6 represents the substrate (stainless steel 316L). The variation in hardness is clearly noticeable, sample $Ta_{0.75}Ti_{0.25}ON$ exhibiting the higher hardness. The notation of the sample is related to the target current, and not to the stoichiometry, for which the chemical

composition analysis is needed. Considering the different reactivity of N_2, and especially of O_2, to Ta and Ti, at this point it is almost impossible to venture an explanation as to the reason of this variation, both in color and hardness. Looking at the enthalpies of formation (Speight, 2017) for a few structural phases that could appear (**TiN** $\Delta_f H^0$ = -265.8 kJ/mol, **TiO** $\Delta_f H^0$ = -519.7 kJ/mol, **TiO_2** $\Delta_f H^0$ = -944 kJ/mol, **Ti_2O_3** $\Delta_f H^0$ = -1520.9 kJ/mol, **Ti_3O_5** $\Delta_f H^0$ = -2454.4 kJ/mol, **TaN** $\Delta_f H^0$ = -251 kJ/mol, **TaO_2** $\Delta_f H^0$ = -201 kJ/mol, **Ta_2O_5** $\Delta_f H^0$ = -2046 kJ/mol), and considering the different sputtering yields for Ta and Ti (85 Å/sec, and 80Å/sec, respectively, if one does not take into account the possibility of target poisoning, which would significantly lower the sputtering yield) the situation is even less clear, without further investigations. At first glance, it would appear that the formation of the oxides is more thermodynamically favored; however, the proportion of oxygen in the reactive gas mixture was specifically chosen to be less than the one in air, in order to stimulate the growth of nitride phases, as well. Moreover, one has to consider that these preliminary results are related to only one configuration of conditions. Therefore, the research directions are relatively limitless, considering the multitude of possible structures that could be obtained. However, the difficulty in understanding the binary oxynitride systems is increased.

B3.2.2 Refractory metal and magnesium-based coatings.

Firstly, due to multiple unanswered questions regarding the WMgN system of coatings, presented in section B2, chapter 4 of this thesis, the research activities will be devoted towards understanding the physical phenomena displayed by this system, through the following means:

- **Chemical composition, surface morphology and structural evaluation.** The chemical composition and stoichiometry will be obtained by EDS (Energy-dispersive X-ray spectroscopy). The surface morphology and structural evaluation will be assessed by AFM (Atomic Force Microscopy) or SEM (Scanning Electron Microscopy), and XRD (X-Ray Diffraction), respectively. New information related to the chemical (composition, stoichiometry), morphological (surface roughness, surface features, deposition defects) and structural evolution (type of structure, phases, grain sizes, etc.) of the W-Mg-N samples, correlated to the deposition parameters, will be obtained.
- **Mechanical characterization.** The surface mechanical characteristics will be determined by instrumented indentation, to assess the variation of surface hardness and elastic modulus due to the deposition processes parameters employed. The results presented in section B2, chapter 4, are obtained using so-called standard settings, according to the ISO 14577 standard. However, the mechanical response of a coating does not necesarilly follow the expected rules. Consequently, a thorough analysis of the samples, using multiple indentation loads and indentation rates will be performed. The adherence of the deposited films to the 100Cr6 steel

substrate material will be determined by scratch resistance or ball impact test. The coating thickness measurements, necessary for the instrumented indentation procedures, in order to limit the substrate influence on the final results, will be done by ball-cratering (calotest), in order to compare the results with the ones obtained through surface profilometry. The wear behavior will be assessed using a rotational tribometer, in various conditions: using various loads and friction couple materials. New information will be obtained, containing: mechanical characteristic values (hardness, elastic modulus, friction coefficient, wear rate, film thickness, critical adhesion loads, etc.), all correlated to the deposition conditions.

The dissemination of the results will be performed by the involved persons in order to strengthen the ties between the institutions and enhance future collaborations. The results will be disseminated through high impact factor journal publications (e.g.: *Applied Surface Science, Surface & Coatings Technology*). The research activities will contribute to the build-up of high-quality research, education and training through the effective exchange of knowledge between the involved persons.

Secondly, considering that a database concerning the corrosion open circuit potential of several refractory metal nitrides was obtained, further research is planed using the same hypothesis, namely pairing a refractory metal target with a magnesium target, to obtain complex MeMgN-type coatings.

B3.2.3 Refractory metal ternary nitrides (Me_1Me_2N).

Multiple component nitride-type compounds (A-B-N, where A, B = Zr, Hf, V, Nb, Ta, Cr, Mo, W, Mg, etc.) have received attention in recent years due to their original properties compared to their nitride parents. Ternary nitrides (A-B-N) may form a composite (multiphase) or a solid solution, determined by the properties and concentration of the metallic elements. If both metallic elements are transition metals, a solid solution with crystal structure and electronic properties similar to the binary nitrides may form. Compared to those of the constituting binary nitrides, solid solutions were found to possess superior hardness, wear resistance, and corrosion resistance.

Theoretical molecular dynamics (MD) and density functional theory (DFT) calculations predicted that mixtures of transition metal nitrides could exhibit higher hardness compared to binary nitrides (Sangiovanni, 2010; Sangiovanni, 2011). Hardness is increased by tuning the material valence electron concentration (VEC) around an 8.4 value, which yields a maximum hardness in cubic transition metal nitride and carbide materials, as shown by Jhi et al. (Jhi, 2001). In previous studies (Kindlund, 2014; Kindlund, 2013), it was predicted that ordered cubic $Ti_{0.5}Mo_{0.5}N$, $Ti_{0.5}W_{0.5}N$, $V_{0.5}Mo_{0.5}N$, and $V_{0.5}W_{0.5}N$ materials are not only harder, but also significantly more ductile than their parent binaries TiN and VN. The enhanced toughness in these ternary materials was shown to be induced by the increased occupation of the metallic states at the Fermi level, due to the higher VEC obtained upon the

substitution of Ti/V with Mo/W atoms on the metallic (Me) sublattice. The higher VEC not only preserves the typically strong Me–N bonds found in binaries, but also enables the formation of stronger Me–Me bonds compared to TiN and VN. Overall, high VEC lowers the shear resistance and energetically promotes dislocation glide, thus leading to increased ductility. The increased toughness could result in lower wear rates for these materials.

Some predictions have been already checked on a few compounds such as TiMoN, which exhibit higher hardness and lower friction coefficient than MoN and TiAlSiN, respectively (Wang, 2015), CrNiN and TiMoN, which exhibit superhardness (~45GPa) (Regent, 2001), TiYN films with lower wear rates and friction coefficient, due to the addition of Y (Ju, 2015), TiMoSiN (34.5 GPa hardness) (Xu, 2014), to name a few.

Since the *ab initio* calculations could not be yet performed for very large numbers of atoms and usually require periodic boundary conditions, the role of crystalline grain sizes on the hardness has not been yet investigated in great detail. There is an experimentally derived Hall-Petch model that predicts an increase of the hardness with the decrease of the grain size (Hall, 1951; Petch, 1953). However, for very small grain sizes, an anti- or inverse Hall-Petch behavior was observed, where the hardness starts decreasing with the decrease of the grain size. The approximate size where this transition occurs has been determined for a handful of materials only and some results are still under debate (Trelewicz, 2007; Carlton, 2007). In general, dislocations could not exist in very small grains, therefore the increase in ductility (or toughness) for such nanostructured materials should depend on the specific grain size. In addition, the predicted lower wear rates would also greatly depend on the value of the friction coefficient, a material constant that is still difficult to evaluate from simulations.

The use of nanostructured transition metal nitrides, due to their particular advantages, is very important for many high-tech applications. For example, a main drawback of Ti implants is the release of rather large crystalline grains into surrounding tissue, causing inflammation (Popescu-Pelin, 2015). The use of a nanostructured protective coating deposited on Ti, besides lowering the friction coefficient and increasing the chemical resistance, would release only very small grains, that would be easily dissolved in the body fluids and not elicit an adverse reaction from the body, therefore significantly decreasing the inflammatory risk.

As many properties investigated in the last decades, the mechanical properties of materials also change when the structure of the film, i.e. the grain size enters into the nanometer range, roughly defined by grain sizes smaller than 100 nm. The densification/refinement of the structure for ternary nitride compounds was reported extensively, considering that the main precursors, i.e. the target-expelled atoms, compete during the formation of the material structure. There are novel aspects that

should be taken into account at this scale such as the absence of dislocations that will influence the way the grains deform under the action of forces. There are very few materials that were investigated to find out if the Hall-Petch model relating the hardness to the grain size applies when the grain size is smaller than 100 nm. There is, in several instances, disagreement between theoretical predictions and experimental results (Trelewicz, 2007; Carlton, 2007).

The multitude of possible applications for A-B-N-type materials stems from the numerous types of structures and chemical compositions that can arise, controllable through the processing parameters (deposition parameters, thermal annealing, etc.). The potential benefit of developing A-B-N-type coatings can be extracted from the literature, as follows. In relation to CrAlN coatings, by extending the binary system CrN with aluminum to the ternary system chromium aluminum nitride (Cr,Al)N, the properties of the coating can be varied by altering the chromium/aluminum ratio. (Cr,Al)N coatings exhibit enhanced mechanical properties, increased abrasion resistance, and a higher adhesion resistance in comparison to CrN coatings (Bobzin, 2016). CrAlN coatings were proposed as films deposited on components of injection molding machines (Bagcivan, 2013). NbAlN was proposed as one of the component layers in the NbAlN/NbAlON/Si_3N_4 tandem absorber for high-temperature solar selective applications (Harish, 2008). The solar thermal power systems use solar collectors to convert solar radiation into thermal energy for producing electricity. Solar selective absorbing coatings are ordinarily used in solar collectors to increase the efficiency of photo-thermal conversion. Several A-B-N-type coatings were proposed for such applications: NbMoN (Yongxin, 2015), TiAlN (Barshilia, 2008), CrMoN (Selvakumar, 2013), HfMoN (Selvakumar, 2012), WAlN (Atasi, 2016). Moreover, SmCoN magnetron sputtered coatings were proposed as materials for solid oxide fuel cell (SOFC) technology, due to their high electrical conductivity, good stability in both reducing and oxidizing atmospheres, and close CTE (coefficient of thermal expansion) match with other SOFC ceramic components (Junwei, 2008). Furthermore, TiAlN coatings were studied in terms of their capacity to be implemented as materials for biomedical applications. The TiAlN coatings were assessed in terms of their surface properties, electrochemical corrosion in simulated body fluid (SBF), and cytotoxicity. It was found that the TiAlN coatings deposited on CP–Ti exhibited superior corrosion resistance compared to the TiON, TiN and the bare CP–Ti substrate (Subramanian, 2011). The addition of Al to the TiN-type coatings was reported to contribute to the improvement of hemocompatibility as compared to the TiN, AlN layers and the bare substrate, as well as to the improved corrosion resistance, which was attributed to the densified microstructure with development of fine grain size and reduced surface roughness (Subramanian, 2010). In terms of mechanical behavior, i.e., coatings with improved wear behavior to be deposited on cutting/milling tools, it was reported that TiCrN coatings, deposited at different pulsed frequencies, grown on steel substrates by pulsed reactive DC magnetron sputtering technique, exhibit denser structure, which may reduce the friction of the coating, increase the mechanical performance,

and increase the resistance against corrosion (Anusha, 2016). Moreover, in the case of TiVN coatings, it was reported that the roughness, corrosion resistance and mechanical properties of the V containing TiVN and TiN/VN coatings were significantly improved compared to the TiN coating, the TiVN ternary thin film coating having the highest hardness and adhesion strength and the lowest oxygen contamination (Uslu, 2015).

After a thorough examination of the available literature concerning these types of compounds (Me_1Me_2N), results concerning certain configurations were observed to be missing from the literature (e.g., coatings based on hafnium, most likely due to the material's cost). Consequently, the intention is to supplement the available results with part of this missing data.

(B4) Bibliography

1	Abbondanza, 2012	Abbondanza, L., Meda, L. - *Supposed Versatile β-TaxOyNz structures: DFT studies*. Energy Procedia 2012.
2	Adlhart, 2018	Adlhart, C.; Verran, J.; Azevedo, N.F.; Olmez, H.; Keinanen-Toivola, M.M.; Gouveia, I.; Melo, L.F.; Crijns, F. *Surface modifications for antimicrobial effects in the healthcare setting: a critical overview*. Journal of Hospital Infection 2018
3	Ahmed, 2016	Ahmed, M.; Guo, X.X. *A review of metal oxynitrides for photocatalysis*. Inorganic Chemistry Frontiers 2016
4	Aiken, 2010	Aiken, Z.A.; Hyett, G.; Dunnill, C.W.; Wilson, M.; Pratten, J.; Parkin, I.P. *Antimicrobial Activity in Thin Films of Pseudobrookite-Structured Titanium Oxynitride under UV Irradiation Observed for Escherichia coli*. Chemical Vapor Deposition 2010.
5	Akbal, 2005	Akbal, F. *Photocatalytic degradation of organic dyes in the presence of titanium dioxide under UV and solar light: Effect of operational parameters*. Environmental Progress & Sustainable Energy 2005.
6	Al-Aqtash, 2013	Al-Aqtash, N., Apostol, F., Mei, W-N., *Sabirianov, R.F. Electronic and optical properties of TaO1-xN1+x-based alloys*. Journal of Solid State Chemistry 2013.
7	AL-Jawad, 2017	AL-Jawad, S.M.H.; Taha, A.A.; Salim, M.M. *Synthesis and characterization of pure and Fe doped TiO2 thin films for antimicrobial activity*. Optik 2017
	Anusha, 2016	V.V. Anusha Thampi, Avi Bendavid, B. Subramanian. *Nanostructured TiCrN thin films by Pulsed Magnetron Sputtering for cutting tool applications*. Ceramics International 2016
8	Arranz, 2000	Arranz, A.; Palacio, C. *Tantalum nitride formation by low-energy (0.5-5 keV) nitrogen implantation*. Surface and Interface Analysis 2000
9	Aryasomayajula, 2006	Aryasomayajula, A., Valleti, K., Aryasomayajula, S., Bhat, D.G. *Pulsed DC magnetron sputtered tantalum nitride hard coatings for tribological applications*. Surface & Coatings Technology 2006.
10	Atanassova, 1998	Atanassova, E., Spassov, D*. X-ray photoelectron spectroscopy of thermal thin Ta2O5 films on Si*. Applied Surface Science 1998.
11	Atanassova, 2006	Atanassova, E., Aygun, G., Turan, R., Babeva, Tz. *Structural and optical characteristics of tantalum oxide grown by pulsed Nd:YAG laser oxidation*. Journal of Vacuum Science & Technology A 2006
12	Atasi, 2016	Atasi Dan, J. Jyothi, Kamanio Chattopadhyay, Harish C. Barshilia, Bikramjit Basu. *Spectrally selective absorber coating of WAlN/WAlON/Al2O3 for solar thermal applications*. Solar Energy Materials & Solar Cells 2016
13	Bagcivan, 2013	N. Bagcivan, K. Bobzin, S. Theiß. (*Cr1– xAlx) N: a comparison of direct current, middle frequency pulsed and high power pulsed magnetron sputtering for injection molding components*. Thin Solid Films 2013
14	Balaz, 2013	Balaz, S.; Porter, S.H.; Woodward, P.M.; Brinson, L.J. *Electronic Structure of Tantalum Oxynitride Perovskite Photocatalysts*. Chemistry of Materials 2013

15	Balzer, 2018	Martin Balzer, Martin Fenker, Herbert Kappl, Th. Müller, Andreas Heyn, Alexander Heiss, Andreas Richter. *Corrosion protection of steel substrates by magnetron sputtered TiMgN hard coatings: Structure, mechanical properties and growth defect related salt spray test results*. Surface & Coatings Technology 2018
16	Banakh, 2004	O. Banakh, M. Balzer, M. Fenker, A. Blatter. *Spectroellipsometric evaluation of colour and oxidation resistance of TiMgN coatings*. Thin Solid Films 2004
17	Barshilia, 2008	H.C. Barshilia, N. Selvakumar, K.S. Rajam, D.V. Sridhara Rao, K. Muraleedharan. *Deposition and characterization of TiAlN/TiAlON/Si3N4 tandem absorbers prepared using reactive direct current magnetron sputtering*. Thin Solid Films 2008
18	Beadle, 2008	K.A. Beadle, R. Gupta, A. Mathew, J.G. Chen, B.G. Willis. *Chemical vapor deposition of phase-rich WC thin films on silicon and carbon substrates*. Thin Solid Films 2008
19	Bell, 1998	T. Bell, H. Dong, Y. Sun, *Realizing the potential of duplex surface engineering*. Tribology International. 1998
20	Berg, 2005	S. Berg, T. Nyberg, *Fundamental understanding and modeling of reactive sputtering processes*. Thin Solid Films 2005
21	Bhaumik, 2000	S.K. Bhaumik, C. Divakar, A.K. Singh, G.S. Upadhyaya, *Synthesis and sintering of TiB2 and TiB2–TiC composite under high pressure*. Materials Science and Engineering: A 2000
22	Bidev, 2013	F. Bidev, Ö. Baran, E. Arslan, Y. Totik. Efeoglu, *Adhesion and fatigue properties of Ti/TiB2/MoS2 graded-composite coatings deposited by closed-field unbalanced magnetron sputtering*. Surface and Coatings Technology. 2013
23	Bobzin, 2016	K. Bobzin, T. Brögelmann, G. Grundmeier, T. de los Arcos, M. Wiesing, N.C. Kruppe. *(Cr,Al)N/(Cr,Al)ON Oxy-nitride Coatings deposited by Hybrid dcMS/HPPMS for Plastics Processing Applications*. Surface and Coatings Technology, 2016
24	Bull, 1991	S.J. Bull, *Failure modes in scratch adhesion testing*. Surface and Coatings Technology. 1991
25	Carlton, 2007	C. E. Carlton, P. J. Ferreira. *What is behind the inverse Hall–Petch effect in nanocrystalline materials?* Acta Materialia 2007
26	Chang, 2014	Chang, Y.Y.; Huang, H.L.; Chen, H.J.; Lai, C.H.; Wen, C.Y. *Antibacterial properties and cytocompatibility of tantalum oxide coatings*. Surface and Coatings Technology 2014
27	Chiang, 2005	K.C. Chiang; C.H. Lai; A. Chin; T.J. Wang; H.F. Chiu; Jiann-Ruey Chen; S.P. McAlister; C.C. Chi. *Very high-density (23 fF/μm2) RF MIM capacitors using high-k TaTiO as the dielectric*. IEEE Electron Device Letters 2005
28	Chiu, 2000	H.T. Chiu C.N. Wang S.H. Chuang. *Tantalum oxide is a high dielectric material suitable for DRAM applications*. Chemical Vapor Deposition 2000
29	Christie, 2005	D. J. Christie, *Target material pathways model for high power pulsed magnetron sputtering*, Journal of Vacuum Science & Technology A 2005

30	Chun, 2003	Chun, W.J.; Ishikawa, A.; Fujisawa, H.; Takata, T.; Kondo, J.N.; Hara, M.; Kawai, M.; Matsumoto, Y.; Domen, K. *Conduction and valence band positions of Ta2O5, TaON, and Ta3N5 by UPS and electrochemical methods*. The Journal of Physical Chemistry B 2003
31	Clapa, 2006	M. Clapa, D. Batory. *Improving adhesion and wear resistance of carbon coatings using Ti:C gradient layers*, Journal of Achievments in Materials Manufacturing Engineering, 2006
32	Cong, 2012	Cong, Y.Q.; Park, H.S.; Dang, H.X.; Fan, F.R.F.; Bard, A.J.; Mullins, C.B. *Tantalum Cobalt Nitride Photocatalysts for Water Oxidation under Visible Light.* Chemistry of Materials 2012
33	Creus, 2000	J. Creus, H. Mazille, H. Idrissi, *Porosity evaluation of protective coatings onto steel, through electrochemical techniques*. Surface and Coatings Technology. 2000
34	Cristea, 2011-1	Cristea, D, Crisan, A. *MeOxNy Thin Film Deposition Particularities - Magnetron Sputtering Method*. Cercetări metalurgice și de noi materiale 2011
35	Cristea, 2011-2	Cristea, D, Crișan, A. *MeOxNy system thin films (Me=Ti, Ta, Zr, Mo) – Properties and applicatio*n. Cercetări metalurgice și de noi materiale 2011
36	Cristea, 2013	Cristea, D., Crisan, A. *Tantalum based thin films (oxides, nitrides and oxynitrides) preparation, structures and properties*. RECENT 2013
37	Cristea, 2014	D Cristea, A Crisan, D Munteanu, M Apreutesei, MF Costa, L Cunha. *Tantalum oxynitride thin films: Mechanical properties and wear behavior dependence on growth conditions*. Surface and Coatings Technology 2014
38	Cristea, 2015-1	D Cristea, A Crisan, N Cretu, J Borges, C Lopes, L Cunha, V Ion, M Dinescu, NP Barradas, E Alves, M Apreutesei, D Munteanu. *Structure dependent resistivity and dielectric characteristics of tantalum oxynitride thin films produced by magnetron sputtering*. Applied Surface Science 2015
39	Cristea, 2015-2	D Cristea, M Pătru, A Crisan, D Munteanu, D Crăciun, NP Barradas, E Alves, M Apreutesei, C Moura, L Cunha. *Composition and structure variation for magnetron sputtered tantalum oxynitride thin films, as function of deposition parameters*. Applied Surface Science 2015
40	Cristea, 2019	Daniel Cristea, Luis Cunha, Camelia Gabor, Ioana Ghiuta, Catalin Croitoru, Alexandru Marin, Laura Velicu, Alexandra Besleaga, Vasile Bogdan. *Tantalum Oxynitride Thin Films: Assessment of the Photocatalytic Efficiency and Antimicrobial Capacity*. Nanomaterials 2019
41	Cunha, 2018	L Cunha, M Apreutesei, C Moura, E Alves, NP Barradas, D Cristea*. *In-situ XRD vs ex-situ vacuum annealing of tantalum oxynitride thin films: Assessments on the structural evolution*. Applied Surface Science 2018
42	Deng, 1998	J.X. Deng, X. Ai, *Microstructure and Mechanical Properties of Hot-Pressed TiB2–SiCw Composites*. Materials Research Bulletin. 1998
43	Depla, 2008	Depla, Diederik, Mahieu, Stijn (Eds.) *Reactive Sputter Deposition*, ISBN 978-3-540-76662-9 Springer, 2008
44	Dionysiou, 2004	Dionysiou, D.D.; Suidan, M.T.; Baudin, I.; Laine, J.M. *Effect of hydrogen peroxide on the destruction of organic contaminants-synergism and*

		inhibition in a continuous-mode photocatalytic reactor. Applied Catalysis B: Environmental 2004
45	Ehiasarian, 2002	A.P. Ehiasarian, R. N, W. Munz, U. Halmerson, V. Kousnetsov, *Influence of high-power densities on the composition of pulsed magnetron plasma*. Vacuum 2002
46	Ehiasarian,2007	A.P. Ehiasarian, J. G. Wen, I. Petrov, *Interface microstructure engineering by high power impulse magnetron sputtering for enhancement of adhesion*, Journal of Applied Physics 2007
47	Erdemir, 2006	Ali Erdemir, Christophe Donnet, *Tribology of diamond-like carbon films: recent progress and future prospects*, Journal of Physics D: Applied Physics. 2006
48	Evans, 2007	Evans, P.; Sheel, D.W. *Photoactive and antibacterial TiO2 thin films on stainless steel*. Surface and Coatings Technology 2007
49	Feinstein, 1974	Feinstein, L.G., Huttemann, R.D. *Annealing and phase stability of tantalum films sputtered in Ar-O2*. Thin Solid Films 1974
50	Feldiorean, 2019	D Feldiorean, D Cristea, M Tierean, C Croitoru, C Gabor, L Jakab-Farkas, L Cunha, NP Barradas, E Alves, V Craciun, A Marin, C Moura, J Leme, M Socol, D Craciun, M Cosnita, D Munteanu. *Deposition temperature influence on the wear behaviour of carbon-based coatings deposited on hardened steel*. Applied Surface Science 2019
51	Feng, 2010	Wenran Feng, Hai Zhou, Si-ze Yang. *Gas pressure dependence of composition in Ta–Ti–N films prepared by pulsed high energy density plasma.* Materials Chemistry and Physics 2010
52	Fenker, 2005	M. Fenker, M. Balzer, H. Kappl, O. Banakh. *Some properties of (Ti,Mg)N thin films deposited by reactive dc magnetron sputtering*. Surface & Coatings Technology 2005
53	Fenker, 2006	M. Fenker, M. Balzer, H. Kappl, *Corrosion behaviour of decorative and wear resistant coatings on steel deposited by reactive magnetron sputtering–Tests and improvements.* Thin Solid Films 2006
54	Fenker, 2014	Martin Fenker, Martin Balzer, Herbert Kappl. *Corrosion protection with hard coatings on steel: Past approaches and current research efforts*. Surface & Coatings Technology 2014
55	Fenker, 2019	Martin Fenker, Martin Balzer, Herbert Kappl, Andreas Heyn, Michael Rohwerder, Nicole Fink, Andrea Mingers. *Corrosion protection of steel substrates by magnetron sputtered TiMgN hard coatings: Influence of surface morphology and Mg content on Mg release in NaCl solutions*. Thin Solid Films 2019
56	Gao, 2011	Gao, Q., Giordano, C., Antonietti, M. *Controlled synthesis of tantalum oxynitride and nitride nanoparticles*. Small 2011
57	Gebretsadik, 2011	D.W. Gebretsadik, J. Hardell, I. Efeoglu, B. Prakash, *Tribological properties of composite multilayer coating*. Tribology - Materials, Surfaces & Interfaces 2011
58	Greenwood, 1997	Greenwood, N, Earnshaw, A. *Chemistry of the elements*, 2nd Edition. Butterworth-Heinemann 1997 ISBN: 0-7506-3365-4. 976-980

59	Grosser, 2009	Grosser, M., Schmid, U. *The impact of sputter conditions on the microstructure and on the resistivity of tantalum thin films*. Thin Solid Films 2009
60	Gu, 2006-1	M.L. Gu, C.Z. Huang, B. Zou, B.Q. Liu, *Effect of (Ni, Mo) and TiN on the microstructure and mechanical properties of TiB2 ceramics tool materials*. Materials Science and Engineering: A 2006
61	Gu, 2006-2	M.L. Gu, C.Z. Huang, J. Wang, *Effect of nano-scale Al2O3 on mechanical properties of TiB2 ceramic tool materials*. Key Engineering Materials. 2006
62	Gu, 2008	M.L. Gu, C.Z. Huang, S.R. Xiao, H.L. Liu, *Improvements in mechanical properties of TiB2 ceramics tool materials by the dispersion of Al2O3 particles*. Materials Science and Engineering: A 2008
63	Hall, 1951	E. O. Hall, *The Deformation and Ageing of Mild Steel: III Discussion of Results*. Proceedings of the Physical Society. Section B, Volume 64, 1951
64	Hara, 2003	Hara, M.; Chiba, E.; Ishikawa, A.; Takata, T.; Kondo, J.N.; Domen, K. *Ta3N5 and TaON thin films on Ta foil: Surface composition and stability*. The Journal of Physical Chemistry B 2003
65	Harb, 2014	Harb, M.; Sautet, P.; Nurlaela, E.; Raybaud, P.; Cavallo, L.; Domen, K.; Basseta, J.M.; Takanabe, K. *Tuning the properties of visible-light-responsive tantalum (oxy)nitride photocatalysts by non-stoichiometric compositions: a first-principles viewpoint*. Physical Chemistry Chemical Physics 2014
66	Harish, 2008	Harish C. Barshilia, N. Selvakumar, K.S. Rajam, A. Biswas. *Spectrally selective NbAlN/NbAlON/Si3N4 tandem absorber for high-temperature solar applications.* Solar Energy Materials and Solar Cells 2008
67	Harish, 2014	Harish C. Barshilia. *Growth, characterization and performance evaluation of Ti/AlTiN/AlTiON/AlTiO high temperature spectrally selective coatings for solar thermal power applications*. Solar Energy Materials & Solar Cells 2014
68	Harrison, 2017	Harrison, P.L.; Harrison, T.; Stockley, I.; Smith, T.J. *Does tantalum exhibit any intrinsic antimicrobial or antibiofilm properties*? The Bone & Joint Journal 2017
69	Hassanien, 2015	Hassanien, A.S.; Akl, A.A. *Influence of composition on optical and dispersion parameters of thermally evaporated non-crystalline Cd50S50-xSex thin films*. Journal of Alloys and Compounds 2015
70	Hassanien, 2018	Hassanien, A.S.; Akl, A.A. *Influence of thermal and compositional variations on conduction mechanisms and localized state density of amorphous Cd50S50-xSex thin films*. Journal of Non-Crystalline Solids 2018
71	Hayt, 2012	Hayt F., William H. Jr., John A. Buck, *Engineering Electromagnetics*, 8th ed., McGraw-Hill, 2012, pp. 131–146
72	He, 2016	He, Y.M.; Thorne, J.E.; Wu, C.H.; Ma, P.Y.; Du, C.; Dong, Q.; Guo, J.H.; Wang, D.W. *What Limits the Performance of Ta3N5 for Solar Water Splitting?* Chem-Us 2016

73	Hermann, 1981	Hermann Jr., W.C. *E-beam deposition characteristics of reactively evaporated Ta2O5 for optical interference coatings*. Journal of Vacuum Science and Technology 1981
74	Hodroj, 2011	A. Hodroj, O. Chaix-Pluchery, P. Steyer, J.F. Pierson. *Oxidation resistance of decorative (Ti, Mg) N coatings deposited by hybrid cathodic arc evaporation-magnetron sputtering process*. Surface & Coatings Technology 2011
75	Hoshi, 2004	Y. Hoshi, T. Takahashi, *High rate sputter-deposition of TiO2 films using oxide target*. IEICE TRANSACTIONS on Electronics. E87-C, 227 2004
76	Houas, 2001	Houas, A.; Lachheb, H.; Ksibi, M.; Elaloui, E.; Guillard, C.; Herrmann, J.M. *Photocatalytic degradation pathway of methylene blue in water*. Applied Catalysis B: Environmental 2001
77	Hsieh, 2011	Hsieh, J.H.; Li, C.; Liang, H.C. *Structures and photocatalytic behavior of tantalum-oxynitride thin films*. Thin Solid Films 2011
78	Huang, 2010	Huang, H.L.; Chang, Y.Y.; Lai, M.C.; Lin, C.R.; Lai, C.H.; Shieh, T.M. *Antibacterial TaN-Ag coatings on titanium dental implants*. Surface and Coatings Technology 2010
79	Ionescu, 2009	Ionescu, C, Munteanu, A., Munteanu, D. *Straturi dure de tip Ti-Si-C, obtinute la temperaturi prin depunere fizică din vapori*. Editura Universității Transilvania, Brașov, România. (2009) ISBN 978-973-598-506-6. Pag.31
80	Ishihara, 2008	Ishihara, A.; Doi, S.; Mitsushima, S.; Ota, K. *Tantalum (oxy)nitrides prepared using reactive sputtering for new nonplatinum cathodes of polymer electrolyte fuel cell*. Electrochimica Acta 2008
81	Jagadeesh, 2008	Jagadeesh Chandra, S.V., Uthanna, S., Mohan Rao, G. *Effect of substrate temperature on the structural, optical and electrical properties of dc magnetron sputtered tantalum oxide films*. Applied Surface Science 2008
82	Jagadeesh, 2010	Jagadeesh Chandra, S.V., Choi, C.J., Uthanna, S., Mohan Rao, G. *Structural and electrical properties of radio frequency magnetron sputtered tantalum oxide films: Influence of post-deposition annealing.* Materials Science in Semiconductor Processing 2010
83	Jagadeesh, 2011	Jagadeesh Kumar, K., Ravi Chandra Raju, N., Subrahmanyam, A. *Properties of pulsed reactive DC magnetron sputtered tantalum oxide (Ta2O5) thin films for photocatalysis.* Surface & Coatings Technology 2011
84	Jankowski, 2007	Jankowski, A.F., Go, J., Hayes, J.P. *Thermal stability and mechanical behavior of ultra-fine bcc Ta and V coatings*. Surface and Coatings Technology 2007
85	Jehn, 1992	H.A. Jehn, M.E. Baumgärtner, *Corrosion studies with hard coating-substrate systems.* Surface and Coatings Technology. 1992
86	Jehn, 1993	H.A. Jehn, I. Pfeiffer-Schäller, *Corrosion of hard coatings - Part 3: Electrochemical corrosion tests on decorative hard coatings*. Galvanotechnik 1993.
87	Jeong, 2002	H.W. Jeong, S.J. Kim, Y.T. Hyun, Y.T. Lee, *Densification and compressive strength ofin-situ processed Ti/TiB composites by powder metallurgy*. Metals and Materials International. 2002.

88	Jhi, 2001	S. H. Jhi, S. G. Louie, M. L. Cohen, and J. Ihm, *Vacancy Hardening and Softening in Transition Metal Carbides and Nitrides*. Physical Review Letters. 2001
89	Jinga, 2015-1	V Jinga, AO Mateescu, G Mateescu, LS Craciun, C Ionescu, C Samoila, D Ursutiu, D Munteanu, D Cristea. *Mechanical and tribological behaviour of the multilayer dry lubricant coatings with ternary composition from compound materials (TixNy; TiB2/TixByNz; WC/WxCyNz).* Journal of Optoelectronics and Advanced Materials 2015
90	Jinga, 2015-2	V Jinga, AO Mateescu, D Cristea, G Mateescu, I Burducea, C Ionescu, LS Crăciun, I Ghiută, C Samoilă, D Ursutiu, D Munteanu. *Compositional, morphological and mechanical investigations of monolayer type coatings obtained by standard and reactive magnetron sputtering from Ti, TiB2 and WC*. Applied Surface Science 2015
91	Jones, 2017	Jones, D.R.; Gomez, V.; Bear, J.C.; Rome, B.; Mazzali, F.; McGettrick, J.D.; Lewis, A.R.; Margadonna, S.; Al-Masry, W.A.; Dunnill, C.W. *Active removal of waste dye pollutants using Ta3N5/W18O49 nanocomposite fibres*. Scientific Reports 2017
92	Ju, 2015	Hongbo Ju, Junhua Xu, *Microstructure, oxidation resistance, mechanical and tribological properties of Ti–Y–N films by reactive magnetron sputtering*. Surface and Coatings Technology 2015
93	Junwei, 2008	Junwei Wu, Chengming Li, Christopher Johnson, Xingbo Liu. *Evaluation of SmCo and SmCoN magnetron sputtering coatings for SOFC interconnect applications.* Journal of Power Sources 2008
94	Kadlec, 1987	S. Kadlec, J. Musil, J. Vyskocil, *Influence of the pumping speed on the hysteresis effect in the reactive sputtering of thin films*. Vacuum 1987
95	Kato, 2009	Kato, K., Toyota, H., Jin, Y., Ono, T. *Characterization of tantalum oxy-nitrides deposited by ECR sputtering*. Vacuum 2009
96	Kaur, 2007	Kaur, S.; Singh, V. *TiO2 mediated photocatalytic degradation studies of Reactive Red 198 by UV irradiation*. Journal of Hazardous Materials 2007
97	Kazuki, 2001	Kazuki Kawata, Hiroyuki Sugimura, Osamu Takai. *Characterization of multilayer films of TiAlOCN system prepared by pulsed D.C. plasma-enhanced chemical vapor deposition.* Thin Solid Films 2001
98	Khemasiri, 2016	Khemasiri, N.; Jessadaluk, S.; Chananonnawathorn, C.; Vuttivong, S.; Lertvanithphol, T.; Horprathum, M.; Eiamchai, P.; Patthanasettakul, V.; Klamchuen, A.; Pankiew, A., et al. *Optical band engineering of metal-oxynitride based on tantalum oxide thin film fabricated via reactive gas-timing RF magnetron sputtering*. Surface and Coatings Technology 2016
99	Kim, 2005	Kim, S.K., Cha, B.C. *Deposition of tantalum nitride thin films by D.C. magnetron sputtering*. Thin Solid Films 2005
100	Kindlund, 2013	H. Kindlund, D. G. Sangiovanni, L. Martinez-de-Olcoz, J. Lu, J. Jensen, J. Birch, I. Petrov, J. E. Greene, V. Chirita, L. Hultman. *Toughness enhancement in hard ceramic thin films by alloy design*. APL Materials 1, 2013

101	Kindlund, 2014	H. Kindlund, D. G. Sangiovanni, J. Lu, J. Jensen, V. Chirita, I. Petrov, J. E. Greene, L. Hultman, *Effect of WN content on toughness enhancement in V1–xWxN/MgO (001) thin films.* Journal of Vacuum Science & Technology A 2014
102	Kubacka, 2009	Kubacka, A.; Ferrer, M.; Cerrada, M.L.; Serrano, C.; Sanchez-Chaves, M.; Fernandez-Garcia, M.; de Andres, A.; Rioboo, R.J.J.; Fernandez-Martin, F.; Fernandez-Garcia, M. *Boosting TiO2-anatase antimicrobial activity: Polymer-oxide thin films.* Applied Catalysis B: Environmental 2009
103	Kuznetsov,1999	V. Kuznetsov, K. Macak, etc, *A novel pulsed magnetron sputter technique utilizing very high power densities*, Surface and Coatings Technolgy 1999
104	Lachheb, 2002	Lachheb, H.; Puzenat, E.; Houas, A.; Ksibi, M.; Elaloui, E.; Guillard, C.; Herrmann, J.M. *Photocatalytic degradation of various types of dyes (Alizarin S, Crocein Orange G, Methyl Red, Congo Red, Methylene Blue) in water by UV-irradiated titania*. Applied Catalysis B: Environmental 2002
105	Lamour, 2008	Lamour, P.; Fioux, P.; Ponche, A.; Nardin, M.; Vallat, M.F.; Dugay, P.; Brun, J.P.; Moreaud, N.; Pinvidic, J.M. *Direct measurement of the nitrogen content by XPS in self-passivated TaNx thin films*. Surface and Interface Analysis 2008
106	Le Dréo, 2006	Le Dréo, H., Banakh, O., Keppner, H., Steinmann, P.-A., Briand, D., de Rooij, N.F. *Optical, electrical and mechanical properties of the tantalum oxynitride thin films deposited by pulsing reactive gas sputtering*. Thin Solid Films 2006
107	Le Paven, 2017	C. Le Paven, R. Benzerga, A. Ferri, D. Fasquelle, V. Laur, L. Le Gendre, F. Marlec, F. Tessier, F. Chevirè, R. Desfeux, S. Saitzek, X. Castel, A. Sharaiha, *Ferroelectric and dielectric study of strontium tantalum-based perovskite oxynitride films deposited by reactive rf magnetron sputtering*. Materials Research Bulletin 2017
108	Lee, 1999	Lee, S.L., Cipollo, M., Windover, D., Rickard, C. *Analysis of magnetron-sputtered tantalum coatings versus electrochemically deposited tantalum from molten salt*. Surface & Coatings Technology 1999
109	Lee, 2005	Lee, C.C., Jan, D.J. *Optical properties and deposition rate of sputtered Ta2O5 films deposited by ion-beam oxidation*. Thin Solid Films 2005
110	Lin, 2006	Lin, W.H.; Cheng, C.; Hu, C.C.; Teng, H.S. *NaTaO3 photocatalysts of different crystalline structures for water splitting into H-2 and O-2*. Applied Physics Letters 2006
111	Liu, 2001	Liu, L., Gong, H., Wang, Y., Wang, J., Wee, A.T.S., Liu, R. *Annealing effects of tantalum thin films sputtered on 001 silicon substrate.* Materials Science and Engineering C 2001
112	Liu, 2004	Liu, Y.; Yang, S.F.; Li, Y.; Xu, H.; Qin, L.; Tay, J.H. *The influence of cell and substratum surface hydrophobicities on microbial attachment*. Journal of Biotechnology 2004
113	Liu, 2010	Liu, L., Huang, K., Hou, J., Zhu, H. S*tructure refinement for tantalum nitrides nanocrystals with various morphologies.* Materials Research Bulletin 2012

114	Liu, 2012	Yu Liu, Cong Wang, Yafei Xue, *The spectral properties and thermal stability of NbTiON solar selective absorbing coating*. Solar Energy Materials & Solar Cells 2012
115	Liu, 2014	Yu Liu, Zhifeng Wang, Dongqiang Lei, Cong Wang, *A new solar spectral selective absorbing coating of SS (Fe3O4)/Mo/TiZrN/TiZrON/SiON for high temperature application*. Solar Energy Materials & Solar Cells 2014
116	Liu, 2017	Liu, X.J.; Gan, K.; Liu, H.; Song, X.Q.; Chen, T.J.; Liu, C.C. *Antibacterial properties of nano-silver coated PEEK prepared through magnetron sputtering.* Dental Materials Journal 2017
117	Long, 2003	Yi Long, R.J. Stearn, Z.H. Barber, J. Lloyd, W.J. Clegg, *Deposition of TiN/NiB Superlattice Hard Coatings by Ionised Magnetron Sputter Deposition*. MRS Proceedings 2003
118	Lopes, 2020	C Lopes, C Gabor, D Cristea, R Costa, RP Domingues, MS Rodrigues, J Borges, E Alves, NP Barradas, D Munteanu, F Vaz. *Evolution of the mechanical properties of Ti-based intermetallic thin films doped with different metals to be used as biomedical devices*. Applied Surface Science 2020
119	Lukosius, 2011-1	M. Lukosius, C. Baristiran Kaynak, Ch. Wenger, G. Ruhl, S. Rushworth, P. Baumann. *Atomic Vapor Depositions of Ti–Ta–O thin films for Metal–Insulator–Metal applications*. Thin Solid Films 2011
120	Lukosius, 2011-2	M. Lukosius, C. Baristiran Kaynak, S. Rushworth, and Ch. Wenger. *HfO2, Sr-Ta-O and Ti-Ta-O High-k Dielectrics for Metal-Insulator-Metal Applications*. Journal of The Electrochemical Society 2011
121	Luthier, 1990	R. Luthier, F. Lévy. *TiAlON black decorative coatings deposited by magnetron sputtering.* Vacuum 1990
122	Ma, 2002	J. Ma, G.E.B. Tan, *Processing and characterization of metal–ceramics functionally gradient materials.* Journal of Materials Processing Technology. 2002
123	Maeda, 2008	Maeda, K.; Terashima, H.; Kase, K.; Higashi, M.; Tabata, M.; Domen, K. *Surface modification of TaON with monoclinic ZrO2 to produce a composite photocatalyst with enhanced hydrogen evolution activity under visible light.* Bulletin of the Chemical Society of Japan 2008
124	Malinsky, 2012	P. Malinsky, et al., *Early stages of growth of gold layers sputter deposited on glass and silicon substrates*. Nanoscale Research Letters. 2012
125	Martin, 1999	N. Martin, C. Rousselot, *Modelling of reactive sputtering processes involving two separated metallic targets.* Surface and Coatings Technology. 1999
126	Mateescu, 2015	AO Mateescu, G Mateescu, V Jinga, D Cristea, C Samoilă, D Ursutiu, D Munteanu. *Physical and technological interpretation of mechanical properties for single and multi-layer films with properties of dry lubricants*. Journal of Optoelectronics and Advanced Materials 2015
127	McKinley, 1996	McKinley, K.A., Sandler, N.P. *Tantalum pentoxide for advanced DRAM applications*. Thin Solid Films 1996

128	Mitrovic, 2012	Mitrovic, J.; Radovic, M.; Bojic, D.; Andelkovic, T.; Purenovic, M.; Bojic, A. *Decolorization of the textile azo dye Reactive Orange 16 by the UV/H2O2 process.* Journal of the Serbian Chemical Society 2012
129	Mukhopadhyay, 2009	A. Mukhopadhyay, G.B. Raju, B. Basu, A.K. Suri, *Correlation between phase evolution, mechanical properties and instrumented indentation response of TiB2-based ceramics*. Journal of the European Ceramic Society. 2009
130	Mungchamnankit, 2008	Mungchamnankit, A.; Limsuwan, P.; Thongcham, K.; Meejoo, S. *The electron spin resonance study of Gd3+ in natural zircon*. Journal of Magnetism and Magnetic Materials 2008
131	Murphy, 2006	Murphy, A.B.; Barnes, P.R.F.; Randeniya, L.K.; Plumb, I.C.; Grey, I.E.; Horne, M.D.; Glasscock, J.A*. Efficiency of solar water splitting using semiconductor electrodes.* International Journal of Hydrogen Energy 2006
132	Nikolova, 2000	V. Nikolova, I. Nikolov, P. Andreev, et al., *Tungsten carbide-based electrochemical sensors for hydrogen determination in gas mixtures*. Journal of Applied Electrochemistry 2000
133	Noguchi, 2003	Noguchi, D.; Kawamata, Y.; Nagatomo, T. *Photocatalytic characteristics of TiO2 thin films prepared by Dc reactive magnetron sputtering with added H2O.* Japanese Journal of Applied Physics 2003
134	Oberle, 1951	T.L. Oberle, *Properties influencing wear of metals*. Journal of Metals. 3 1951
135	Oliver, 1992	W.C. Oliver, G.M. Pharr, *An improved technique for determining hardness and elastic modulus using load and displacement sensing indentation experiments.* Journal of Materials Research. 1992
136	Onder, 2013	Sakip Onder, Fatma Nese Kok, Kursat Kazmanli, Mustafa Urgen. *Magnesium substituted hydroxyapatite formation on (Ti,Mg)N coatings produced by cathodic arc PVD technique*. Materials Science and Engineering C 2013
137	Onder, 2015	Sakip Onder, Ayse Ceren Calikoglu-Koyuncu, Kursat Kazmanli, Mustafa Urgen, Gamze Torun Kose, Fatma Nese Kok. *Behavior of mammalian cells on magnesium substituted bare and hydroxyapatite deposited (Ti,Mg)N coatings.* New Biotechnology. 2015
138	Ono, 2006	Ono, T., Kato, K., Toyota, H., Fukuda, Y., Jin, Y. *Characterization of metal insulator metal electrical properties of electron cyclotron resonance plasma deposited Ta2O5*. Japanese Journal of Applied Physics 2006
139	Park, 1990	M.J. Park, A. Leyland, A. Matthews, *Corrosion performance of layered coatings produced by physical vapour deposition.* Surface and Coatings Technology. 1990
140	Perez, 2017	Perez, I.; Carrejo, J.L.E.; Sosa, V.; Perera, F.G.; Mancillas, J.R.F.; Galindo, J.T.E.; Rodriguez, C.I.R. *Evidence for structural transition in crystalline tantalum pentoxide films grown by RF magnetron sputtering*Journal of Alloys and Compounds 2017
141	Petch, 1953	N. J. Petch, *The Cleavage Strength of Polycrystals*. The Journal of the Iron and Steel Institute. 1953

142	Popescu-Pelin, 2015	G. Popescu-Pelin, D. Craciun, G. Socol, D. Cristea, L. Floroian, M. Badea, M. Socol, V. Craciun, *Investigations of pulsed laser deposited tin thin films for titanium implants*. Romanian Reports in Physics 2015
143	Raju, 2009	G.B. Raju, B. Basu, N.H. Tak, S.J. Cho, *Temperature dependent hardness and strength properties of TiB2 with TiSi2 sinter-aid.* Journal of the European Ceramic Society. 2009
144	Ranade, 2012	A.N. Ranade, K.L. Rama, Z. Li, J. Wang, C.S. Korach, Y.-W. Chung, *Relationship between hardness and fracture toughness in Ti–TiB2 nanocomposite coatings.* Surface and Coatings Technology. 2012
145	Rawal, 2010	Rawal, S.K., Chawla, A.K., Chawla, V., Jayaganthan, R., Chandra, R. *Effect of ambient gas on structural and optical properties of titanium oxynitride films*. Applied Surface Science 2010
146	Rebouta, 2012	L. Rebouta, A. Pitães, M. Andritschky, P. Capela, M.F. Cerqueira, A. Matilainen, K. Pischow. *Optical characterization of TiAlN/TiAlON/SiO2 absorber for solar selective applications.* Surface & Coatings Technology 2012
147	Reckewe, 2001	Olaf Reckewe, Jay C. Molstad, Francis J. DiSalvo. *Magnesium nitride chemistry.* Journal of Alloys and Compounds 2001
148	Regent, 2001	F. Regent, J. Musil, *Magnetron sputtered CrNiN and TiMoN films: comparison of mechanical properties*. Surface & Coatings Technology 2001
149	Renaud, 2017	Renaud, A.; Wilmet, M.; Truong, T.G.; Seze, M.; Lemoine, P.; Dumait, N.; Chen, W.; Saito, N.; Ohsawa, T.; Uchikoshi, T., et al. *Transparent tantalum cluster-based UV and IR blocking electrochromic devices*. Journal of Materials Chemistry C 2017
150	Renuka, 2017	Renuka, L.; Anantharaju, K.S.; Vidya, Y.S.; Nagaswarupa, H.P.; Prashantha, S.C.; Sharma, S.C.; Nagabhushana, H.; Darshan, G.P. *A simple combustion method for the synthesis of multi-functional ZrO2/CuO nanocomposites: Excellent performance as Sunlight photocatalysts and enhanced latent fingerprint detection.* Applied Catalysis B: Environmental 2017
151	Riekkinen, 2003	Riekkinen, T., Molarius, J. *Reactively sputtered tantalum pentoxide thin films for integrated capacitors*. Microelectronic Engineering 2003
152	Ristova, 1998	Ristova, M.; Ristov, M. *Silver-doped CdS films for PV application*. Solar Energy Materials & Solar Cells 1998
153	Rouahi, 2012	A. Rouahi, A. Kahouli, F. Challali, M. P. Besland, C. Vallée, S. Pairis, B. Yangui, S. Salimy, A. Goullet and A. Sylvestre. *Dielectric relaxation study of amorphous TiTaO thin films in a large operating temperature range*. Journal of Applied Physics 2012
154	Rouahi, 2013	A Rouahi, A Kahouli, F Challali, M P Besland, C Vallée, B Yangui, S Salimy, A Goullet and A Sylvestre. *Impedance and electric modulus study of amorphous TiTaO thin films: highlight of the interphase effect*. Journal of Physics D: Applied Physics 2013
155	Rouahi, 2016	A. Rouahi, F. Challali, I. Dakhlaoui, C. Vallée, S. Salimy, F. Jomni, B. Yangui, M.P. Besland, A. Goullet, A. Sylvestre. *Structural and dielectric*

		characterization of sputtered Tantalum Titanium Oxide thin films for high temperature capacitor applications. Thin Solid Films 2016
156	Rumble, 1992	Rumble, J.R.; Bickham, D.M.; Powell, C.J. *The Nist X-Ray Photoelectron-Spectroscopy Database*. Surface and Interface Analysis 1992
157	Rupa, 2014	P. Karuna Purnapu Rupa, P.C. Chakraborti, S.K. Mishra, *Structure and indentation behavior of nanocomposite Ti–B–N films*. Thin Solid Films 2014
158	Sakai, 1998	Sakai, N.; Wang, R.; Fujishima, A.; Watanabe, T.; Hashimoto, K. *Effect of ultrasonic treatment on highly hydrophilic TiO2 surfaces*. Langmuir 1998
159	Salimy, 2013	S. Salimy, F. Challali, A. Goullet, M-P. Besland, M. Carette, N. Gautier, A. Rhallabi, J. P. Landesman, S. Toutain, and D. Averty. *Electrical Characteristics of TiTaO Thin Films Deposited on SiO2/Si Substrates by Magnetron Sputtering.* ECS Solid State Letters, 2013
160	Sangiovanni, 2010	D. G. Sangiovanni, V. Chirita, and L. Hultman*, Electronic mechanism for toughness enhancement in TiMN (M=Mo and W).* Physical Review. B 81, 2010
161	Sangiovanni, 2011	D. G. Sangiovanni, L. Hultman, and V. Chirita, *Supertoughening in B1 transition metal nitride alloys by increased valence electron concentration*. Acta Materialia. 2011
162	Schalka, 2016	Nina Schalka, J.F. Thierry, Simonet Fotso, David Holeca, Georg Jakopic, Alexander Fian Velislava L. Terziyska, Rostislav Daniel, Christian Mitterer. *Influence of varying nitrogen partial pressures on microstructure, mechanical and optical properties of sputtered TiAlON coatings*. Acta Materialia 2016
163	Schildhauer, 2006	Schildhauer, T.A.; Robie, B.; Muhr, G.; Koller, M. *Bacterial adherence to tantalum versus commonly used orthopedic metallic implant materials*. Journal of Orthopaedic Trauma 2006
164	Selvakumar, 2012	N. Selvakumar, N.T. Manikandanath, A. Biswas, H.C. Barshilia, *Design and fabrication of highly thermally stable HfMoN/HfON/Al2O3 tandem absorber for solar thermal power generation applications.* Solar Energy Materials and Solar Cells 2012
165	Selvakumar, 2013	N. Selvakumar, S. Santhoshkumar, S. Basu, A. Biswas, H.C. Barshilia, *Spectrally selective CrMoN/CrON tandem absorber for mid-temperature solar thermal applications*. Solar Energy Materials and Solar Cells 2013
166	Shi, 2005	Shi, L.; Yang, Z.H.; Chen, L.Y.; Qian, Y.T. *Synthesis and characterization of nanocrystalline TaN*. Solid State Communications 2005
167	Shibata, 1976	Shibata, S., Murasugi, K., Kaminishi, K. *New type thermal printing head using thin film.* IEEE Transactions on Parts, Hybrids and Packaging 1976
168	Shinichi, 2009	Shinichi Yamamoto, Yoshio Ohashi, Yuji Masubuchi, Takashi Takeda, Teruki Motohashi, Shinichi Kikkawa. *Niobium–aluminum oxynitride prepared by ammonolysis of oxide precursor obtained through the citrate route.* Journal of Alloys and Compounds 2009

169 Song, 2012-1 J. Song, C. Huang, B. Zou, H. Liu, J. Wang, *Microstructure and mechanical properties of TiB2–TiC–WC composite ceramic tool materials*. Materials & Design. 2012

170 Song, 2012-2 J. Song, C. Huang, B. Zou, H. Liu, L. Liu, J. Wang, *Effects of sintering additives on microstructure and mechanical properties of TiB2-WC ceramic-metal composite tool materials.* International Journal of Refractory Metals and Hard Materials 2012

171 Speight, 2017 Dr. James G. Speight. Lange's *Handbook of Chemistry*, Seventeenth Edition McGraw-Hill Education, 2017. p. 1:274-275

172 Srivastava, 1986 P.K. Srivastava, V.D. Vankar, K.L. Chopra, *Very hard W–C coatings on stainless steel by rf reactive magnetron sputtering*. Journal of Vacuum Science & Technology A 1986

173 Stampfl, 2005 Stampfl, C., Freeman, A.J. *Stable and metastable structures of the multiphase tantalum nitride system*. Physical Review B 2005

174 Subramanian, 2010 Balasubramanian Subramanian, Ramadoss Ananthakumar, Muthirulandi Jayachandran. *Microstructural, mechanical and electrochemical corrosion properties of sputtered titanium–aluminum–nitride films for bio-implants*. Vacuum 2010

175 Subramanian, 2011 B. Subramanian, C.V. Muraleedharan, R. Ananthakumar, M. Jayachandran. *A comparative study of titanium nitride (TiN), titanium oxy nitride (TiON) and titanium aluminum nitride (TiAlN), as surface coatings for bio implants*. Surface & Coatings Technology 2011

176 Sun, 1993 Sun, X., Kolawa, E., Chen, J.-S., Reid, J.S., Nicolet, M.A. *Properties of reactively sputter-deposited Ta-N thin films*. Thin Solid Films 1993

177 Swisher, 1972 Swisher, J.H., Read, M.H. *Thermodynamic properties and electrical conductivity of Ta3N5 and TaON.* Metallurgical Transactions 1972

178 Tezza, 2012 Tezza, V.B.; Scarpato, M.; Bernardin, A.M. *Wettability of anatase ceramic glazes.* Chim Oggi 2012

179 Thornton, 1974 J. A. Thornton, *Influence of apparatus geometry and deposition conditions on the structure and topography of thick sputtered coatings*. Journal of Vacuum Science and Technology 1974

180 Todorova, 2006 Todorova, Z., Donkov, N., Ristic, Z., Bundaleski, N., Petrovic, S., Petkov, M. *Electrical and optical characteristics of Ta2O5 thin films deposited by electron-beam vapor deposition*. Plasma Processes & Polymers 2006

181 Tönshoff, 1998 K. Tönshoff, B. Karpuschewski, A. Mohlfeld, T. Leyendecker, G. Erkens, H. GFuß, R. Wenke. *Performance of oxygen-rich TiAlON coatings in dry cutting applications.* Surface and Coatings Technology 1998

182 Trelewicz, 2007 J. R. Trelewicz, C. A. Schuh, *The Hall–Petch breakdown in nanocrystalline metals: a crossover to glass-like deformation*. Acta Materialia 2007

183 Tsai, 1995 Tsai, M.H., Sun, S.C., Lee, C.P., Chiu, H.T., Tsai, C.E., Chuang, S.H., Wu, S.C. *Metal-organic chemical vapor deposition of tantalum nitride barrier layers for ULSI applications*. Thin Solid Films 1995

184 Ullah, 2018 Ullah, H.; Tahir, A.A.; Bibi, S.; Mallick, T.K.; Karazhanov, S.Z. *Electronic properties of beta-TaON and its surfaces for solar water splitting*. Applied Catalysis B: Environmental 2018

185 Uslu, 2015 Merve Ertas Uslu, Aykut Can Onel, Gokhan Ekinci, Burcu Toydemir, Salih Durdu, Metin Usta, Leyla Colakerol Arslan. *Investigation of (Ti,V)N and TiN/VN coatings on AZ91D Mg alloys*. Surface & Coatings Technology 2015

186 Valente, 2006 Valente, J.P.S.; Padilha, P.M.; Florentino, A.O. *Studies on the adsorption and kinetics of photodegradation of a model compound for heterogeneous photocatalysis onto TiO2*. Chemosphere 2006

187 Veprek, 2008 Stan Veprek, J.G. Maritza, Beijman Veprek, *Industrial applications of superhard nanocomposite coatings,* Surface & Coatings Technology, 2008

188 Verchiani, 2008 Verchiani, M., Bouyssou, E., Fiannaca, G., Cantin, F., Anceau, C., Ranson, P. *Reliability study of TaON capacitors: From leakage current characterization to ESD robustness prediction*. Microelectronics Reliability 2008

189 Voevodin, 2000 A.A Voevodin; J.S. Zabinski, *Supertough wear-resistant coatings with "chameleon" surface adaptation*, Thin Solid Films, 2000

190 Wang, 2014 L. Wang, H. Liu, C. Huang, B. Zou, X. Liu, *Effects of sintering processes on mechanical properties and microstructure of Ti (C, N)–TiB2–Ni composite ceramic cutting tool material*. Ceramics International. 2014

191 Wang, 2015 T. Wang, G. Zhang, B. Jiang, *Microstructure, mechanical and tribological properties of TiMoN/Si3N4 nano-multilayer films deposited by magnetron sputtering*. Applied Surface Science 2015

192 Wei, 2011 Wei, A.X., Ge, Z.X., Zhao, X.H., Liu, J., Zhao, Y. *Electrical and optical properties of tantalum oxide thin films prepared by reactive magnetron sputtering*. Journal of Alloys and Compounds 2011

193 Westergard, 1997 Westergard, R., Bromark, M., Larsson, M., Hedenqvist, P., Hogmark, S. *Mechanical and tribological characterization of DC magnetron sputtered tantalum nitride thin films*. Surface & Coatings Technology 1997

194 Xiao, 2017 Xiao, M.; Wang, S.C.; Thaweesak, S.; Luo, B.; Wang, L.Z. *Tantalum (Oxy)Nitride: Narrow Bandgap Photocatalysts for Solar Hydrogen Generation*. Engineering 2017

195 Xu, 2014 Junhua Xu, Hongbo Ju, Lihua Yu. *Influence of silicon content on the microstructure, mechanical and tribological properties of magnetron sputtered Ti–Mo–Si–N films*. Vacuum 2014

196 Yamajo, 2019 Yamajo, S.; Yoon, S.; Liang, J.; Sodabanlu, H.; Watanabe, K.; Sugiyama, M.; Yasui, A.; Ikenaga, E.; Shigekawa, N. *Hard X-ray photoelectron spectroscopy investigation of annealing effects on buried oxide in GaAs/Si junctions by surface-activated bonding.* Applied Surface Science 2019

197 Yang, 2007 Yang, W.M., Liu, Y.W., Zhang, Q., Leng, Y.X., Zhou, H.F., Yang, P., Chen, J.Y., Huang, N. *Biomedical response of tantalum oxide films deposited by DC reactive unbalanced magnetron sputtering*. Surface & Coatings Technology 2007

198	Yongxin, 2015	Yongxin Wu, Cong Wang, Ying Sun, Yafei Xue, Yuping Ning, Wenwen Wang, Shuxi Zhao, Eric Tomasella, Angélique Bousquet. *Optical simulation and experimental optimization of Al/NbMoN/NbMoON/SiO2 solar selective absorbing coatings.* Solar Energy Materials & Solar Cells 2015
199	Yoon, 2005	Yoon, S.G., Kim, H.K., Kim, M.J., Lee, H.M., Yoon, D.H. *Effect of substrate temperature on surface roughness and optical properties of Ta2O5 using ion-beam sputtering*. Thin Solid Films 2005
200	Zarfl, 2015	C. Zarfl, P. Schmid, G. Balogh, U. Schmid. *Electro-mechanical properties and oxidation behaviour of TiAlNxOy thin films at high temperatures*. Sensors and Actuators A: Physical 2015
201	Zhang, 1997	Zhang, Q.Y.; Mei, X.X.; Yang, D.Z.; Chen, F.X.; Ma, T.C.; Wang, Y.M.; Teng, F.N. *Preparation, structure and properties of TaN and TaC films obtained by ion beam assisted deposition*. Nuclear Instruments and Methods B 1997
202	Zhang, 2013-1	Zhang, Q.; Li, C.L.; Li, T. *Rapid photocatalytic decolorization of methylene blue using high photon flux UV/TiO2/H2O2 process*. Chemical Engineering Journal 2013
203	Zhang, 2013-2	Zhang, X.X.; Wang, L.; Levanen, E. *Superhydrophobic surfaces for the reduction of bacterial adhesion*. Rsc Advances 2013
204	Zhang, 2014	Zhang, P.; Zhang, J.J.; Gong, J.L. *Tantalum-based semiconductors for solar water splitting*. Chemical Society Reviews 2014,
205	Zhu, 2013	H.B. Zhu, H. Li, Z.X. Li, *Plasma sprayed TiB2–Ni cermet coatings: Effect of feedstock characteristics on the microstructure and tribological performance*. Surface and Coatings Technology. 2013